

## CHAPTER 3

# Impact of Climate Change on Infrastructure Performance

Bruce R. Ellingwood, Dist.M.ASCE; Paolo Bocchini, M.ASCE; Zoubir Lounis, M.ASCE; Michel Ghosn, M.ASCE; Ming Liu, M.ASCE; David Yang, A.M.ASCE; Luca Capacci; Sofia Diniz, M.ASCE; Ning Lin, A.M.ASCE; George Tsiatas, M.ASCE; Fabio Biondini, F.ASCE; John van de Lindt, F.ASCE; Dan M. Frangopol, Dist.M.ASCE; Mitsuyoshi Akiyama, M.ASCE; Yue Li, M.ASCE; Michele Barbato, F.ASCE; Hanping Hong; Therese McAllister, Dist.M.ASCE; Georgios Tsampras, A.M.ASCE; Farshid Vahedifard, F.ASCE

### 3.1 INTRODUCTION

Structural codes and standards provide criteria for the design of buildings, bridges, and other civil infrastructure to withstand demands imposed by their service requirements and by environmental events or climatic hazards such as snow and ice, rain, windstorms, and riverine and coastal flooding. These codes and standards are revised periodically (typically at intervals of 5 to 10 years) to ensure that they continue to represent the state-of-the-art in engineering science and knowledge.

For the past four decades, structural codes and standards worldwide, including the *Minimum Design Loads and Associated Criteria for Buildings and Other Structures*, ASCE 7-22 ([ASCE 2022b](#)), *AASHTO LRFD Bridge Design Specifications* ([AASHTO 2020](#)) *International Building Code* (IBC 2021a), *National Building Code of Canada* (NBCC 2020), and *Eurocodes* have adopted the principles of limit states (or strength) design. The structural engineering and regulatory communities have also learned over that period that structural reliability and risk analysis tools are essential for modeling uncertainties associated with structural loads and response to ensure satisfactory performance in service. Following the transition from allowable stress design (ASD) to limit states design (often referred

to as load and resistance factor design or LRFD), the evolution of criteria for climatic loads has been gradual and deliberate. Existing criteria for climatic loads, based on historical climatological records and assessments of structural reliability levels underlying these criteria, have treated the operational and climatic loads as stationary in nature (i.e., the past is representative of the future).

The reality of climate change promises to have a disruptive and substantial impact on this gradual evolution of risk-informed codes and standards as well as on structural design practice (ASCE 2015a, 2018). The assumption of stationarity in natural hazard analysis is not tenable when climate change effects are considered. Moreover, uncertainties in climate effects projected over the remainder of the 21st century are extremely large, especially for wind, ice, and snow loads (Tye et al. 2021). More aggressive climatic factors may accelerate structural deterioration in some situations as well as increase hazard intensities and durations. Finally, climate change has become a volatile economic and political issue. Achieving the necessary consensus on climate change effects on infrastructure systems within a code committee will require skillful technical management and careful separation of politicized issues (e.g., what are the causes of climate change) from technical issues (e.g., what is the impact of climate change on structures). There may also be resistance from the public to the costs incurred by climate-related code changes because of their controversial nature. Conversely, failure to address the impact of climate change on the long-term performance of structures and infrastructure facilities could lead to an increased risk of damage and failure of civil infrastructure, increased costs of infrastructure design, construction and maintenance, public health and safety issues, disruption of public services, and negative socioeconomic and environmental impacts nationwide.

Several key questions must be addressed to consider the imperatives of climate change in code and standard development, among them

- How should one model the nonstationarity in climatic hazard event occurrences and intensities that arises because of climate change?
- How should these uncertainties be integrated into a time-dependent structural reliability analysis to estimate future behavior and to demonstrate compliance with performance objectives expressed on reliability terms?
- How should the structural engineering profession and the public be persuaded to accept such changes in the national interest (Cooke 2015), even if the costs of infrastructure systems increase in some instances?

Chapter 3 is designed to answer these and other questions.

## 3.2 OBJECTIVES AND SCOPE

### 3.2.1 Objectives

Chapter 3 addresses the challenges posed by climate change in structural engineering practice to advance the performance of infrastructure systems

through guidelines for recommended code and standard provisions as well as for best engineering practices for design, rehabilitation, and risk management of future climate extremes. Moreover, because current standards and codes for structural design are based on historic climatic data and associated loads and load combinations, Chapter 3 promotes further research to apply the scientific principles of structural reliability and risk analysis to incorporate climate change effects in structural design codes and standards, evaluation and rehabilitation of existing infrastructure, performance-based design (PBD) of structures, and community resilience.

The following tasks are undertaken to achieve these objectives:

- Identify and characterize hazards that are significant for the design of buildings and other structures and are susceptible to climate effects, including extreme temperatures, precipitation, riverine and coastal flooding, landslides, sea level rise, extratropical winds, tropical cyclones and associated storm surge, ice accretion, snow and freeze–thaw cycles, among others.
- Summarize the principles of reliability-based structural design and risk-informed decision-making, as applicable to a changing climate.
- Investigate the issue of the nonstationarity of climate and its implications on climatic loads, load combinations, and structural reliability levels and develop methods for modeling uncertainties in climate variables.
- Identify and assess the impact of changes in climatic hazards and climate-related loads on the performance of structures and resilience of communities.

### 3.2.2 Scope

The scope of Chapter 3 includes climatic loads and structural performance that are also found in ASCE 7 (ASCE 2022b), the *International Building Code* (ICC 2021a), and the *AASHTO LRFD Bridge Design Specifications* (AASHTO 2020). It does not include time-dependent performance of structural components and systems (discussed in Chapter 4), which are the purview of material standards and specifications, such as *ACI 318 Building code requirements for structural concrete* (ACI 2019), or the *AISC Specification for Steel Building Structures* (AISC 2022). Nor does it include special structures that are outside the scope of building and bridge codes and standards.

Many climate effects in infrastructure systems, such as wildland–urban interface (WUI) fires, landslides and droughts, and pluvial flooding, are better addressed through zoning or land-use regulations than through structural engineering practice. Chapter 3 does not address these issues.

The hazard analyses needed to identify and determine climatic structural load parameters are provided and adopted by reference from Chapter 2.

Many fundamental concepts of the problem have already been presented in the ASCE report, *Adapting Infrastructure and Civil Engineering Practice to a Changing Climate* (ASCE 2015a). Chapter 3 focuses on how these concepts can be implemented in structural engineering practice.

The focus of this chapter is on structures. Readers are referred to the ASCE MOP 140, *Climate-Resilient Infrastructure: Adaptive Design and Risk Management*

(ASCE 2018), for a more general discussion of other applications in civil and environmental engineering, such as lifelines, dams and hydraulic structures, and environmental systems.

### 3.2.3 Overview

The chapter begins with an overview of climatic loads appearing in structural design guidelines, standards, and codes used for buildings, bridges, and coastal infrastructure. It draws upon recent activities in the United States (ASCE 2015a, 2018; Tye et al. 2021) as well as in Canada under the Climate-Resilient Buildings and Core Public Infrastructure Initiative (CRBCPI) to develop future climate-based design criteria for the *National Building Code of Canada* (NBCC 2020) and the *Canadian Highway Bridge Design Code* (CSA 2019). That overview is followed by a brief summary of principles of risk-informed decision-making and the use of reliability targets for setting design criteria in ASCE 7 (ASCE 2022b) and the *AASHTO Bridge Design Specifications* (AASHTO 2020).

A major portion of Chapter 3 addresses the treatment of nonstationarity in analysis of climate-dependent building code parameters and a detailed discussion of those parameters on an individual basis, drawing on an extensive review of the literature, with a comprehensive reference list. The need to address climate change impacts on geotechnical systems is summarized. Performance-based approaches to climate change are introduced because it is likely that structural engineers will address client needs under the alternative means and methods clauses of the building codes.

The last major section deals with climate change impacts on community resilience, a topic of urgency in light of increasing losses to infrastructure systems as a result of extreme climate hazards with large geographic footprints and the issuance of PPD 21 (PPD 2013). A summary of recommendations for improving structural design practices concludes the chapter.

## 3.3 CLIMATE CHANGE AND ITS IMPACT ON LOADS FOR CIVIL INFRASTRUCTURE

### 3.3.1 Fundamentals of Structural Design for Climatic Loads

The primary objective of building codes and standards is to protect life safety under extreme (or design-basis) conditions. The national resource document in the United States for structural loads on buildings is ASCE 7, *Minimum Design Loads and Associated Criteria for Buildings and Other Structures* (ASCE 2022b), which is adopted by the *International Building Code* (ICC 2021a) and local building departments in the United States. In Canada, the *National Building Code of Canada* (NBCC 2020) is the national resource, which receives technical support from the National Research Council of Canada and is adopted by the provincial and territorial government authorities. These documents are very similar in their

philosophical basis, and they may be discussed together for this special project. The Eurocodes and many other national structural design codes throughout the world take a similar approach.

The major climatic loads covered in these codes and standards are flood, wind (including extratropical winds, hurricanes, and tornadoes), snow, ice, and rain loads, summarized as follows. The climatic variables affected by climate change are in **boldface** text:

- Hydrostatic flood load per unit width (lb/ft, N/m):  $F = (1/2) \gamma_w \mathbf{d}_f^2$ , in which  $\gamma_w$  is the unit weight of water and  $\mathbf{d}_f$  is the depth of water. If hydrodynamic effects are present, there is an additional term that is dependent on the square of water velocity,  $\mathbf{V}_f^2$ .
- Wind pressure (psf, kPa):  $\mathbf{W} = C_w \mathbf{V}^2$ , in which  $\mathbf{V}$  is the wind speed (mph, m/s) measured at 10 m elevation in open terrain (climate-dependent) and  $C_w$  is the exposure and aerodynamic coefficients (climate-independent). The wind speed depends on averaging time; in the United States,  $\mathbf{V}$  is the  $= 3$  s gust wind speed, whereas in Canada,  $\mathbf{V}$  is the mean hourly wind speed. The aerodynamic coefficients,  $C_w$ , are stipulated so that the design wind pressures in Canada and the United States are virtually the same in most instances. Note that the wind load is proportional to the square of  $\mathbf{V}$ , which makes the estimate of wind speed in a changing climate particularly important.
- Snow load per unit area (psf, kPa):  $\mathbf{S} = C_s \mathbf{S}_g + \mathbf{S}_r$  in which  $\mathbf{S}_g$  is the ground snow load (psf, kPa) (climate-dependent) and  $C_s$  is the ground-to-roof conversion factor, which depends on roof exposure, roof slope, and roof insulation (climate-independent). A rain-on-snow surcharge,  $\mathbf{S}_r$  (psf, kPa), may be added in certain areas where rain may accompany snow.
- Ice loads and atmospheric icing: Atmospheric ice loads caused by freezing rain, snow, and in-cloud icing should be considered, where appropriate. The ice load is determined from the weight of glaze ice formed on all exposed surfaces, determined from the design ice thickness,  $\mathbf{t}_d$  (climate-dependent), on those surfaces. Ice accreted on structural components also increases the projected area of the component exposed to wind, thereby increasing the effect of wind.
- Rain load per unit area (psf, kPa):  $\mathbf{R} = 5.2 (\mathbf{d}_s + \mathbf{d}_h + \mathbf{d}_p)$  in psf (or **0.0098**  $(\mathbf{d}_s + \mathbf{d}_h + \mathbf{d}_p)$  in kPa, in which  $\mathbf{d}_s$  is the depth of water on undeflected roof up to the inlet of the secondary drainage system when the primary drainage system is blocked (static head, in. or mm),  $\mathbf{d}_h$  is the depth of water on the undeflected roof above the inlet of the secondary drainage system at its design flow (hydraulic head, in. or mm),  $\mathbf{d}_p$  is the ponding depth arising from roof deflections caused by unfactored dead and rain load, and the constant 5.2 (or 0.0098) equals psf/in. of water (or kPa/mm of water). Rain loads,  $\mathbf{R}$  (distinguished from the aforementioned  $\mathbf{S}_r$ ), are required for designing drainage for flat roofs or for checking ponding instability.

The climate-related parameters,  $\mathbf{d}_p$ ,  $\mathbf{V}_p$ ,  $\mathbf{V}$ ,  $\mathbf{S}_g$ ,  $\mathbf{S}_r$ ,  $\mathbf{t}_d$ ,  $\mathbf{d}_s$ ,  $\mathbf{d}_h$ , etc., customarily have been presented in maps or tables constructed for a stipulated return period (or

annual probability of being exceeded) to achieve uniformity in hazard at different geographic locations. Until recently, these return periods typically were 50 years for ordinary buildings and 100 years for critical facilities; in addition, a load factor (typically on the order of 1.4 to 1.6) was applied to the specified nominal load to achieve a desired level of structural reliability. [Mapping the load parameters at their return periods and applying a load factor greater than 1.0 (typically on the order 1.4 to 1.6, depending on the level of uncertainty in load) is referred to as a *uniform hazard* approach to load specification. The uniform hazard approach has been traditionally found in ASCE 7 and in the NBCC until recently.] More recently, the load factor on climatic loads has been set equal to 1.0 and the return periods have been increased to the order of 500 years for ordinary buildings to 1,000 years or more for critical facilities to achieve uniform reliability at all sites. [Recent research in probability-based codes has revealed that uniform reliability across geographical boundaries is better achieved by mapping the design-basis event directly and using a load factor of 1.0 (a so-called *uniform risk or uniform reliability* approach to distinguish it from traditional methods).] The conversion of climate parameters to design loads is discussed subsequently in Chapter 3.

In addition to the aforementioned major climate parameters, temperature effects,  $T$ , may be significant for deformation-related limit states, particularly in tall buildings and bridge decks, but they seldom impact structural safety (as discussed in Section 3.7.1).

In contrast to life safety under extreme conditions, current guidelines and standards also contain minimal requirements to ensure *serviceability* under ordinary conditions. Serviceability is viewed primarily as an economic rather than a public safety issue, making it difficult to codify. Serviceability is usually controlled by providing adequate stiffness to minimize deflections, deformations, or vibrations that adversely affect the intended use of the building or comfort of its occupants under ordinary conditions. The loads used to check serviceability have much shorter return periods than those used to verify that safety objectives have been met.

Natural hazard mitigation and community resilience have achieved prominence in the past decade as losses caused by natural hazard events have increased in severity, to a total of approximately USD 80 billion in insured catastrophe losses in 2020 worldwide ([Swiss Re 2020](#)) [see also data in Section 4] and questions of property protection and ability to maintain function during a severe event or to recover function following an event are increasingly debated by public decision-makers. In ASCE 7, buildings are assigned risk categories for planning and design purposes by importance to the community. The most important civilian facilities are designated Risk Category IV facilities, which include hospitals and critical care facilities, fire and police stations, telecommunication facilities, and other essential facilities needed to perform their critical functions and manage emergency in the postdisaster period. In NBCC, the *postdisaster* occupancy class has similar performance requirements. In both the United States and Canada, such facilities are typically designed for longer return periods than ordinary facilities on the order of 1,000 to 3,000 years, and additional performance criteria deemed necessary for them to achieve their postdisaster performance objectives are imposed.

### 3.3.2 Issues and Challenges in Climate Data Analysis for Structural Design

Climatic variables in codes and standards used in structural design such as those mentioned previously are based primarily on historical data. Extratropical winds, snow, temperature, and precipitation are purely data-based; for hurricanes, the historical data are analyzed within a framework that models their genesis in the North Atlantic basin, their growth along tracks into fully developed hurricanes that impact coastal infrastructure, and their dissipation following landfall. It is assumed in these analyses that the climatic variables can be evaluated as if they were stationary—the past being representative of the future—and their intensities can be stipulated by their return periods. These data have been collected for many purposes other than building design—commercial aviation, local hydrology and water resources management, and agriculture—and typically cover fewer than 100 years. Most of the climatic variables found in ASCE 7 and NBCC have been determined by fitting the annual extreme parameter to a probability distribution—the Type I distribution of the largest values and the generalized extreme value (GEV) distribution being two of the most common types of distribution used for this purpose—and the return period (RP) [or mean recurrence interval (MRI)] of a load is determined as the reciprocal of the annual probability,  $p$ , that the load is exceeded:  $RP = 1/p$ . The sampling error on the estimate of the design-basis events in a stationary sequence for return periods greater than 100 years can be quite large, but the estimates of the sample means are reasonably stable when the estimates are updated at intervals of typically 10 years using additional climatic data.

The assumption of stationarity in the data cannot be justified in a changing climate (Pandey and Lounis 2023), and the concept of an event associated with a specified return period, strictly speaking, does not apply (Section 3.5). The increase (or decrease) in climatic variables and the large growth in uncertainty in climate modeling forecasts, particularly beyond 2060, will affect the manner in which the data are analyzed and specified for structural design purposes. Perhaps more important, it will affect the manner in which the design hazards are communicated to the professional engineering community and its client base (Cooke 2015), as discussed further in Section 3.3.3. The authors remember well the confusion over the concept of a return period (or a mean recurrence interval) when it was introduced in the late 1960s. The return period was a way of recognizing that the load parameter is random and defining (indirectly) the annual probability that its design intensity is exceeded without dealing with small probabilities that were not commonly used by structural engineers at the time. This might explain why some climate researchers have attempted to couch their parameter estimates using a notion of a return period (Ribereau et al. 2008, Salas and Obeysekera 2014). This issue requires careful consideration when dealing with a changing climate where the annual probabilities are not constant over a structure's service life.

The projected growth in climatic variables and their uncertainties beyond 2060 suggests that methods will have to be developed for dealing with the *epistemic*

*uncertainty* in parameter estimates that heretofore have not been considered in estimating climatic variables for structural code development. Although the accuracy of overall climate forecasting techniques has been improving through continuous data collection, as explained in Chapter 2, current climate models can predict the impact of climate change on temperature and precipitation with better accuracy than the impact on flooding, snow, and wind, which will be problematic at probability levels deemed appropriate for structural safety analysis.

### **3.3.3 Implementation of Climate Data in Structural Codes and Standards**

Structural codes and standards are developed differently by different groups. The reality of these differences must be considered if climate change effects are to be successfully implemented in professional practice.

First, contrary to popular belief, the choice of return periods (typically 50 to 100 years) for specifying climatic load intensities for design has absolutely nothing to do with the service life of a building or a bridge but serves as a base period for load evaluation. In fact, the concept of a return period was first introduced in the United States in the late 1960s (and two decades earlier in Canada), long before life-cycle analysis became an academic discipline in civil engineering. Parameter samples were much smaller than they are nowadays, and the sampling errors on the estimate of return periods longer than 50 years were very large, placing some limits on estimates of long return period values from available datasets. Furthermore, developers of commercial and multistory residential buildings do not think in terms of 50-year lives because the buildings change hands in the commercial market every 5 to 10 years. In short, the 50-year service life for buildings cannot be verified. The 75-year service life of bridges has more meaning because bridges are designed and maintained by the same entity (state Departments of Transportation in the United States or Provincial and Territorial Ministries of Transportation or municipalities in Canada) during their entire service lives and records are kept on their performance. However, in many cases, functional obsolescence rather than structural safety is problematic for older bridges.

Second, in the United States, standards and codes are developed through a “voluntary consensus standard approval approach,” which is a bottom-up process involving a balance (partnership) of professional engineers and architects, academics, trade association representatives, and building officials. Unlike in most parts of the world where the process is top-down, the United States has no national building code or code-developing organization (NIST provides technical support to standard development but has no regulatory authority in the building and construction industries), and therefore, the ultimate path to risk-informed treatment of climate effects cannot be mandated by any national body. Instead, ASCE (and other professional organizations) facilitates the development of new code provisions on a 5-year cycle, which must be adopted by consensus before being proposed to the International Code Council, where it is voted on

by building code officials who make the final determination of code content. (The International Code Council publishes the *International Building Code*, which is a Model Code that can be adopted by local jurisdictions, often with local amendments. It includes provisions for plumbing, electrical systems, and HVAC systems, in addition to structural provisions. New editions appear every three years, but the major changes occur less frequently because standards such as ASCE 7, ACI 318, ANSI/AISC 360, and others on which the building code relies are revised less frequently.) The process is similar with the *LRFD Bridge Code* ([AASHTO 2020](#)), and in Canada, where NRCC plays a similar role as that of ASCE.

The implications of this second point are far-reaching. The specification of  $d_p$ ,  $V_p$ ,  $V$ ,  $S_g$ ,  $S_r$ ,  $t_d$ ,  $d_s$ ,  $d_h$ ,  $T$ ,  $R$ , and other parameters affected by climate change must reflect the education that has taken place in the building code community during the last four decades and the composition of the standard and code committees and must be understandable to them if improvements in structural engineering practice are to be achieved.

### **3.4 PROBABILITY-BASED LIMIT STATES DESIGN: AN ADVANCE TOWARD RISK-INFORMED DECISION-MAKING**

The failure of a structure or a major portion of it has severe safety and financial consequences to its users, its owners, and the surrounding community. For these reasons, the design and construction of structural systems must meet strict criteria stipulated in design codes and standards to ensure the safety of the public. At the same time, construction costs should be maintained at a level that does not discourage development. Code-writing authorities inevitably seek a proper balance between these conflicting goals.

This section summarizes commonly accepted procedures for developing structural design codes to provide for public safety and to minimize the risk of structural failure. The section also provides a review of the history of structural design code developments and outlines a process for updating current codes to account for the effect of climate change.

#### **3.4.1 Historical Background: Earlier Design Approaches**

The evolution of structural design codes during the past century is a reflection of an improved understanding of the behavior of structural members and systems subjected to design-basis hazard events and the development of more advanced tools to model their behavior and assess their capacities. Laboratory and field data, as well as in situ investigations following structural failures or other performance issues, have also helped verify the applicability of structural mechanics and material models as well as the frequency and intensity of the loads that structural members and systems may experience during their service lives. Such data have

prompted the progression of structural design codes from experience-based codes to uniform hazard codes prior to modern uniform reliability codes as detailed in Section 3.4.2.

### 3.4.1.1 *Experience-Based Codes*

In the early years of the twentieth century, structural code provisions were based on what is commonly known as allowable stress design (ASD) or working stress design (WSD) methods. These methods were based on the assumption that the behavior of structural members and components could be modeled as linear-elastic. A single factor of safety was applied in the design checking equation to ensure that member capacity exceeded the demand imposed by applied loads by an appropriate margin. The nominal loads and the safety factors used in checking structural safety were specified by the code writers on the basis of experience and engineering judgment rather than scientific principles. In the 1950s, the structural engineering community began to recognize that linear elastic models were not representative of structural behavior at design-level loading situations of concern for public safety, nor did they take full advantage of the actual member capacities. Furthermore, utilizing a single safety factor in the design check equation did not properly account for the differences in the uncertainties associated with different structural loads and strengths. Accordingly, some standard-writing groups began adopting concepts of limit states design and specified load and resistance factors that were thought to better reflect these differences in uncertainty in their design specifications. The 1956 edition of ACI 318, *Building Code Requirements for Reinforced Concrete*, introduced such methods in an appendix, calling them ultimate strength design. In bridge engineering ([AASHTO 1973](#)), these design specifications were known as load factor design (LFD) methods. Although the improved structural models for analyzing the load effects and structural resistance capacities using the load and resistance factors were more representative of the actual structural behavior, the specified load and resistance factors were still based on experience and engineering judgment.

### 3.4.1.2 *Uniform Hazards in Codified Design*

Design codes of the earlier era provided empirical equations to determine the nominal design loads associated with environmental and climatic hazards. For example, design wind loads were based on code-specified uniform wind pressures as a function of height; snow loads on roofs were a uniform 20 psf (958 Pa). Neither regional variations nor building exposure were taken into account explicitly. In other cases, the codes gave recommendations to the designer to “compile hazard data applicable for the site by including historical and maximum hazards of records to determine distributions to be considered in design” [see, e.g., the section on hydrological analysis in the *Standard Specification for Highway Bridges* ([AASHTO 1973](#))]. The random nature of climatic hazard intensities eventually was recognized by tying climatic load parameters, such as wind speed or ground

snow load, to return periods (alternatively known as mean recurrence intervals, or MRI) in ANSI A58.1-1972, the forerunner of ASCE 7 (ASCE 2022b). For common building design, a 50-year return period (equivalently, a probability of 1/50 that a given hazard intensity would be exceeded in any year, assuming that the sequence of annual extremes is identically distributed and statistically independent) was chosen in the United States, whereas hydraulic design loads for bridges were associated with 100-year floods. As noted in Section 3.3.3, the service life of the structure did not play a role in the selection of these return period events; the notion of return period was selected for ease of communication because most engineers at the time were unfamiliar with probabilistic analysis and found it easier to think in terms of a return period. Hazard intensities for design were set in terms of a fixed return period regardless of geographical location and without a specific consideration of the random nature of other variables that influence structural design. (The return period was 50 years for ordinary building structures, as noted previously, 100 years for essential facilities, and 25 years for buildings posing no threat to human life. Designating different return periods for different classes of structures was a first attempt to differentiate between failure risks for different building occupancies. It was of limited effectiveness because only one climatic variable in the typical design equation was affected. Moreover, the difference in nominal loads based on 100-year versus 50-year return periods for wind and snow is typically on the order of 10% in the highly populated regions of the Northern United States, which is insufficient, in and of itself, to manage risk.) This approach is known as a uniform hazard approach.

### 3.4.2 Probability-Based Limit States Design: Moving toward Uniform Risk

Advances in the field of structural reliability during the 1970s made it possible to extend structural design beyond the uniform hazard approach to develop safety checking equations that reflect the level of uncertainties in all variables, including those that define applied loads, member capacities, and the analysis methodologies. *Probability-based limit states design*, which remains the basis of modern structural engineering practice, stipulates that design criteria must meet an acceptable level of safety for each limit state of interest, measured in terms of either the reliability index,  $\beta$ , or the limit state probability,  $P_f$ , which are related by Equation (3-1):

$$\beta = -\Phi^{-1}(P_f) \quad (3-1)$$

where  $\Phi^{-1}(\dots)$  is the inverse of the standard Gaussian cumulative distribution function (CDF). For ultimate limit states,  $P_f$  is determined as the convolution of member capacity represented by member strength,  $R$ , and combined load effects for the given design event,  $S$  (Ellingwood et al. 1980):

$$P_f = P(R < S) \quad (3-2)$$

Because Equations (3-1) and (3-2) are unmanageable for practical structural design, a code optimization process was developed to transform them into a set of design equations (Ellingwood et al. 1980, 1982):

$$\text{Required strength} \leq \text{Design strength} \quad (3-3)$$

$$\sum_{i=1}^m \gamma_i Q_{ni} \leq \phi R_n \quad (3-4)$$

in which the nominal load effects,  $Q_{ni}$ , including climatic variables(s) [see Equation (3-3)], are computed by structural analysis, the load factors,  $\gamma_i$ , are defined in appropriate design codes, such as Section 2.3 of ASCE 7-22, and the design strength, described by the right-hand side of the inequality, is determined by the material specification of interest, for example, ACI 318-19 (ACI 2019), *AISC Specification for Steel Building Structures* (AISC 2022), and *AASHTO LRFD Bridge Design Specifications* (AASHTO 2020). Each load and resistance factor depends on the target reliability and the bias and uncertainty in the parameter. Equation (3-4) is known as the load and resistance factor design (or LRFD) format, which has been familiar to structural engineers since the 1950s, hence its selection to implement probability-based limit states design.

The safety levels inherent in any standard or code represent a value judgment on the part of the code writers based on experience, as noted in Section 3.4.1. The target reliabilities for LRFD in ASCE 7 and other material standards and specifications are based on reliability measures that have been established from a structural reliability-based review and assessment of structures that historically have demonstrated satisfactory safety and performance. This process, referred to as *code calibration* (Galambos et al. 1982), was necessary to ensure that the structural engineering profession had confidence in the level of safety provided by the LRFD approach and constituted a major part of the work leading to the load combinations that first appeared in ANSI A58.1-1982 (ANSI 1982) and are the source of those now found in ASCE 7. The benchmark target reliability for most structural members was set in ASCE 7 at  $\beta = 3.0$  for a 50-year service life or, equivalently, at  $P_f = 0.135\%$  in 50 years. By calibrating the target reliability to the successful performance of previous generations of structures, the target probability of failure during a service period arbitrarily set at 50 years reflects the risk level tolerated by society, which implicitly gives a proper consideration of cost, safety, and our ability to adequately characterize safety. A similar criterion is used in the *National Building Code of Canada* (NBCC 2020). However, the *AASHTO Bridge Design Specifications* used a reliability index  $\beta = 3.5$  for a 75-year service life as a basis for calibration (Nowak 1999).

The ASCE 7 target reliability levels for failure modes and risk categories are listed in Table 3-1, which is reproduced from Table 1.3-1 of the ASCE 7-22 General Requirements and are presented in two forms: a reliability index,  $\beta$ , based on a

Table 3-1. Target Reliabilities.

Basis	Risk Category			
	I	II	III	IV
Failure that is not sudden and does not lead to a widespread progression of damage	$P_f = 1.25 \times 10^{-4}$ $\beta = 2.5$	$P_f = 3.0 \times 10^{-5}$ $\beta = 3.0$	$P_f = 1.25 \times 10^{-5}$ $\beta = 3.25$	$P_f = 5.0 \times 10^{-6}$ $\beta = 3.5$
Failure that is either sudden or leads to a widespread progression of damage	$P_f = 3.0 \times 10^{-5}$ $\beta = 3.0$	$P_f = 5.0 \times 10^{-6}$ $\beta = 3.5$	$P_f = 2.0 \times 10^{-6}$ $\beta = 3.75$	$P_f = 7.0 \times 10^{-7}$ $\beta = 4.0$
Failure that is sudden and results in a widespread progression of damage	$P_f = 5.0 \times 10^{-6}$ $\beta = 3.5$	$P_f = 7.0 \times 10^{-7}$ $\beta = 4.0$	$P_f = 2.5 \times 10^{-7}$ $\beta = 4.25$	$P_f = 1.0 \times 10^{-7}$ $\beta = 4.5$

Source: ASCE 7-22 (ASCE 2022b).

Note: Annual probabilities of failure,  $P_f$ , and 50-year reliability indexes,  $\beta$ , for load combinations that do not include earthquakes, tsunamis, or extraordinary events.

50-year service period and an annual limit state probability,  $P_f$ , for the convenience of the user, depending on the requirements of the reliability analysis. (The notion of risk categories was introduced in ASCE 7-10. Prior to that time, consequences of failure for wind, snow, and earthquake loads were distinguished by multiplicative Importance factors on individual load intensities for different occupancy categories.) The annual limit state probability, which is numerically equivalent to the mean annual frequency of failure for rare events, has often been used in recent years in considering extreme natural hazard events, such as tornadoes, tsunamis, flooding, and so on. The reliability index and the annual probability of failure in Table 3-1 are equivalent measures of structural safety, provided that the load processes are stationary in nature. Code development during the last four decades has stabilized around the reliability targets in Table 3-1 as well as those in current bridge design specifications, as experience has shown that they are adequate for structural design. (The Special Project organized a workshop held on September 30, 2022. A preworkshop survey and discussion during the workshop indicated that some consideration might be given to increasing the 50-year and 75-year

basic service periods for certain categories of buildings and bridges exposed to climate change. A summary of the survey and discussion are found in Appendixes A and B of this report.)

With a few exceptions, the load combination requirements in ASCE 7 (summarized in Section 3.6.8) were developed for individual members for use with common material specifications. (Load combinations for earthquake-resistant design, which are based on the performance of the structural system, are an exception to this general rule.) Additional guidance on reliability targets for different failure modes for use by material specification committees is provided in the first column of [Table 3-1](#). For example, because connection failures are usually sudden and additional safety can be provided at little cost, the target reliability index,  $\beta$ , is 4.0 rather than 3.0. Furthermore, to account for the different levels of risk associated with different types of buildings, ASCE 7 classifies buildings into the following four risk categories:

1. Buildings and other structures that represent low risk to human life in the event of failure.
2. All other buildings and other structures not in Risk Categories I, III, and IV.
3. Buildings and other structures that could pose a substantial risk to human life or cause a substantial economic impact or disruption of everyday life in the event of failure.
4. Buildings and other structures designated as essential facilities or the failure of which could pose a substantial hazard to the community.

In general, different return periods on climate parameters may be required to achieve the reliability targets in [Table 3-1](#) for each risk category. For example, [McAllister et al. \(2018\)](#) observed that, for the four building categories in which member failures are not sudden and do not lead to a widespread progression of damage, wind load calculations would require return periods on 3 s gust wind speed of 300 years, 700 years, 1,700 years, and 3,000 years, respectively, to achieve the target reliability levels in Line 1 of [Table 3-1](#). The development of the wind and snow hazard maps in ASCE 7 can be described schematically as in [Figure 3-1](#), in which  $\nu_{\text{hazard}}$  is the mean annual frequency of maximum hazard intensity.

### **3.4.3 Hazard Analysis and Application to Climate Change: An Illustration**

#### *3.4.3.1 Design Hazard Return Period*

Data on the frequencies and intensities of annual extreme events have been used to identify probability models for annual extreme climate variables which, in turn, permit cumulative distribution functions (CDFs) of maximum intensities over a service period of  $T$  years to be developed, provided that the annual extremes form a stationary sequence. Such maximum intensities are utilized in reliability

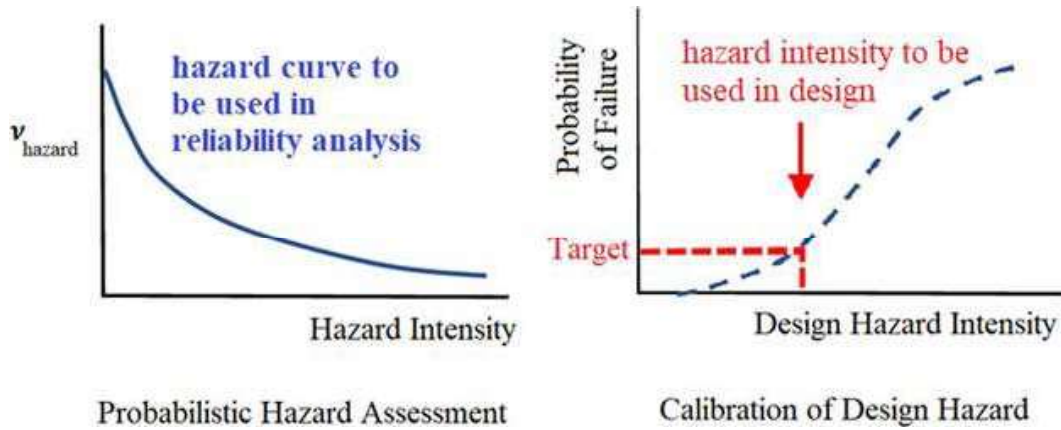


Figure 3-1. Method for establishing design hazard maps.

Source: Adapted from NEHRP (2020).

analyses to assess the probability of failure or to calibrate design codes and specify design loads, as described in Section 3.4.2. In many cases, the probability distributions of these annual extremes,  $F_{H_1}(\dots)$ , can be modeled using a Type I distribution of the largest values (otherwise known as a Gumbel distribution function), a two-parameter form of the generalized extreme value distribution (Coles 2001), where the CDF can be expressed as

$$F_{H_1}(x; u, \gamma) = e^{-e^{-(x-u)/\gamma}} \quad (3-5)$$

where the location parameter,  $u$ , is the mode and the scale parameter,  $\gamma$ , is related to the standard deviation,  $\sigma$ , and approximately equals to  $0.78\sigma$ . Thus, the maximum hazard intensity  $H_T^*$  that has a probability of being exceeded in any given year of  $p = 1/T_R$ , in which  $T_R$  = the return period, is

$$H_T^* = F_{H_1}^{-1}\left(1 - \frac{1}{T_R}\right) = F_H^{-1}(1 - p) = \mu - \gamma \ln(-\ln(1 - p)) \quad (3-6)$$

where  $F_{H_1}^{-1}(\dots)$  is the inverse of the CDF of the maximum yearly hazard  $H_1$ . Equation (3-6) gives the hazard intensity that has a probability of being exceeded in any given year equal to  $p = 1/T_R$ . If it is assumed that the return period gives the mean rate of occurrence, the hazard occurrence can then be modeled with a Poisson distribution with a mean recurrence rate  $\nu = 1/T_R$ . The probability of exceeding the return period hazard in a given period of  $t$  years is obtained as

$$P(H > H_T^*) = 1 - P(H \leq H_T^*) = 1 - e^{-\nu t} = 1 - e^{-t/T_R} \quad (3-7)$$

which for  $t = T_R$  gives a probability of exceedance  $P(H > H_T^*) = 63.2\%$ . Structures designed with such a probability of hazard exceedance would usually lead to reliability indexes much lower than those in Table 3-1. Therefore, design

codes often use return periods much higher than expected service lives or else apply additional safety (load) factors to reduce the likelihood that the structure will fail within its service life. For example, the return period for the base design wind load is set for 700 years for a period of service equal to 50 years, with a load factor of 1.0.

### 3.4.3.2 *T*-year Maximum Hazard

Given the CDF of annual extreme hazard events, the CDF for the extreme hazard event in a period of  $T$  years depends on the number of loading events (in this case, the number of events,  $N$ , is equal to the number of years  $T$ ) that occur during this period. These events are designated as  $H_1, H_2, \dots, H_N$ . The maximum of these events,  $H_T$ , is represented by

$$H_T = \max_{i=1}^N(H_i) \quad (3-8)$$

The probability that  $H_T$  is smaller than some value,  $h$ , implies that each of  $H_1, H_2, \dots, H_N$  is smaller than  $h$ . Assuming independence between events, the cumulative probability distribution of  $H_T$ ,  $F_{H_T}(\dots) = P(H_T < h)$  can then be obtained from

$$F_{H_T}(h) = F_{H_1}(h) \times F_{H_2}(h) \times \dots \times F_{H_N}(h) \quad (3-9)$$

Assuming that the CDF of each event is represented by the same CDF,  $F_{H_1}(h) = F_{H_2}(h) = \dots = F_{H_N}(h)$ , Equation (3-9) reduces to

$$F_{H_T}(h) = [F_{H_1}(h)]^N \quad (3-10)$$

Although Equation (3-9) is always valid for the annual sequence of independent random variables, Equation (3-10) is valid only if the CDFs are the same, which implies that the process is stationary. This assumption is clearly not valid for climatic hazards where the intensities and the rate of occurrence vary, which is the focus of Chapter 3 and this book.

Note that if  $h$  in Equation (3-10) is set equal to  $H_T^*$ , and the return period,  $T_R$ , is high, by setting  $N = t$  and taking the first two terms of the Taylor series expansion,

$$F_{H_T}(H_T^*) = \left[1 - \frac{1}{T_R}\right]^{N=t} \approx 1 - \frac{t}{T_R} \quad (3-11)$$

Given that the CDF  $F_{H_T}(H_T^*) = 1 - P(H > H_T^*)$ , it is observed that Equation (3-11) gives approximately the same result as the first term of the Taylor series expansion of Equation (3-7). The similarity between the results of Equations (3-7) and (3-11), which is valid only in the case of stationary hazards, is attributed to the fact that the concept of return period is applicable only when the maximum yearly hazards are stationary.

### 3.4.3.3 Nonstationarity of Climatic Hazards

Chapter 2 shows that owing to climate change, the frequencies and intensities of climatic hazards may vary over time. Because of the large level of uncertainty in projecting future changes, sample functions of climatic hazards may look as shown in [Figure 3-2](#), where the confidence bounds around the expected intensity levels would also increase over the projection period. The increased uncertainties are a result of both natural variations in the climatic hazard, known as aleatory uncertainties, and our limited ability to estimate future climate change and how it might affect these climatic hazard intensities, known as epistemic uncertainties. Epistemic uncertainties are caused by limitations in available data, shortcomings in the scientific models that account for all the complexities of the problem, and the analytical tools used to implement these models, as well as the unpredictability of future economic activities, human reactions to the climate crisis, and political decisions and actions.

Regardless of the levels of uncertainty involved, if the probability distributions of the maximum yearly climatic hazards are available and can still be considered as independent (see [Section 3-5](#)), then [Equation \(3-9\)](#) is still valid and can be used, as schematically presented previously in [Figure 3-1](#), to obtain the limit state probability for different safety check equations and determine which design load will result in the target reliability.

### 3.4.3.4 Projection of Maximum Service Life Hazard

A process describing how to calibrate design load factors that account for the nonstationary nature of climatic hazards has been presented by [Ghosn and Ellingwood \(2024\)](#). A similar simple example is presented in this section to illustrate how the distribution of the maximum service life hazard might be

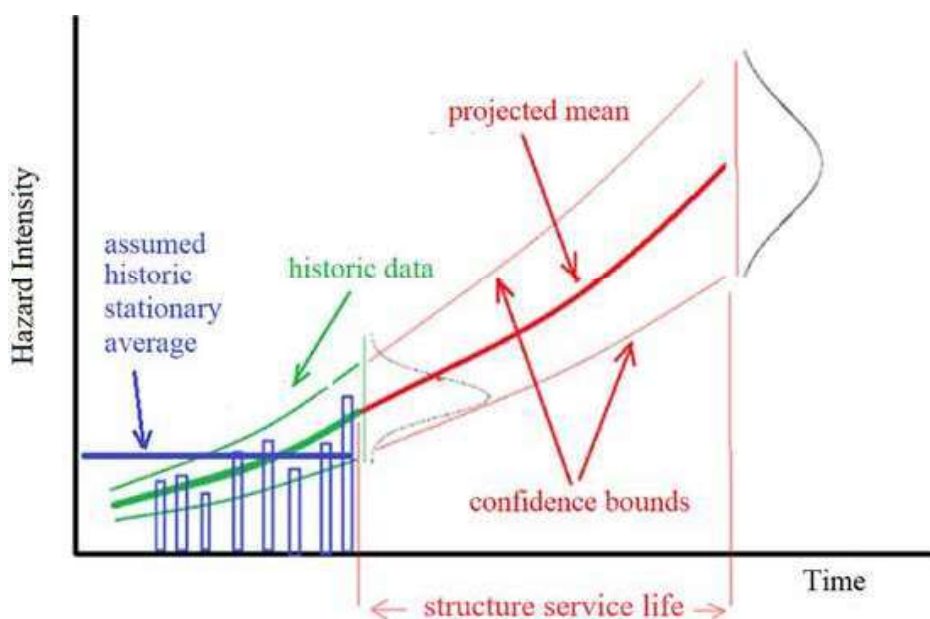


Figure 3-2. Projection of hazard intensities.

obtained. In this example, historical data on hydraulic discharge rates were collected for the Schoharie Creek USGS Station 01350000 at Prattsville, New York (Molodecka et al. 2020). The statistical analysis of the historic upward trend in the maximum yearly flood event indicates that the discharge rate starting with the year 1908 can be modeled as a Gumbel distribution with a location parameter,  $u_t$ , and a scale parameter,  $\gamma_t$ , both of which vary linearly over time,  $t$ , measured in years, such that

$$u_t = 10,371 + 51.71 t \quad (3-12)$$

$$\gamma_t = 5,869 + 43.30 t \quad (3-13)$$

where the discharge rate is in  $\text{ft}^3/\text{s}$  ( $1 \text{ ft}^3/\text{s} = 0.0283168 \text{ m}^3/\text{s}$ ). Available data show that the rate of change for the location parameter per year equals 0.50% per year, and for the scale parameter, it is 0.74% per year. If the Gumbel distribution is used in Equation (3-6) for a return period  $T_R = 100$  years, for the first year, the design hazard would be equal to  $37,332 \text{ ft}^3/\text{s}$  ( $1,057 \text{ m}^3/\text{s}$ ).

Table 3-2 compares the results obtained for the maximum 100-year discharge rate assuming stationary or nonstationary models on the basis of the data in Equations (3-11) and (3-12).

The calculations show that the application of Equation (3-9) would produce a probability distribution for the maximum 100-year flood that can be approximated by a Gumbel distribution. Accounting for the increase in the flood discharge rates over the 100 years beginning in 1908 leads to an expected maximum discharge rate equal to  $57,000 \text{ ft}^3/\text{s}$  ( $1,614 \text{ m}^3/\text{s}$ ) with a coefficient of variation (COV) of 20.3%. This value is 40% higher than one would have predicted assuming no change over the years. This table also shows that even under stationary assumptions, the flood with 100-year return period for this river data would underestimate the mean value of the maximum 100-year flood by about 9%. As shown in the last two rows of the table, using the end year's data to conservatively develop design standards to account for climate change, as some researchers have advocated, would lead to overconservative designs. Alternatively, using the average yearly statistics would underestimate the maximum flood rate by about 5%.

Figure 3-3 indicates that the calculated expected maximum 100-year discharge rate covers all the actual measured peaks in this period. However, the data from Hurricane Irene in the year 2011 are almost six standard deviations above the mean, presenting an anomaly to the statistical trends observed over the period of data collection.

### 3.4.4 Reliability Targets for a Changing Climate

Probability-based limit states design currently is the fundamental basis for dealing with the uncertainties that lead to risk in buildings, bridges, and other civil infrastructure designed by following building codes and is likely to remain so in the foreseeable future.

Table 3-2. Comparison of Projections of 100-Year Maximum Flood Rates for Different Stationary and Nonstationary Cases

Case	Yearly dist., location (ft <sup>3</sup> /s)	Yearly dist. scale (ft <sup>3</sup> /s)	Yearly mean (ft <sup>3</sup> /s)	Yearly standard dev. (ft <sup>3</sup> /s)	Mean of 100-year max. (ft <sup>3</sup> /s)	Std. dev of 100-year max. (ft <sup>3</sup> /s)	COV of 100-year max. (%)	100 year return Q, (ft <sup>3</sup> /s)
Stationary model with statistics from (year 1908)	10,371	5,869	13,754	7,517	40,745	7,517	18.4	37,332
Stationary with average statistics (1908–2007)	12,938	7,808	17,560	10,271	54,438	10,271	18.9	49,775
Stationary model with statistics from (year 2007)	15,505	10,155	21,366	13,024	68,130	13,024	19.1	62,218
Nonstationary					57,000	11,548	20.3	

Note: 1,000 ft<sup>3</sup>/s = 28.32 m<sup>3</sup>/s.

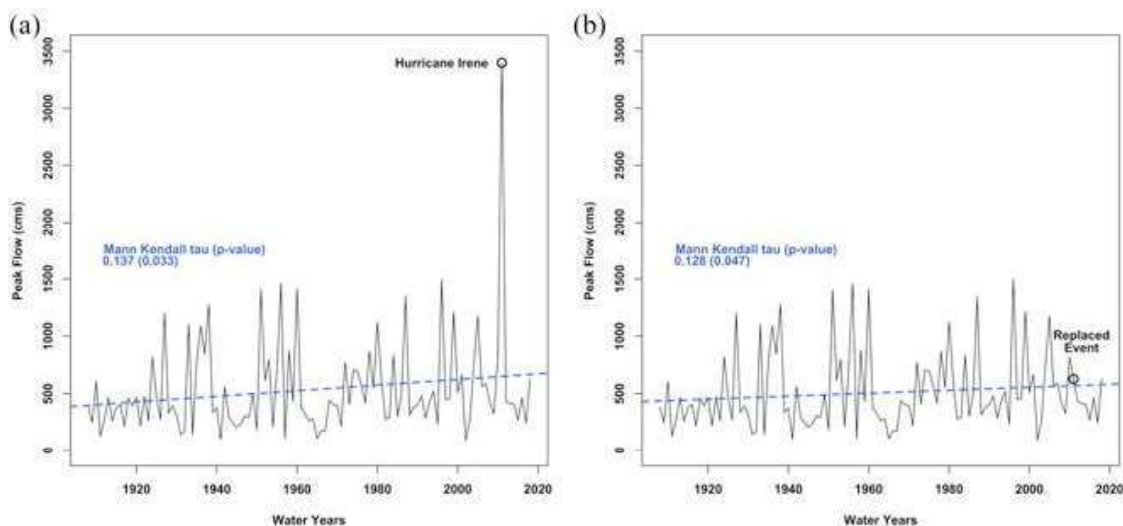


Figure 3-3. Analysis of historical trends for Schoharie Creek peak streamflow: (a) Time series with the underlying historical linear trend, (b) evidence that the historical trend is still significant even with the Hurricane Irene–induced flood event replaced.

Source: Molodecka et al. (2020).

Structural safety involves low failure probabilities and high consequences of failure. The safety levels inherent in structural design codes represent a value judgment on the part of the code writers based on experience and the evolution of engineering practices over the past century. Although it is not possible to assign target limit state probabilities or reliability indexes a priori, the target reliabilities during a service life, arbitrarily set at 50 years for most structures, obtained by calibrating them to the successful performance of previous generations of structures, implicitly reflect the risk level tolerated by society, given a proper consideration of cost, safety, and our ability to adequately characterize safety. The target reliability indexes in [Table 3-1](#), taken from the General Requirements in ASCE 7-22, were determined through an exhaustive set of reliability analyses of structural members and have been reviewed periodically at approximately 6-year intervals over the last four decades. There is no evidence that these target reliabilities require a reconsideration for a changing climate and such changes are not recommended. However, maintaining the current reliability targets in light of climate change, combined with a possible increase in the baseline service period, might necessitate an increase in the specified design loads. The acceptance of such increases by the construction industry and developers as well as highway infrastructure agencies will depend on their levels, which according to some experts, must remain within a range of 5% to 10% with a similar range of increase in the associated construction costs ([Appendixes A and B](#)). It may be difficult to build a business case for code changes beyond these levels.

### 3.4.5 Risk-Informed Structural Design

At a fundamental level, risk is considered to be the product of the probability of failure and the consequences of failure ([Elms 1992](#); [Kunreuther et al. 2004](#)):

$$\text{Risk} = P_f \times \text{Consequences of failure} \quad (3-14)$$

If failure is defined as the situation when a member reaches some predefined limit state, the consequences of failure take two forms: structural consequences of a member's failure (i.e., the possibility of excessive deformations or collapse) and the impact of failure on owners, users, and the community that the structure is intended to serve. It is common to monetize the consequences of failure. These costs may include direct costs, such as the cost of replacing or repairing the structure and loss of life, as well as indirect and user costs including downtime, economic losses, environmental, societal, and political costs.

In [Section 3.4.2](#), failure consequences were taken into account qualitatively by the assignment of buildings to risk categories. Such an approach is necessary because building codes are applicable to a broad range of building occupancies and structural systems (e.g., [Tables 4.3-1 and 12.2-1](#) in ASCE 7-22) and it is not possible to monetize risk for such a broad range for building regulatory purposes.

However, individual buildings designed using a performance-based approach or for enhanced resilience (Sections 3.7 and 3.9) can be designed to minimize total costs subject to code-imposed safety constraints of the type discussed in Section 3.4.2. Further details may be found in Chapter 4.

A conceptual expression for risk, measured by the probability of loss owing to damage caused by single or multiple hazards, is

$$Risk = P(Loss > c) = \sum_H \sum_D \sum_{LS} P(Loss > c | D)P(D | LS)P(LS | H)P(H) \quad (3-15)$$

where

$P(H)$  = Probability of occurrence of an input intensity level associated with hazard ( $H$ );

$P(LS|H)$  = Conditional probability of exceeding a structural limit state (LS) given the hazard ( $H$ );

$P(D|LS)$  = Conditional probability of a damage state ( $D$ ) given the exceedance of the structural limit state (LS);

$P(Loss > c|D)$  = Conditional probability of a loss ( $Loss$ ) given the damage state ( $D$ ); and

$c$  = Appropriate loss metric.

The term  $P(D|LS)$  is an intermediate step that is usually necessary to relate the damage state (minor, moderate, severe), which is used by underwriters to estimate a loss, to a limit state (e.g., flange-local buckling, connection rupture), which is difficult to quantify in monetary terms. Alternatively, risk may be measured as an expected loss:

$$Risk = E[Loss] = \sum c_i P[Loss = c_i] \quad (3-16)$$

The last two terms in Equation (3-15),  $\sum_H P(LS|H) P(H)$ , are equivalent to the probability of failure in Equation (3-2). For example, for the analysis of most hazards, ASCE 7 and most structural design codes require assessing the structural response of individual members such that  $P(LS|H)$  in Equation (3-2) represents the probability of limit state exceedance, given the occurrence of an event with a given intensity (often denoted as “fragility”). The term  $P(D|LS)$  represents the physical damage expected when the limit state is exceeded and is indirectly reflected by the difference in the lines of [Table 3-1](#).

Evaluating the probability of failure, whether failure is defined in terms of a member limit state or in terms of structural collapse, involves a three-step process: (1) establishing a hazard curve, which expresses the mean annual frequencies (rates) at which different intensity levels of a hazardous event are exceeded,  $\nu_H$ ; (2) developing a fragility [Fragility analyses sometimes are used in performance-based earthquake and wind engineering ([Shinozuka et al, 2000](#)). They usually require a system reliability analysis, which may preclude their use for ordinary building

design but can offer considerable value for large projects.] curve for the structure, each point of which represents the conditional probability of failure, given that a certain intensity of the hazard has occurred,  $P(LS|H)$ ; and (3) integrating the hazard and fragility curves to compute the unconditional probability of structural failure. Although an estimation of the damage probabilities,  $P(D|LS)$ , is within the reach of leading structural engineers, the loss probability,  $P(Loss > c|D)$ , is more difficult to determine. Recent efforts to develop next-generation PBD procedures (FEMA P-58-1) (FEMA 2018a) are providing the necessary databases to estimate such damage probabilities and costs.

### 3.5 ANALYSIS OF NONSTATIONARY DATA AND IMPLEMENTATION FOR PRACTICAL DESIGN PURPOSES

#### 3.5.1 Nonstationary Climate and How It Can Be Described

The results presented in Chapter 2 of this book show how general circulation models based on emission and temperature increases project a clear nonstationarity of the physical parameters that determine structural loads. In particular, mean values of several key climatic parameters in many regions of the world are expected to increase over the coming decades, and the fluctuations around the means will also increase, rendering extreme weather events, and, in turn, extreme structural loads, significantly more frequent with potentially higher intensities and larger uncertainties. These trends will have a major impact on the entire calibration of design loads. Moreover, the changes in environmental load-related statistics will exhibit different characteristics over time and space, which will require periodic recalibrations of the design codes. In fact, there is aleatory uncertainty in the future climate and epistemic uncertainty in our climate models (Jun et al. 2008, ASCE 2015a). An exhaustive list of these variables is provided in Chapter 2 and is discussed in Section 3.3, and some examples include the wind speed determining wind loads, the precipitation rate determining snow loads, and the ice thickness, which determines ice loads.

The relationship between climate projections and extreme weather events that drive design loads, such as tropical cyclones, is very complex (see Chapter 2). The return period is a metric commonly used in structural design to identify the magnitude of an extreme event, and it is defined as the inverse of the annual probability of exceedance. It has the crucial advantage of being hazard-agnostic, enabling the comparison of different types of natural hazards. When the random processes describing the occurrence of an extreme event and its magnitude are nonstationary, the annual probability of exceedance changes over time, and the calibration process of the design load needs to be rethought because the notion of return period is not applicable (Sections 3.3 and 3.4). Sections 3.5.2 and 3.5.3 present different approaches to address this issue. Nonstationarity in the capacity of a structure owing to aging or deterioration processes is addressed in Chapter 4.

### 3.5.2 Design Criteria for a Nonstationary Climate

In the last decade, several proposals for replacement of the return period have been made (e.g., [Hunter 2012](#), [Rootzén and Katz 2013](#), [Buchanan et al. 2016](#), [Xu et al. 2020](#)). In particular, [Xu et al. \(2020\)](#) proposed to set the design criteria based on the cumulative exceedance probability (CEP) over the analysis time horizon, and they applied it to determine the design wind speed in a changing climate. [Rootzén and Katz \(2013\)](#) also proposed such a design level targeting the CEP, termed a *design life level* as a rational criterion for hydrologic engineering design accounting for climate change. [Hunter \(2012\)](#) and [Buchanan et al. \(2016\)](#) pointed out that, when modifying designs based on stationary assumptions to account for future nonstationary climate changes, the designer may want to conserve the level of hazard deemed appropriate. As discussed by [Xu et al. \(2020\)](#), CEP-based design is consistent with the traditional stationary design in conserving the level of hazard measured by various probabilistic metrics.

The CEP provides a rigorous consideration of climate nonstationarity, while also allowing structural designers to continue relying on maps for the assessment of design loads. In this case, the maps associated with the CEP will be related to the target service life of the structure, rather than a fixed return period ([Lin et al. 2016](#), [Xu et al. 2020](#)). Although it is expected that to preserve a familiar tool, design loads will continue to be presented through hazard maps; these maps will have to be a function of a set of parameters and will evolve over time. Hence, it is expected that rather than being printed in design manuals, they will be available through an online tool, along the lines of what has already been done by the ASCE 7 Hazard Tool Online ([ASCE 2022a](#)).

The CEP-based approach may be applied in different forms for different loads. For example, ASCE 7-22 provides design wind speed maps for the United States, for Risk Categories I, II, III, and IV. The maps show contours of the 3-s gust wind speed at a height of 10 m for the mean return period of 300, 700, 1,700, and 3,000 years, corresponding to the CEP over 50 years of 0.15, 0.07, 0.03, and 0.016, respectively, if climatic parameters are assumed stationary. Thus, similar maps of design wind speed can be developed for the CEP targets for the nonstationary climate case. The CEP targets can be defined to be consistent with the existing reliability indexes ([Table 3-1](#)). A digital tool can be developed to extend the maps for other CEP targets and service lives. Following the approach of [Xu et al. \(2020\)](#), [Hintermaier and Lin \(2024\)](#) developed CEP-based design wind speed maps for the Eastern United States using the Coupled Model Intercomparison Project Phase 6 (CMIP6) downscaled climate projections of tropical cyclones over the 21st century. [Hintermaier and Lin \(2024\)](#) also compared the CEP-based design wind speeds with the design wind speeds determined for the most extreme year over the analysis time horizon; the later criterion controls annual exceedance probabilities rather than the CEP and is more conservative.

### 3.5.3 Design Loads That Account for a Nonstationary Climate

Current codes and standards are based on the assumption of stationary loads over the service life. The series of steps provided subsequently may be used by

code developers to obtain the data to compile digital maps for climatic variables. Although the use of CEP maps follows the *uniform hazard* concept, this section presents an approach to determine design loads that is consistent with the *uniform risk* concept adopted by ASCE. Building on the work of [Ellingwood et al. \(1982\)](#), the analytical details of this uniform risk approach are provided by [McAllister et al. \(2018\)](#), [Maguire et al. \(2021\)](#), and [Ghosn and Ellingwood \(2024\)](#).

- Step 1. Fix the location, the structural class (which will also determine the target probability of failure over the entire service life), and the target service life.
- Step 2. Compute the probability density function of the maximum annual load  $L_a$  for each year of service life, using models described in Chapter 2.
- Step 3. Combine the annual loads to obtain the probability distribution of the maximum load,  $L$ , expected within the service life of the structure.
- Step 4. Based on the distributions of  $L$ , perform structural analyses for a representative portfolio of archetype components/structures to determine the probability distribution of the demand  $D$  for each component over the target service life.
- Step 5. Determine the general functional form (e.g., lognormal) of the probability distribution of the capacity  $C$  of each component.
- Step 6. By combining the probability distributions of  $C$  and  $D$  (computed at Steps 4 and 5), it is possible to assess the cumulative probability of failure over the service life, by simulation or simple integration. Hence, in this step, the parameters of  $C$  can be iteratively tuned so that the resulting cumulative probability of failure over the service life matches the target value defined in Step 1.
- Step 7. Determine the design load that would lead to such distribution of  $C$  for the structural components being considered ([Ellingwood et al. 1982](#), [Galambos et al. 1982](#), [Maguire et al. 2021](#)).
- Step 8. Repeat Steps 1 to 7 for each combination of location, structural class, and target service life, to provide designers with nominal loads that are a function of these three parameters.

It is important to note that calculations in Step 5 should be done in such a way as to account for the fact that the resistance,  $C$ , of each component is a random variable. Assuming no deterioration,  $C$  remains constant over the service life and the simulated capacity is a single stationary value that remains constant for the life of the structure. In contrast, the demand,  $D$ , each year has a different distribution and a different realization of the random variable that describes the yearly maximum. If different values of the capacity are sampled for each year, an implicit assumption of independence of  $C$  during each year of the service life is made, which is unrealistic. However, the difference in the results obtained by either approach should be numerically negligible for small probabilities of failure.

If the proposed approach is adopted, the entire process that accounts for the nonstationarity of climate and loads would not change the workflow for structural

designers. In fact, they could access an online tool similar to the aforementioned ASCE 7 Hazard Tool Online (ASCE 2022a), and for a given location and target analysis time horizon based on risk category or other considerations, they will automatically receive a value of the design load or of the representative climate parameters that account for climate change, and then, usual techniques to convert the climate parameters into design loads can be adopted. A possible alternative to be investigated is for the designer to be involved in a semiprobabilistic or fully probabilistic analysis.

For illustrative purposes, a hypothetical example code calibration process is provided, for the case of wind loads on a bridge structural member (Ghosn and Ellingwood 2024).

- Step 1. The considered bridge is located in Rochester, New York, and it is to be designed to have a target reliability index  $\beta = 3.5$  for 75 years of service (Nowak 1999).
- Step 2. In this example, it is hypothetically assumed that climate projections indicate that the mean  $\mu_V$  of the maximum yearly wind speed,  $V$ , will increase by 0.1% per year, and its standard deviation  $\sigma_V$  will increase with a yearly rate of 0.2%:

$$\mu_V = 86 + 0.086 t \quad (3-17)$$

$$\sigma_V = 8.6 + 0.0172 t \quad (3-18)$$

- where  $t$  indicates times in years from the present year and speeds are expressed in km/h. It is also assumed that the maximum yearly wind speed  $V$  is well described by a Gumbel distribution, with parameters calibrated based on  $\mu_V$  and  $\sigma_V$ , for instance by using the method of moments.
- Step 3. If the annual maxima of the speed are assumed to be associated with independent events, the cumulative distribution function of the maximum 75-year wind speed  $V$  is well described by a Gumbel distribution with a mean of 121 km/h (which is 5% higher than the 75-year wind speed assuming stationarity) and a standard deviation of 9.4 km/h.
- Step 4. As an example, the bending moment in a bridge column with diameter 1.8 m and height 8.8 m is considered (Ghosn and Ellingwood 2024). The demand on the column can be computed as the product  $C_W \cdot (\lambda_V \cdot V)^2$ , where  $C_W$  is a coefficient that accounts for aerodynamic factors, structural parameters, and site parameters, lognormally distributed with a mean of 0.0764 and a coefficient of variation of 23%;  $\lambda_V$  is a coefficient that captures the uncertainties in estimating future maximum wind speed, normally distributed with a mean of 1 and a coefficient of variation of 7.5%. Based on this information, the distribution of the demand can be easily assessed numerically.
- Step 5. The moment capacity of the column is assumed to have a lognormal distribution with mean value to be determined and a coefficient of variation equal to 13% (Nowak 1999).

- Step 6. By comparing the distributions of capacity and demand, it is found that the 3.5 target reliability index is achieved if the capacity has a mean of 3,740 kN m.
- Step 7. The nominal moment capacity  $M_n$  for the column can be determined knowing that the mean of the actual capacity is  $1.14 \cdot M_n$  (Nowak 1999), which indicates that the required nominal capacity is 3,280 kN m, which would be achieved by a factored design wind load equal to 197 km/h (for a resistance factor equal to 0.9) or 155 km/h if a load factor equal to 1.6 is used. Thus, in keeping with ASCE 7's approach that does not apply load factors for extreme events, the value of 197 km/h would be specified for this site.
- Step 8. Steps 1 to 7 can be repeated when actual data for expected regional changes in wind speeds are available for various locations, structural classes, and target service lives. This will help code writers map the corresponding design wind loads for implementation in appropriate design standards.

The approach described in the aforementioned steps are consistent with current structural design standards that are calibrated assuming no member deterioration. Chapter 4 outlines methods for considering the effects of climate change on the capacity,  $C$ .

### 3.5.4 New Opportunities and Challenges

The use of the CEP will present some new opportunities and challenges for designers, which need to be understood by scientific and professional communities.

The maps describing the CEP can be static like the current hazard maps based on the concept of return period, which will support an easy transition in practice. However, they will have to be a function of the target service life, in addition to the class of structure. Moreover, given the large uncertainty in the climate projection, these maps can be periodically updated to reflect new science and observations. Such updates will also support the new concept of *adaptive design* proposed to account for climate uncertainties (ASCE 2018), as also discussed in Chapters 2 and 4. For this reason, they are expected to be delivered as a digital service. This is consistent with new trends also adopted for the ASCE 7 hazard maps, but although now the online service is a convenient option, it will become a necessary integral part of the design practice. This will also require a commitment from the code-issuing organizations to guarantee continued access and website maintenance to such online services.

The climate parameters must be converted into a load for the structural reliability analyses described in Step 4 of the aforementioned example (e.g., from wind speed to pressure, to be used to find moments and shearing forces). If the nonstationarity of climate and structural loads is considered by using the CEP approach, the probability that a structure experiences an event exceeding a given threshold will grow more than linearly with the increase in duration of the service life, because in general, the years that are added at the end will be subject to larger hazards. Therefore, choosing the target service life will become a major decision in the design or analysis process.

For infrastructure systems for which it is expected that the owner and operator will remain the same during the entire life cycle, this will be an opportunity to create an even more integrated design and management plan. For structures for which ownership changes frequently (e.g., residential and commercial buildings), this aspect may exacerbate existing challenges in valuing long-term investments in structural quality and safety. This aspect is also important for the safety assessment of existing structures. In this case, the analysis will have to be conducted with an analysis time horizon that accounts for the fact that the structure has already been in service for some time.

It is important to realize that engineers and their clients will have to deal with the fact that even disregarding structural deterioration, the annual probability of failure will not be constant in a nonstationary climate. To sidestep this issue, engineers may be tempted to make simplistic assumptions as, for example, design only considering the loads associated with the most extreme year (e.g., the last year) of the target service life. However, this approach may result in overly conservative designs with an associated excessive increase in the cost of construction. To avoid this problem, an approach similar to that presented in this section that looks holistically at the probability of failure over the service life, such as CEP-based design, is recommended.

In most cases, the concept of adaptive design, with multiple design and construction points during the service life, will yield the best approach, allowing designers to update the design as the climate and climate science evolve, which will minimize the level of climate uncertainty to be considered. In this way, they will not have to design and build for a climate that will manifest itself only decades later and on which there are large uncertainties. At the same time, the conceptual design and construction details must have built-in flexibility to facilitate future updates and strengthening should better information become available, for example, *adaptive design* in [ASCE \(2018\)](#).

### 3.5.5 Concluding Remarks

The considerations and ideas presented in Section 3.5 allow readers to draw some important conclusions. First, it must be pointed out that, although the inclusion of climate change considerations in structural design codes is a paradigm shift, the science to do so effectively is already available. The proposed transition mechanism is relatively simple in concept and puts the burden of the change on code developers but leaves the protocols almost unchanged for structural designers. This is an important feature to encourage widespread early adoption by the professional community.

Second, it is important for structural engineers to provide feedback to climatologists on which statistics are needed from climate models (global and downscaled). In fact, the entire code development process, and, in turn, the structural design process, rely on the load distributions used. It is important to have accurate statistics of the load evolution in time, to avoid unsatisfactory performance on the one hand or overdesigned structures on the other hand. In this sense, it is necessary that structural code developers and climate scientists collaborate closely during the continuous update of the digital design load maps.

Third, it is important to stress that, although some global circulation models focus on the evolution of the mean values of climatic parameters, structural design needs to focus on extreme events. For this reason, it will be important to accurately model the tails of the distributions of climatic parameters and promote studies that can correctly capture extreme events and improve our estimates of extreme structural loads to reduce the risk of failures.

### 3.6 ANALYSIS OF CLIMATIC LOADS

The scope of Chapter 3 includes climatic variables and loads that are found in *ASCE Standard 7*, the *International Building Code*, and the *AASHTO LRFD Bridge Design Specifications*. The primary objective of such standards and codes is to *protect life safety* under design-basis conditions. The major climatic loads covered in these codes and standards are flood, wind (including extratropical winds and hurricanes), snow and ice, temperature effects, and rain loads. Section 3.6 shows how the climatic variables identified in Section 3.3— $d_p$ ,  $V_p$ ,  $V$ ,  $S_g$ ,  $S_p$ ,  $t_d$ ,  $d_s$ ,  $d_h$ ,  $R$ , and  $T$ —are incorporated in code and standard provisions to advance structural engineering practices and the performance of civil infrastructure under future climate extremes and to suggest revisions that may be required by a changing climate.

#### 3.6.1 Temperature Effects on Structural Systems

Temperature effects in modern steel and concrete tall buildings and long-span bridges can be significant. Temperature changes cause an imposed internal strain or deformation in a structural system, accompanied by self-equilibrating stresses or forces. The thermal strain,  $\varepsilon_{th}$ , is equal to  $\alpha\Delta T$ , in which  $\alpha$  = coefficient of thermal expansion and  $\Delta T$  = increment in temperature. If the structure is statically determinate, the internal deformation is unrestrained and no internal stresses or forces are developed. In contrast, if the structure is statically indeterminate, the internal deformation is restrained. In the extreme, if the system is an elastic truss and the joints are fully restrained, the axial force  $(P_{th})_k$  developed in member  $k$  with axial rigidity  $(EA)_k$  is equal to the product of the modulus of elasticity,  $E$ , cross-sectional area,  $A$ , and coefficient of thermal expansion,  $\alpha$   $(EA\alpha\Delta T)_k$ , and the intensity of the thermal action may approach that of the dead and live loads. Thus, the thermal effects in a statically indeterminate structural system depend foremost on the stiffness properties (e.g., axial rigidity  $EA$  or flexural rigidity  $EI$ , where  $I$  is the moment of inertia) of the members and connections in the system (El-Tayib 2017).

If the response of a structure is limited to or remains within the elastic range, the thermal and load-induced effects superpose. Thus, thermal effects may be significant for assessing performance related to serviceability/functionality requirements for the structure. Conversely, if the structural system behaves in a ductile fashion, the ultimate load capacity of the system is virtually independent

of the thermal actions. The dependence of the design load on the behavior of the structural system (ductile versus nonductile) makes it difficult to codify the impact of temperature effects on structural design and is the reason why guidance on load combinations for temperature effects are addressed in the Commentary of ASCE 7-22.

As discussed in Chapter 2 of this book, the uncertainties associated with projections of temperature increases owing to climate change are lower than those associated with projections of precipitation, riverine or coastal flooding, and wind and snow loads. For most engineered structures, temperature effects are more likely to be of importance for checking serviceability or functionality than for checking strength.

### 3.6.1.1 Buildings

Interior columns in buildings are subjected to relatively small temperature variations owing to building climate control systems. However, exterior columns may sustain large temperature variations. In the case of tall buildings, these variations in temperature over the height of the building may lead to significant axial deformations in the exterior columns (Fintel and Khan 1965, Khan and Fintel 1966, McLaughlin 1970, West and Kar 1970). These, in turn, may impose large stresses at their connections to the floor systems, leading to potential cracking in the floors themselves (Khan and Fintel 1968, Khan and Nassetta 1970, Ahmed 2011). Climate change may lead to more frequent and larger temperature variations and longer periods of extreme temperatures, thus accelerating connection cracking. Such problems can be minimized by proper connection detailing.

### 3.6.1.2 Bridges

Structural effects in bridges owing to thermal actions include time-dependent fluctuations of the average (effective) bridge temperature and temperature differentials (gradients) over the bridge superstructure. Bridges have to be designed to account for stresses and movements resulting from these effects based on temperature hazard maps. Expansion and contraction of the bridge deck should be accommodated by proper joints and sliding bearings to minimize damage at the interface between framing and abutments or piers. If such movements are partially or totally restrained, as may occur in statically indeterminate systems and integral bridges, the structure must resist the forces developed and a calculation of thermally induced stresses is essential (AASHTO 2020, Imbsen et al. 1985, Roeder 2002).

Climate change and its effect on weather include more frequent temperature fluctuations and longer periods of extreme temperatures, resulting in larger demands on bridge joints and bearings, with possible malfunctioning, and higher stresses on structural members over the bridge service life. An overview of thermal effects on steel bridges considering the possible implications of climate change on bridge design assessment and maintenance can be found in Palu and

[Mahmoud \(2019\)](#). The results showed that ignoring climate change may jeopardize the integrity of many existing steel bridges and that efficient maintenance to keep the expansion joints functional is necessary to avoid undesirable thermal demands. The impact of temperature extremes on prestressed concrete bridges is investigated in [Hagedorn \(2016\)](#) and [Hagedorn et al. \(2019\)](#), who found that temperature gradients may become more extreme owing to extreme heat events and that design procedures should be updated to account for these gradients. The importance of assessing the detrimental impact of temperature extremes on prestressed concrete bridges is also highlighted in [He et al. \(2021\)](#). Furthermore, bridge nonstructural components that are potentially exposed to damage under temperature loading, such as pavements and rails, may also be significantly affected by climate change effects ([Lindgren et al. 2009](#), [Nasr et al. 2020](#)).

### **3.6.2 Riverine (Fluvial) Flooding**

#### *3.6.2.1 Background*

There is a concern that, owing to climate change, the US Northeast, Pacific Northwest, and Northern Great Plains will witness increases in the frequency and magnitudes of floods, which will increase the threats to civil infrastructures (Climate Change Indicators: River Flooding | US EPA). Historically, floods have accounted for 38% of all bridge failures and the total annual flood insurance claims in the United States average more than \$3.5 billion ([Sharma and Mohan 2011](#), [FEMA 2016](#), [Molk 2016](#)). Major floods can be divided into three broad groups: (1) coastal (ocean) flooding, (2) pluvial in its two forms of surface and flash flooding, and (3) fluvial or riverine flooding. Other types include groundwater flooding and drainage flooding. This section addresses riverine flooding and their effects on structural systems.

Section 3.6.2 reflects the state of knowledge as of June, 2022. However, a supplement to the flood loading in Chapter 5 of ASCE 7-22 was being prepared at the time of completion of the SEI Special Project. This supplement may modify how flood loads from both riverine and coastal floods are estimated for structural design.

#### *3.6.2.2 Modeling the Effect of Climate Change on Maximum Riverine Floods*

As explained in Sections 3.4 and 3.5, evaluating the safety of structures exposed to potential riverine floods requires a hazard assessment process that models the maximum intensity of the hazard over the service life of the structure accounting for future changes in the hazard. This can be done using either of two approaches: (1) performing a direct study of historical changes of the hazard over time and performing a statistical projection to estimate future floods, or (2) modeling changes in the primary climate parameters such as temperature and precipitation and using these models to project their influence on flooding hazards (see Chapter 2, Section 2.6.3). The first approach requires the availability of a long historical record at specific locations and assumes that future changes will continue at the same historic trend. The second approach requires an

integrated hydrological–hydraulic model that relates the intensity of the flood to the underlying climatic parameters. Chapter 2 provides explanations on how such climate-dependent riverine flood hazard data can be obtained.

#### 3.6.2.2.1 *Projection of Historical Riverine Flood Data*

In an example analysis of historic trends, reported in Section 3.4.3, [Molodecka et al. \(2020\)](#) showed that the maximum yearly flood discharge rate,  $Q$ , for Schoharie Creek at Prattsville, New York, starting with the year 1908 can be modeled as a Type I Extreme Value Gumbel distribution with a location parameter,  $u_t$ , and a dispersion parameter,  $\gamma_t$ , both of which vary linearly over time,  $t$ , as described by Equations (3-12) and (3-13).

#### 3.6.2.2.2 *Integrated Hydrological–Hydraulic Model*

A study by [Xue et al. \(2018\)](#) describes an integrated modeling framework that couples a hydrological model with a hydraulic analysis module. The hydrological model uses precipitation data at a coarse resolution, whereas the hydraulic module computes localized flood depths, velocities, and inundated areas at a finer spatial resolution. The input data consist of precipitation and air temperature, which are combined with topographic data, land cover type and soil texture type, flow direction, flow accumulation, river network, and slope. Hence, the integrated model approach applies climate projection data to estimate future flood discharge rates in a pertinent geographical region or a river location ([Yang and Frangopol 2019](#)).

#### 3.6.2.2.3 *Maximum Service Life Flood*

For the design and the safety assessment of infrastructure systems, the trends in the maximum yearly flood rates are used as explained in Chapter 2 along with Section 3.4 of this document to obtain the probability distribution of the maximum service life flood. The flood model is subsequently implemented in a structural reliability analysis process to extract a design flood level for use in structural design and safety check equations. The uniform reliability/risk analysis process followed to obtain the design flood is described in Sections 3.4 and 3.5.

### 3.6.2.3 *Effect of Riverine Floods on Structures*

The effects of riverine floods on structures are related to: (1) flood depth, (2) flood velocity, (3) structural exposure, and (4) type and depth of their foundations. Good estimates of flood depth and velocity are obtained on the basis of flood discharge rate data as well as the topographical profile of the river and flooded zone and the type of soils in the vicinity of the structure using computationally intensive or sometimes simplified hydraulic models ([Xue et al. 2018](#), [Ghosn et al. 2003](#)). As an example, the discharge rate,  $Q$ , at a cross section of a river is computed by dividing the cross section into  $n$  elements ([Genç et al. 2015](#)):

$$Q = \sum_{i=1}^n U_i d_i \Delta w_i \quad (3-19)$$

where  $U_i$ ,  $d_i$ , and  $\Delta w_i$  are the mean velocity, mean flood depth, and width in the cross-sectional element,  $i$ , respectively. The flow velocity can be estimated from Manning's equation (Chow et al. 1988):

$$U_i = \frac{R_i^{2/3} S_i^{2/3}}{n_i} \quad (3-20)$$

where

$R_i = A_i/P_i$  = Hydraulic radius of section  $i$  of the channel with  $A_i$  as the cross-section area;

$P_i$  = Wetted perimeter;

$S_i$  = Friction slope, which is equal to the bed slope for a steady uniform flow; and

$n_i$  = Manning's coefficient.

Given a value for  $Q$ , the solution of Equations (3-19) and (3-20) leads to the determination of the flood depth and velocity in each flooded subarea of width  $\Delta w_i$ . The flood depths and velocities are used to study the two types of hydraulic effects of a flood on a structure: (1) hydraulic forces on structural components and foundations, and (2) foundation scour.

#### 3.6.2.3.1 Hydraulic Forces on Structural Components

Flood pressure at each point of a submerged structural component is attributed to hydrostatic and hydrodynamic effects, such that

$$p = \rho gz + \frac{1}{2} a \rho U^2 \quad (3-21)$$

where

$\rho$  = Density of water,

$g$  = Gravity,

$z$  = Depth below the water surface at the point where the pressure is evaluated,

$U$  = Average water velocity, and

$a$  = Drag coefficient or shape factor.

The structure may also be subject to impact forces from debris carried by a flooded river. However, the difficulty of determining the type of debris being carried may require the consideration of various site-specific scenarios. A more complex situation arises when openings between different structural elements (or different structures) are obstructed by large-size debris causing a blockage of water flow, which can itself collect smaller debris resulting in a debris jam. The blockage adds to the forces applied on the structural elements at contact debris-structure areas.

Ignoring the effects of debris-related forces, a simple free body diagram of a submerged structural component may be represented as shown in Figure 3-4, where  $H$  is the water depth. The structure may fail because of bending or shearing forces or because of general equilibrium instability, or from foundation scour.

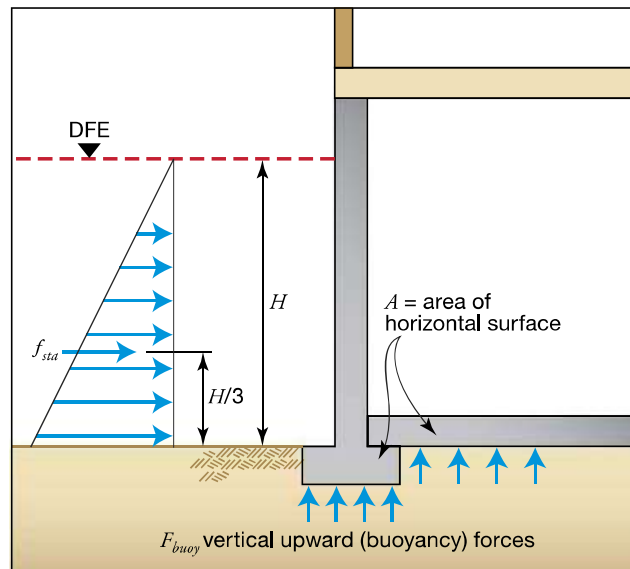


Figure 3-4. Free body diagram of a submerged simple structure.

Source: FEMA (2001).

### 3.6.2.3.2 Foundation Scour

Foundation scour is the erosion of soil around piers and abutments owing to fast-flowing waters. The three types of scour addressed in HEC-18 (FHWA 2012) are: (1) local pier scour, (2) abutment scour, and (3) contraction scour. As an example, the HEC-18 design equation for local scour around bridge piers is a function of the flow depth, pier nose shape, angle of attack of the flow, streambed conditions, soil material size, dimension of the pier, and Froude number. The empirically developed equation used to predict the depth of maximum local scour for design purposes takes the following form (Lagasse et al. 2013):

$$y_{\max} = 2y_0 K_1 K_2 K_3 K_4 \left( \frac{D}{y_0} \right)^{0.65} F_0^{0.43} \quad (3-22)$$

where

$y_{\max}$  = Maximum depth of scour;

$y_0$  = Depth of flow just upstream of the pier excluding local scour;

$D$  = Pier diameter;

$K_1, K_2, K_3,$  and  $K_4$  = Coefficients that account for the nose shape of the pier, the angle between the direction of the flow and the direction of the pier, the streambed conditions, and the bed material size, respectively; and

$F_0$  = Froude's number defined by

$$F_0 = \frac{U}{\sqrt{gy_0}} \quad (3-23)$$

where

$U$  = Mean flow velocity at the pier, and

$g$  = Acceleration owing to gravity.

The flow depth,  $y_0$ , and flow velocity,  $U$ , are related to the flow discharge rate,  $Q$ , and the shape of the channel as given in Equation (3-19).

HEC-18 provides additional information on the local scour as well as equations to model abutment and contraction scour.

### 3.6.2.4 Simplified Design Example

In this simplified example, the analysis of the effect of the static water pressure on a hypothetical reinforced concrete flood wall that is built in the flood plain of the Schoharie River at Prattsville NY in the vicinity of the site where the data of Equations (3-6-1) and (3-6-2) were collected is demonstrated. The schematics of the flooded area and the protective flood wall are shown in Figure 3-5.

The hydraulic static force and the corresponding moment at the base of the flood wall per unit wall width will be respectively equal to  $F = \rho g d_w^2 / 2$  and  $M = \rho g d_w^3 / 6$ , where  $d_w$  is the height of the water level in the flood plain. According to the USGS Flood Indicator Mapper (USGS 2024), the implementation of Equations (3-6-3) and (3-6-4) with the site-specific values of river channel dimensions, bed slope, and Manning coefficient leads to a rating curve that can be approximated by the following relationship between the total flood depth,  $d$ , in feet and the discharge rate  $Q$  in  $\text{ft}^3/\text{s}$ :

$$d = 12 \text{ ft} + d_w = 0.66 Q^{0.31} \quad (3-24)$$

where 12 ft (3.7 m) is the overtopping water depth in the channel. The design and safety assessment of the flood wall must consider various failure modes, including shear and bending moment failure, sliding and overtopping, and foundation failures.

In this example, we demonstrate the design and reliability analysis for bending moment at the base of the concrete flood wall. It is assumed that the design criteria require that the moment capacity of the flood wall be able to withstand an applied water pressure resulting from the 100-year flood level plus an additional one foot of water with a load factor equal to 2.0 and a resistance factor equal to 0.9. The required moment capacity per unit wall width is obtained as follows:

$$0.9 M_{\text{cap}} \geq 2.0 \rho g (d_w + 1)^3 / 6 \quad (3-25)$$

where  $\phi = 0.9$  is the resistance factor and  $\gamma_{\text{Fa}} = 2.0$  is the load factor; a 1 ft water height is added to the calculated height  $d_w$  as traditionally done to provide an additional margin of safety. As mentioned in Table 3-2, assuming that the

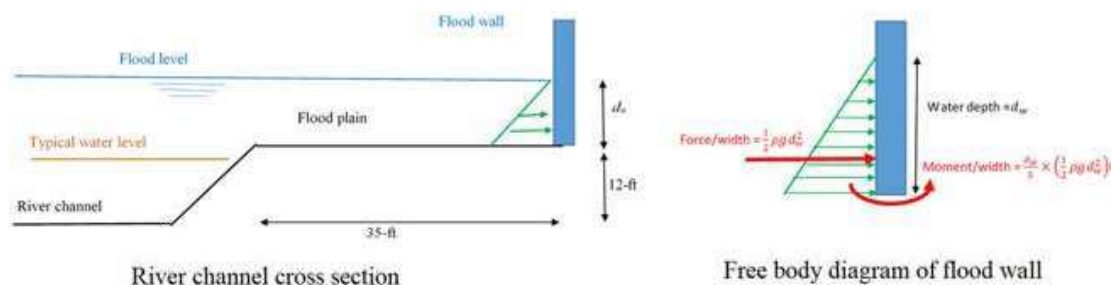


Figure 3-5. Schematic analysis of a flood wall.

engineer ignores the effects of climate change, the design flood corresponding to a 100-year return period is obtained as  $Q_{\text{design}} = 37,332 \text{ ft}^3/\text{s}$ , leading to water depth at the wall level equal to  $d_w = 5.25 \text{ ft}$ . Using the specific weight for water equal to  $\rho g = 62.4 \text{ lb}/\text{ft}^3$ , the required moment capacity per unit width is obtained as  $M_{\text{cap}} = 5.64 \text{ kip ft}/\text{ft}$ .

Table 3-2 shows that a yearly maximum discharge rate  $Q_1 = 13,754 \text{ ft}^3/\text{s}$  yields a 100-year maximum discharge rate  $Q_{100} = 40,745 \text{ ft}^3/\text{s}$  with a standard deviation  $= 7,517 \text{ ft}^3/\text{s}$ . The random generation of the flood discharge rate yields a mean value for  $d_w = 5.67 \text{ ft}$  and a COV  $= 17.7\%$ . Given a bias equal to 1.14 and a COV  $= 13\%$  for the bending strength of reinforced concrete members, the probability of failure for a wall built to meet the  $M_{\text{cap}} = 5.64 \text{ kip-ft}/\text{ft}$  is equal to  $P_f = 1.03\%$  or a reliability index  $\beta = 2.31$ . This reliability index associated with a design discharge rate obtained for a 100-year return period that has a probability of occurrence equal to 63.2% is a reflection of the cubic power for the depth in Equation (3-25) indicating that a live load factor of 2.0 is not consistent with the target reliability  $\beta = 3.0$  set in ASCE-7 even without considering climate change (keeping in mind that these calculations assumed a 100-year service life rather than the 50-year of ASCE-7). A load factor equal to 2.94 in Equation (3-25) giving a moment capacity  $M_{\text{cap}} = 8.29 \text{ kip ft}/\text{ft}$  corresponding to a design flood  $Q_{\text{design}} = 43,600 \text{ ft}^3/\text{s}$  with the original load factor equal to 2.0 would raise the reliability index to  $\beta = 3.0$ . That  $Q_{\text{design}} = 43,600 \text{ ft}^3/\text{s}$  design flood corresponds to the 69.5 percentile of the 100-year flood.

As shown in Table 3-2, accounting for climate change, the 100-year maximum discharge rate has a mean  $Q_{100} = 57,000 \text{ ft}^3/\text{s}$  with a standard deviation  $\sigma_Q = 11,548 \text{ ft}^3/\text{s}$ . This yields a mean value for  $d_w = 7.59 \text{ ft}$  and a COV  $= 16\%$ . The probability of failure for a wall built to meet the  $M_{\text{cap}} = 8.29 \text{ kip ft}/\text{ft}$ , which was originally obtained assuming flood nonstationarity, is equal to  $P_f = 6.06\%$  or a reliability index  $\beta = 1.55$ . Raising the reliability index to the target  $\beta = 3.0$  will require a design moment capacity  $M_{\text{cap}} = 17.51 \text{ kip ft}/\text{ft}$ , which is associated with a design depth  $d_w = 8.12 \text{ ft}$  or a design discharge rate  $Q_{\text{design}} = 61,260 \text{ ft}^3/\text{s}$ . This design discharge corresponds to the 69.4 percentile of the 100-year nonstationary flood, in which the probability of exceedance in a 100-year period (31%) is practically the same as obtained in the stationary case. It is also noted that the ratio of the two design charge rates  $Q_{\text{design}}$  for the nonstationary case compared to the stationary one is equal to 1.41 ( $= 61,260/43,600$ ), which is practically the same ratio of the mean of the nonstationary to the stationary 100-year maximum discharge rates,  $Q_{100}$ , which is 1.40 ( $= 57,000/40,745$ ). These comparisons indicate the possibility of using a simple scaling approach to adjust design load intensities for the nonstationary climate change conditions by scaling the design loads obtained from current load maps that did not account for climate change.

### 3.6.2.5 Summary

This section reviewed how the safety and reliability of structures exposed to riverine floods may be affected by increases in river discharge rates owing to climate change. Using a simple example of the design of a flood wall under static

water pressure, it is observed that maintaining the same target reliability level set in current design standards would require a major change in the specified design flood loads. For the particular hypothetical case analyzed, it appears that using a design flood that has the same probability of exceedance within the specified design period of the structure as that used in the current standards without the consideration of climate change would lead to reliability levels similar to those currently specified. Specifically, if one uses for design flood the discharge rate that has 63.2% probability of exceedance within a 100-year period based on the probability distribution of the maximum flood accounting for climate change, the reliability index would be similar to the one obtained by using in design the flood corresponding to a 100-year return period assuming stationary flood discharge rates. This situation appears to be valid as long as the COV of the maximum design-life-flood under climate change remains reasonably close to the COV for the stationary condition. Additional work is needed to verify the validity of this observation for various limit states and conditions.

### **3.6.3 Coastal Inundation caused by Sea Level Rise**

#### *3.6.3.1 Introduction*

Coastal infrastructure is constantly exposed to extreme sea levels as a result of natural hazards, including hurricane storm surges, tsunami, and beach erosion. In the United States, more than US \$3 trillion has been invested in infrastructure development along the Atlantic and Gulf coasts, making these regions vulnerable to storm surge (Gayathri et al. 2017). One notable instance was Hurricane Katrina in 2005, where the extreme storm surge overtopped levees, causing extensive damage to 200,000 dwellings in New Orleans and a loss estimated to exceed US \$100 billion (Deryugina et al. 2018). Another example is the 2011 Great East Japan Earthquake, which destroyed most of the coastal infrastructure in the Tohoku region and generated prolonged socioeconomic impacts. Accelerating sea level rise (SLR) resulting from climate change could exacerbate such hazards (Koshimura and Shuto 2015), leading to disproportionate increases in coastal inundations and their occurrence frequency over time. Hence, sea level rise assessment plays a vital role in implementing appropriate countermeasures to reduce substantial coastal infrastructure losses.

According to the most recent Annual Report 6 (AR6) of the Intergovernmental Panel for Climate Change (IPCC 2022), the global average sea level could rise 0.56 m in the year 2100 for a modest greenhouse gas emission scenario (i.e., SSP2-4.5) (Fox-Kemper et al. 2021). In addition, IPCC has pointed out that sea level rise could vary considerably on a regional basis, with several locations experiencing significantly higher sea level rise than the global average (Church et al. 2013). Another study (Buchanan et al. 2017) stressed that under a high-end emission scenario (i.e., Representative Concentration Pathway RCP 8.5 scenario of the AR5, as described in Chapter 2), the expected annual number of present-day 100-year storm surge events in the United States could increase by 40-fold because of sea

level rise, indicating a rapid increase of flooding risk along the US coast over the upcoming decades. To comprehend how projected sea level rise would intensify the compounding effects of coastal inundations, a recent numerical study in the Macau Special Administrative region was conducted and it was found that 0.5 m of sea level rise is sufficient to double the tsunami hazard in the cities analyzed (Li et al. 2018). Therefore, it is of critical importance to consider future sea level rise in coastal inundation assessments.

Section 3.6.3 reflects the state of knowledge as of June, 2022. However, a Supplement to the flood loading in Chapter 5 of ASCE 7-22 was being prepared at the time of completion of the SEI Special Project. This Supplement may modify how flood loads from both riverine and coastal floods are estimated for structural design.

### 3.6.3.2 *Modeling Sea Level Rise*

Considerable research has been devoted to projecting sea level rise on the basis of several models. Currently, there are two types of widely accepted models: process-based and semi-empirical models. The process-based approach employs a mathematical model that dynamically simulates the physical processes of atmospheric, ocean density, circulation, and sea level conditions, known as the General Circulation Model (GCM) (Church et al. 2013). This approach has been developed by numerous climate model groups worldwide and is collectively archived in the Coupled Model Intercomparison Project 5 (CMIP5) (Taylor et al. 2012). In the semi-empirical approach, a statistical relationship between past-observed global mean sea levels (GMSLs) with other correlated variables such as global mean temperature (Rahmstorf 2007) or total radiative forcing (Jevrejeva et al. 2009) is established. Based on this statistical relationship, future trends are projected using climate data. Both approaches have been used to estimate each sea level rise contributor on both global and regional scales. Because the semi-empirical approach tends to overestimate the sea level rise projection significantly, the process-based approach is preferred because it uses more representative physical models (Orlić and Pasarić 2013).

The inherent uncertainties associated with sea level rise projections make applying the appropriate countermeasures for future disasters intricate. These uncertainties arise from the differences in modeling approaches on various sea level rise components and the choice between several greenhouse gas emission scenarios, defined as the RCPs for AR5 and SSP for AR6 (Church et al. 2013) (Section 2.4). To account for these inherent uncertainties, probabilistic projections of sea level rise were carried out for each sea level rise component separately, such as sea level rise caused by thermal expansion of the ocean, melting glaciers, or ice-sheet sea level rise (e.g., Kopp et al. 2014, Jackson and Jevrejeva 2016). However, these projections of future sea level rise from past studies must be developed further, particularly for the ice sheet sea level rise, because it was evaluated according to expert elicitation. In addition, the assessments were carried out by disregarding the statistical dependencies between sea level rise components.

Sea level rise can be further integrated with other coastal hazards to achieve an accurate structure reliability assessment and promote resilience for coastal communities. A framework for probabilistic regional sea level rise hazard assessment can be developed by utilizing several sea level rise projections under different climate change scenarios and considering their correlation. Because the intensity of sea level rise substantially depends on location, it is necessary to perform probabilistic sea level rise assessments on a local scale, as summarized by [Alhamid et al. \(2022\)](#). First, regional sea level rise (i.e., sea level rise in a particular location in the ocean) is estimated by multiplying each global mean sea level rise component with its corresponding spatial variability ([Jackson and Jevrejeva 2016](#)). As explained in Chapter 2, the major components for sea level rise have been identified as: (1) the combination of volumetric thermal expansion of the ocean and the ocean currents (hereafter referred to as the sterodynamic sea level rise), (2) surface mass balance of glaciers worldwide (i.e., glacier sea level rise), and (3) the ice sheet sea level rise from the surface mass balance and dynamic thinning of the Greenland and Antarctica Ice Sheets ([Church et al. 2013](#)). Although other components such as land-water storage and other nonclimatic factors might play a role in sea level rise ([Church et al. 2013](#)), their contributions are negligible and therefore disregarded herein.

[Figure 3-6](#) shows the flowchart for the probabilistic sea level rise hazard assessment. Each probability distribution function (PDF) of the regional sea level rise hazard is estimated on the basis of their corresponding uncertainties. In terms of sterodynamic sea level rise (PDF  $S$ ), a conventional statistical analysis is performed using numerous climate models under different RCPs. These models are obtained from CMIP5 by combining the thermosteric sea level rise projection over time with the spatiotemporal projections of the sea level deviation above the ocean geoid (i.e., dynamic sea level rise owing to ocean currents). It should be noted that several preprocessing steps should be carried out prior to utilizing the data, such as model drift corrections and interpolation of ocean grid resolution, to ensure uniform spatial resolution of the data used ([Jackson and Jevrejeva 2016](#)). Similarly, the PDF of global mean glacier sea level rise ( $G$ ) can be estimated by

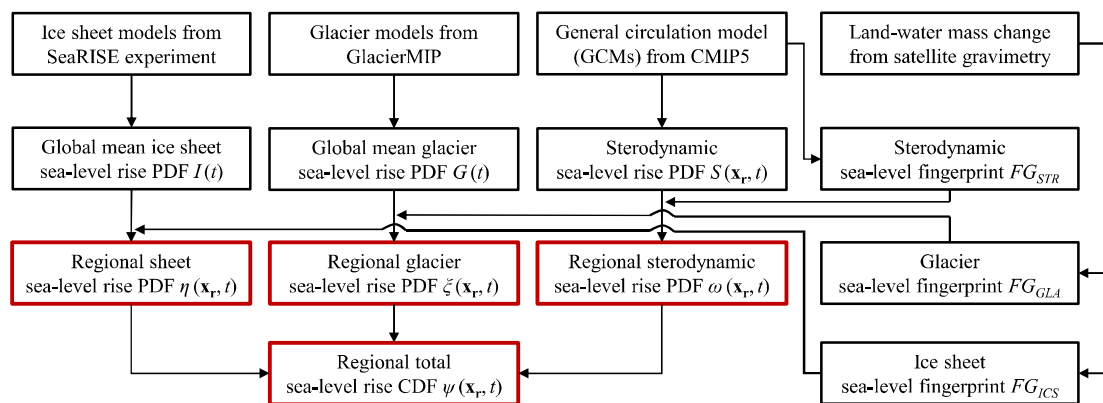


*Figure 3-6. Flowchart of a framework for estimating regional total sea level rise hazard.*

Source: [Alhamid et al. \(2022\)](#).

utilizing Glacier Model Intercomparison Project (GlacierMIP) (Hock et al. 2019). Finally, the global mean ice sheet sea level rise (PDF  $I$ ) is estimated using the volume above floatation change projections for the surface mass balance (Bindschadler et al. 2013) and ice sheet dynamics assessments following the framework of Levermann et al. (2014). The details for each component's assessment can be found in Alhamid et al. (2022).

The sea level fingerprints for each sea level rise component are estimated differently depending on their corresponding sources. The sea level fingerprint for the steric sea level rise  $FG_{STR}$  is calculated using the ocean bottom pressure (OBP) change data from GCM, particularly from the Norwegian Earth System Model (i.e., NorESM1-M), as suggested by Richter et al. (2013). The OBP change is assumed as a static loading and then converted into sea level fingerprints using the sea level equation solver provided by Adhikari et al. (2016) and normalized with its associated global mean value. In terms of the glacier sea level fingerprint  $FG_{GLA}$  and ice sheet sea level fingerprint  $FG_{ICS}$ , the land–water mass change measurement from satellite gravimetry is used from the Gravity and Recovery Climate Experiment (GRACE) (Landerer and Swenson 2012). The land–water mass change data in the corresponding location of the glacier and ice sheet are translated into sea level fingerprints by employing the sea level equation solver provided by Adhikari et al. (2016) and normalized with the global mean value. Finally, the PDF of sea level rise components is multiplied with its corresponding sea level fingerprint using Monte Carlo simulation (MCS) to obtain each component's regional sea level rise PDF, as shown in Figure 3-6.

After obtaining each component's regional sea level rise, the regional total sea level rise cumulative distribution function (CDF) can be assessed based on the convolution of multiple probability distribution concepts. By incorporating the RCPs and assuming that each sea level rise component is perfectly correlated with each other, the regional total sea level rise CDF can be estimated according to Alhamid et al. (2022) based on convolution of multiple probability distributions.

Figure 3-7 shows the regional total SLR hazard and the estimated SLR hazard curve for the southern coast of Japan ( $33.5^{\circ}N$ ,  $136^{\circ}E$ ) in the year 2100 relative

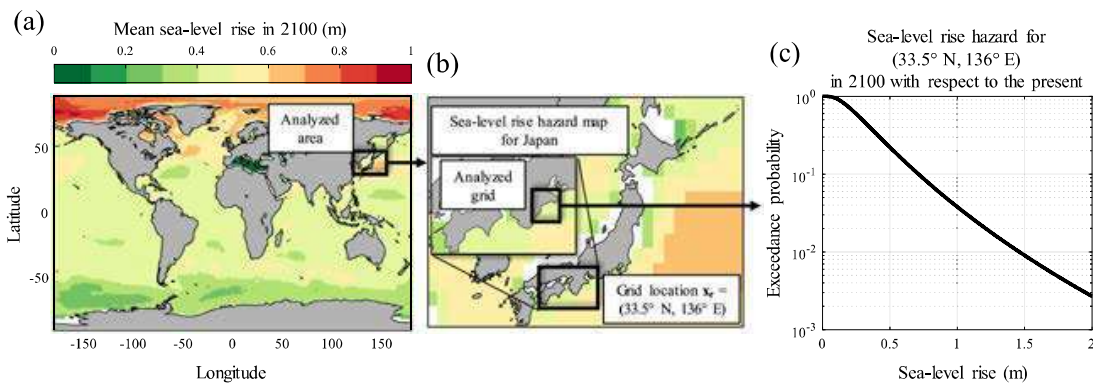


Figure 3-7. SLR hazard: (a) Regional total SLR hazard map, (b) SLR hazard map for Japan and its corresponding analyzed grid, (c) SLR hazard curve for ( $33.5^{\circ}N$ ,  $136^{\circ}E$ ), Japan, in 2100.

to the present (2021), where the mean SLR is predicted to vary between 0.5 and 0.7 m. In the United States, the SLR is predicted to be between 0.4 and 0.6 m. The SLR hazard provided in [Figure 3-7](#) can be utilized further to estimate the potential intensifications of coastal inundations, as discussed in the following subsections.

### 3.6.3.3 Effects of Tide, Storm Surge, and Tsunami Combined with Sea Level Rise on Coastal Inundation and Infrastructures

#### 3.6.3.3.1 Effect of Tides

As the sea level rise persists, daily maximum and minimum tides may reach higher levels. Thus, flood thresholds along the coast are more likely to be exceeded because of the impact of tides alone even without the influence of any extreme natural hazards (e.g., storm surges, tsunami). Hence, quantifying tidal contribution to coastal inundation is essential for achieving meaningful coastal risk assessments. However, frameworks for quantifying tide-only coastal inundation have varied between studies because of different approaches partitioning the observed sea levels into mean sea level, tides, and nontidal residual components ([Hague and Taylor 2021](#)). A recent study by [Hague and Taylor \(2021\)](#) has bridged the gap by introducing metrics to quantify coastal inundations caused by tides alone considering the effects of sea level rise. In their study, the still water level (SWL), as shown in [Figure 3-8](#), can be mathematically expressed as follows:

$$SWL = \delta_{MSL} + \delta_A + \delta_{NTR} = \delta_{MSL} + \delta_A + \delta_{SLR} + \delta_{SLV} \quad (3-26)$$

where

$\delta_{MSL}$  = Mean sea level (MSL),

$\delta_A$  = Harmonic astronomical tide,

$\delta_{NTR}$  = Nontidal residual,

$\delta_{SLR}$  = Long-term change in mean sea level (i.e., sea level rise), and

$\delta_{SLV}$  = Sea level variability.

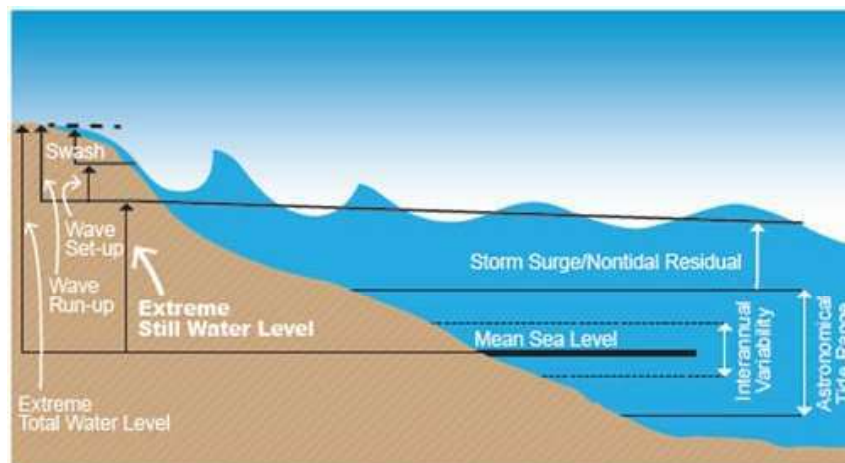


Figure 3-8. Components of the extreme total water and extreme still water measurements.

Source: [Hall et al. \(2016\)](#).

Based on the combination of these components, six tidal analyses that represent the tide-only inundation are presented in [Table 3-3](#). The approach used for the *recent trend* analysis is similar to that for the *full trend*. Both use a linear regression of the observational records obtained from the tide gauge, except that the full trend utilizes the observation data extensively up to a decadal scale. Both global reconstruction and local reconstruction analyses apply the annualized values of a sea level reconstruction, except that the local reconstruction considers the sea level spatial variability. The details of the methodology and data utilization for each tidal analysis combination, including assessing the most appropriate alternative using the physical coherence and scalability criteria, have been comprehensively described in [Hague and Taylor \(2021\)](#).

In the analyses demonstrated by [Hague and Taylor \(2021\)](#), it was found that each combination selected would generate substantially different tide-only inundation results. By analyzing the data from tide gauges in the southern hemisphere around Australia from 1996 to 2015, the low-impact coastal inundation (LICI) of combinations 1, 5, and 6 in [Table 3-3](#) produced values of 10.5, 23.2, and 16.5 days exceeding each threshold per year, respectively. Therefore, to ensure the safety of coastal defense, it is preferable to select the local reconstruction tidal analysis, in which the variability representing the local mean sea level (MSL) is considered. As discussed in the previous subsection, the probabilistic approach of sea level rise can be introduced in these analyses to promote better risk-informed decision-making to mitigate tide-only coastal inundation.

### 3.6.3.3.2 Storm Surges

Storm surges are generated because of vigorous wind intensity, which induces a vertical motion of oceanic waters. Similar to existing approaches for projecting sea level rise, there are two common ways to simulate storm surges: physics-based and empirical approaches. The physics-based approach typically employs shallow water equations (SWEs) to model the hydrodynamics process of storm surges. Conversely, the empirical or approximate approach involves constructing the relationship between the input and the output of the physics-based model or observation data within a spatial domain. The customary physics-based model to simulate the storm surges and the effects of sea level rise on storm surges are

*Table 3-3. Different Combinations for Tidal Analysis.*

	Combination 1	Combination 2	Combination 3	Combination 4	Combination 5	Combination 6
<i>Analysis definition</i>	<i>No trend</i>	<i>Full trend</i>	<i>Recent trend</i>	<i>Global reconstruction</i>	<i>Local reconstruction</i>	<i>Annual means</i>
Tidal analysis	$\delta_{MSL}, \delta_A$	$\delta_{MSL}, \delta_A, \delta_{SLR}$	$\delta_{MSL}, \delta_A, \delta_{SLR}$	$\delta_{MSL}, \delta_A, \delta_{SLR}$	$\delta_{MSL}, \delta_A, \delta_{SLR}, \delta_{SLV}$	$\delta_{MSL}, \delta_A, \delta_{SLR}, \delta_{SLV}$
Residuals	$\delta_{SLR}, \delta_{SLV}, \delta_{MSL}$	$\delta_{SLV}, \delta_{MSL}$	$\delta_{SLV}, \delta_{MSL}$	$\delta_{SLV}, \delta_{MSL}$	$\delta_{SLV}, \delta_{MSL}$	$\delta_{MSL}$

Source: [Hague and Taylor \(2021\)](#).

briefly introduced herein. A more detailed discussion can be found in [Bastidas-Arteaga and Stewart \(2019\)](#) and [Yang et al \(2020\)](#).

Two widely acknowledged models associated with the physics-based approach have been reported in the literature: the Advanced Three-Dimensional Circulation (ADCIRC) and Sea, Lakes and Overland Surge from Hurricanes (SLOSH) models. The ADCIRC model has increasingly been used because of its greater accuracy, which is attributable to the inclusions of several components, including wind stress, wave stress, tides, and river discharge ([Ceyhan et al. 2007](#)). Attention must be drawn to selecting the appropriate mesh to balance model accuracy and computational cost. The Simulating WAVes Nearshore (SWAN) software is regularly coupled together with ADCIRC to aid in solving the wave action balance equation to generate the wave parameters in the numerical domain ([de Lima et al. 2020](#)). In contrast to ADCIRC, the SLOSH model requires less numerical computational effort ([Bastidas and Stewart 2019](#)). However, a recent evaluation of SLOSH carried out by [Mayo and Lin \(2019\)](#) suggested that this model could underestimate the maximum storm surge height by up to 22%. It has thus been suggested that the observed maximum wind speeds should be applied to increase the model accuracy with the knowledge that this will also increase model uncertainty ([Mayo and Lin 2019](#)).

One example of the ADCIRC utilization for climate change studies has been demonstrated by [Marsooli et al. \(2019\)](#), where roughly 65,000 synthetic tropical cyclones were simulated under historical and future climate projections. A probabilistic projection of sea level rise performed by [Kopp et al. \(2014\)](#) was applied in the study, suggesting that changes to the tropical cyclone climatology and intensified sea level rise effects might cause the historical 100-year flood level to occur annually near the mid-Atlantic regions. Another study conducted by [Yin et al. \(2017\)](#) based on ADCIRC simulations suggested that 0.5 m of sea level rise would yield an additional storm surge wave height between 0.00 and 0.46 m under the simulated typhoon Hagupit. In addition, storm surge intensities are more sensitive to sea level rise in near-shore regions with spatially non-uniform and nonlinear characteristics. Hence, the nonlinear effects of sea level rise on storm surge assessment should be taken into consideration. In addition, considering the substantial uncertainties associated with storm surge analysis processes, a probabilistic analysis of storm surge based on surrogate modeling can be adopted ([Zhang et al. 2018](#)). Thus, a probabilistic framework of sea level rise, combined with the storm surge analysis, enables the development of an accurate hazard map that fully considers climate change effects and supports mitigation and adaptation strategies to promote resilient coastal communities.

#### 3.6.3.3.3 *Tsunami*

A rigorous tsunami propagation simulation under various sea level rise scenarios is required to integrate the effects of sea level rise on tsunami hazards. This is because the sea level rise will decrease the effects of bathymetry and modify the roughness coefficient, which are the two important factors in the tsunami

propagation simulation. In the study conducted by [Alhamid et al. \(2022\)](#), tsunami propagation analyses are carried out with several cases of earthquake fault movements (i.e., slip angle and displacement) and a predetermined number of sea level rise cases.

The tsunami hazard curve, representing the relationship between tsunami intensity measure and the exceedance probability, is estimated at a particular location for each sea level rise case, resulting in a tsunami hazard curve that is conditional on sea level rise. Because the simulations required to develop these conditional tsunami hazard curves are computationally demanding, several studies have suggested applying a response surface method with an appropriate experimental design, for example, [Alhamid et al. \(2022\)](#), [Kotani et al. \(2020\)](#). Accordingly, the inclusive tsunami hazard curve considering the effects of sea level rise can be estimated according to the total probability theorem as follows:

$$P(H(\mathbf{x}_r, t) > h) = \int_0^{\infty} \{P(H > h | \Psi = \psi(\mathbf{x}_r, t)) \cdot f_{\Psi}(\psi(\mathbf{x}_r, t))\} d\psi \quad (3-27)$$

where  $P(H(x_r, t) > h)$  is the tsunami hazard representing the probability of tsunami intensity  $H(x_r, t)$  exceeding a predefined value  $h$  considering the effects of sea level rise over the targeted ocean location  $x_r$  at time  $t$ ,  $P(H > h | \Psi = \psi(x_r, t))$  is the conditional tsunami hazard curve, given that the sea level rise intensity  $\Psi$  over  $x_r$  at time  $t$  equals  $\psi(x_r, t)$ , and  $f_{\Psi}(\psi(x_r, t))$  is the PDF of sea level rise. Because the sea level rise is a time-variant and site-specific variable, the tsunami intensity,  $H(x_r, t)$ , is also time-variant and site-specific.

[Figure 3-9a](#) illustrates the tsunami propagation results in Yokkaichi city of Mie Prefecture, Japan, subjected to an anticipated Nankai Trough earthquake with an assumed 0.6-m sea level rise. As shown in [Figure 3-9b](#), increases in tsunami hazards become significant as sea level rise increases. The final tsunami hazard curve considering sea level rise effects is obtained by convolving the conditional tsunami hazard curve in [Figure 3-9b](#) with the sea level rise hazard in [Figure 3-9c](#) [Equation (3-11)]. As shown in [Figure 3-9c](#), the tsunami hazard curve

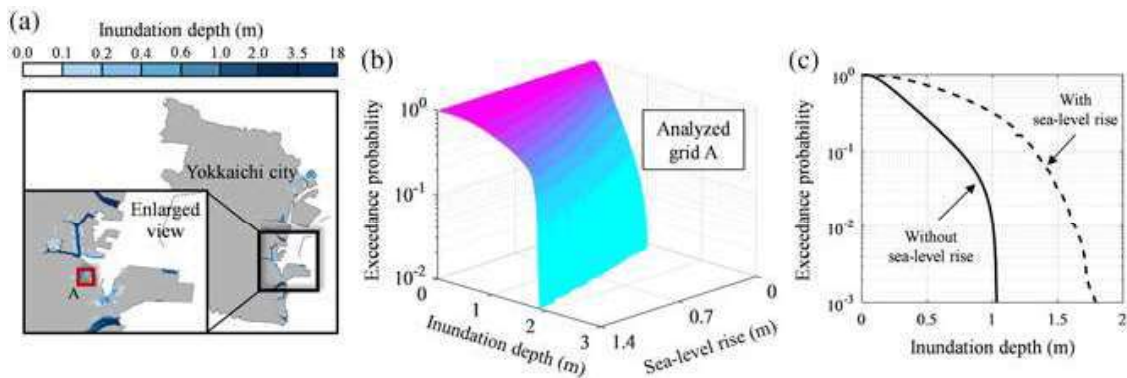


*Figure 3-9. (a) Inundation map of Yokkaichi city, (b) conditional tsunami hazard given sea level rise, (c) tsunami hazard considering the effects of sea level rise.*

Yokkaichi city is amplified by a factor of roughly 1.5 (Alhamid et al. 2022, Li et al. 2018). Hence, the effects of sea level rise should be systematically considered in the tsunami hazard assessment to avoid underestimating the structural risk of failure.

### **3.6.4 Wind Hazard**

#### *3.6.4.1 Introduction*

This section discusses the effects of an increasing sea surface and global temperature on the basic, hurricane, and tornadic wind speeds used by structural engineers for the design of structures subject to wind hazard in the United States. Changes in the design wind speed can produce significant changes in the design loads for both structural and nonstructural components of buildings and other structures, as the wind-induced loads are proportional to the square of the wind speed. Thus, accurate projections of design wind speeds are necessary to ensure that newly designed structures satisfy their reliability requirements.

#### *3.6.4.2 Current Methodology for Basic Wind Speed Maps*

The basic design wind speeds are determined from Figure 26.5-1 in ASCE 7-22 (ASCE 2022b). To be consistent with the target reliabilities in the first row of Table 1.3-1 in ASCE 7-22 (ASCE 2022b), the following return periods in the wind maps for each risk are used: Risk Category I, 300 years; Risk Category II, 700 years; Risk Category III, 1,700 years; Risk Category IV, 3,000 years. The wind speeds correspond to 3 s gust wind speeds at 33 ft (10 m) above ground for Exposure Category C.

The wind maps in ASCE 7-22 use contours to better reflect regional variations, whereas point values are provided to aid the interpolation. Location-specific basic wind speeds can be determined from the ASCE Wind Design Geodatabase using the ASCE 7 Hazard Tool Online (ASCE 2022a), which provides wind speeds to the nearest mile per hour on the basis of a location defined using either latitude/longitude or a specific address. The winds are assumed to be from any horizontal direction. The basic wind speed must be increased if records or experience indicate that the wind speeds are higher than those shown in Figure 26.5-1 of ASCE 7-22 (ASCE 2022b).

#### *3.6.4.3 Effects of Climate Change on Basic Wind Speeds*

Numerous studies have demonstrated a direct relationship between climate change and the intensification of wind speeds from hurricanes in the Atlantic region (e.g., Elsner 2006). Emanuel (2005) showed that hurricane destructiveness has increased drastically since 1970 because of an increase in the sea surface temperature (SST). He also concluded that for every 1 degree Celsius increase in SST, the peak wind speed of hurricanes is expected to increase by about 5%. Subsequently, Emanuel et al. (2008, 2013) used downscaling methods to simulate the effect of climate change on hurricane intensities, projecting increased tropical cyclone activity over the 21st century. The hurricane winds and damage potential associated with this increase in tropical cyclone intensities poses a threat

to exposed populations in coastal areas, as shown by studies such as those by [Rappaport \(2000, 2014\)](#). More recently, hurricane path simulation has been used to predict future hurricane wind speeds in a warmer climate with a focus on the basic wind speeds used for the design of structures and infrastructure systems. [Mudd et al. \(2014\)](#) developed a framework for assessing climate change effects on hurricane wind hazard for the US East Coast by modeling hurricane paths and decay. They combined Georgiou's hurricane wind speed model ([Georgiou et al. 1983](#)), an empirical hurricane track model ([Vickery et al. 2000](#)), and a hurricane genesis model depending on the SST changes predicted by different climate scenarios ([Stocker et al. 2013](#)). Considering the worst-case scenario, they found that, to achieve the same target safety and expected performance levels assumed by existing design standards in the year 2100, the design wind speeds given by *ASCE 7-10* ([ASCE 2010](#)) for the US Northeast region need to be increased by up to 15 m/s for structures of Risk Categories I and II and up to 30 m/s for structures of Risk Categories III and IV ([Mudd et al. 2014](#)).

[Cui and Caracoglia \(2016\)](#) developed a framework for estimating the lifetime costs of tall buildings subject to hurricane-induced damage under different climate change scenarios by means of a statistical hurricane track path model. This framework is based on Weibull distributions for the maxima of the annual wind speed with nonstationary parameters. [Lee and Ellingwood \(2017\)](#) developed a framework for risk assessment of infrastructures with long expected service lives accounting for the effects of climate change by incorporating SST rise in the model by [Vickery et al. \(2000\)](#). More recently, [Pant and Cha \(2018\)](#) accounted for the effects of climate change on hurricane wind-induced damage and losses for residential buildings in the Miami-Dade County, Florida. They used Georgiou's model ([Georgiou et al. 1983](#)), in conjunction with a transition matrix, to simulate the hurricane track, and developed relationships between average yearly SST and hurricane parameters used for hurricane genesis. They found that, for each 1°C SST increase, the 3 s gust wind speed for a 700-year return period is expected to increase by about 6.7 to 8.9 m/s for the county, with significant effects on the accumulated hurricane-induced losses. [Esmaili and Barbato \(2021\)](#) developed a model to predict the effects of climate change on hurricane wind hazard for locations along the US Gulf and Atlantic Coasts. The SST projections for future years were taken from the fifth assessment report (AR5) from the Intergovernmental Panel on Climate Change (IPCC) ([Stocker et al. 2013](#)). The simulation results indicated that different climate change scenarios could produce significant changes in the design wind speeds in future decades. In particular, the results of their study showed that, by the year 2060, the design wind speeds corresponding to the *ASCE 7-22* different mean return intervals (i.e., 300, 700, 1,700, and 3,000 years for Risk Categories I, II, III, and IV, respectively) are expected to increase on average between 14% and 26%, with a corresponding average increase in the design wind-induced loads between 30% and 59%. Other studies ([Emanuel 2005](#), [Emanuel et al. 2010](#), [Lee et al. 2018](#), [Xu et al. 2020](#)) have suggested that climate variables other than the STT may also play an important role in wind speed changes.

Most of the existing literature in civil engineering focuses on assessing the climate change effects on hurricane-induced wind speeds. Climate research has shown that the impact of climate change on noncyclone wind speeds may be significant (Chapter 2). In terms of the mean wind speed, IPCC reports find that under the select emission scenarios, lower noncyclone wind speeds would occur over western and eastern North America. Most simulation reports, including IPCC/AR6 (IPCC 2022), focus on mean wind speed; projections of extreme wind speed are very scarce or *ad hoc*. Some researchers have suggested that downloaded climate models may be necessary to reveal extreme wind speeds for nonhurricane surface winds. Additional investigation is required to assess the climate change effects on nonhurricane wind speeds on civil structures, including a consideration of improved wind pressure profiles, wind field modeling (Kepert and Wang 2001), and along-height wind profiles (Vickery et al. 2010).

#### 3.6.4.4 Effects of Climate Change on Tornado Wind Speeds

Studies in the literature have investigated possible changes in frequency and/or intensity of tornadoes as a result of climate change. However, a lack of consensus still persists (Brooks 2013, Brooks et al. 2014) and thus more comprehensive data and studies are needed to determine whether there is an impact from climate change on tornado frequency and/or intensity.

#### 3.6.4.5 Recommended Climate Analysis Methods for Different Structures

ASCE 7-22 (ASCE 2022b) for minimum design loads for buildings and other structures in the United States does not account for climate change effects on wind loads. Steenbergen et al. (2009) identified three different strategies to update building codes and standards: (1) changing the standards only after full evidence of extreme events driven by climate change is gathered; (2) changing the building codes to ensure safe design for the next 50 years and periodically updating them as new information is collected; or (3) changing the codes by accounting for nonstationarity through a climate change factor that is a function of the year of construction. The ASCE Report on adapting infrastructure to climate change (ASCE 2015a) recommends that civil engineers “should use low-regret, adaptive strategies, such as the Observational Method” to design structures and infrastructure that are resilient to future weather extremes driven by climate change. Engineers should also strive to achieve a better understanding of the uncertainties and probabilities involved in the characterization of such extremes by collaborating with climate, weather, social, and life scientists. The same report highlights how ASCE 7 (as well as other standards) set minimum design criteria; thus, engineers can recommend more conservative designs when warranted. ASCE MOP 140 (ASCE 2018) proposes additional methods to adapt and manage risk in infrastructures beyond the Observational Method. Although ASCE MOP 140 focuses mostly on flood loads, the methodological approach to the adaptive design presented in Tables 7-3 and 7-4 of MOP 140 could be easily adapted to wind loads (and other climatic loads). In particular, Table 7-3 of MOP 140 presents a

Table 3-4. Suggested Modification of Table 7-3 from ASCE MOP 140 for design wind load calculations.

Risk category	Design life <30 years	Design life 30–75 years	Design life >75 years
I	Climate analysis level 1	Climate analysis level 1	—
II	—	Climate analysis level 2	Climate analysis level 3
III	—	Climate analysis level 3	Climate analysis level 4
IV	—	Climate analysis level 4	Climate analysis level 4

Source: ASCE (2018).

matrix of climate analysis levels for different risk category structures as a function of their design life. A suggested modification of this approach is presented in Table 3-4, with the additional recommendation that results obtained for design life length lower than 50 years should be used only if they provide a design that is more conservative than current ASCE 7 wind loads based on the stationarity assumption.

As defined in ASCE MOP 140 (ASCE 2018), the four levels of climate analysis correspond to (1) use of published values of weather and climate extremes based on historical observations, (2) use of published values of weather and climate extremes based on historical observations and climate projections, (3) use of published values of weather and climate extremes based on historical observations and climate projections, while accounting for the sensitivity to uncertainty in the projections, and (4) independent, transparent, and rigorous analysis of risk posed by future weather and climate extremes based on historical observations and climate projections.

### 3.6.5 Snow Loads

#### 3.6.5.1 Introduction

Snow load is one of the climatic loads specified in structural design codes. It is important for designing structures in regions experiencing long winter seasons and heavy snowfalls. Failures owing to snow load have been documented in Holicky and Sykora (2009) and Geis et al. (2012). The actual snow load on a roof depends on the process of the snow and rain-on-snow accumulation as well as melting, evaporation, and wind-induced snowdrift (Ellingwood and O'Rourke 1985). However, measurements of the roof snow load are rarely available, and the ground snow load is used instead as a proxy for its evaluation by including a ground-to-roof snow load transformation factor (O'Rourke et al. 1982, Bartlett et al. 2003, Bean et al. 2021). Therefore, the ground snow load is specified in

structural design codes for evaluating the design roof snow load. The specified ground snow loads in ASCE-7-22 (ASCE 2022b) as well as in the *National Building Code of Canada* (NBCC 2015, NBCC 2020) consider that the roof snow loads consist of a snow component and a rain component. ASCE-7-22 has also shifted away from uniform hazard basis to uniform risk (or uniform reliability) basis for assigning the snow load (Section 3.4). This shift is currently contemplated by NBCC for its future edition as well (Hong et al. 2021).

The analysis of ground snow load is further complicated by the fact that only the ground snow depth rather than the ground snow load, or snow water equivalent (SWE), is routinely measured in most meteorological stations. The lack of SWE measurements is attributed to the effort and resources involved in these measurements that are much greater than those involved in measuring ground snow depth (Sturm et al. 2010). Moreover, the effect of future climate change on snow load is not taken into account in the current structural design codes. Such effects could be incorporated into the future design snow load in NBCC (Hong et al. 2021) by taking into account nonstationary climate projection data for a selected global mean temperature or Representative Concentration Pathway (RCP) (IPCC 2014, 2022).

### 3.6.5.2 Site-Dependent Extreme Snow Statistics and Snow Hazard Mapping

Given historical snow depth data and snow water equivalent records, the historical annual maximum ground snow depth record,  $S_{DA}$ , or the annual maximum snow load,  $S_{LA}$ , at a site, can be extracted and an extreme-value analysis (Jones and Daly 2016, Bean et al. 2021) of  $S_{DA}$  or  $S_{LA}$  can be conducted. Commonly used probability distributions to model these annual extremes include the Gumbel distribution, the Generalized Extreme Value (GEV) distribution, and the lognormal distribution. It was found that the lognormal distribution is the preferred distribution model for  $S_{LA}$  (Ellingwood and Redfield 1983, Lee and Rosowsky 2005) for many sites in the United States, but the use of Gumbel distribution for  $S_{DA}$  is favored by design code writers in several countries, including Canada (Newark et al. 1989, Hong and Ye 2014), Western Europe, and China (Mo et al. 2016). The use of the GEV distribution for  $S_{LA}$  was adopted by Bean et al. (2021).

Because the historical ground snow depth record may be short (i.e., less than 20 years), rather than carrying out a site-specific analysis for  $S_{DA}$ , the analysis must be based on regional models (Mo et al. 2016, Bean et al. 2021). This is an attempt to reduce the statistical uncertainty in estimating the  $T$ -year return period values of  $S_{DA}$  or  $S_{LA}$ , denoted as  $s_{DA-T}$  and  $s_{LA-T}$ .

### 3.6.5.3 Relationship between Extreme Ground Snow Load and Ground Snow Depth

The snow load factor  $s_{LA-T}$  (kPa) may be approximated by  $\rho_{SB}gs_{DA-T}$  where  $s_{DA-T}$  is in m,  $g$  is the gravitational acceleration, and  $\rho_{SB}$  ( $\text{kg/m}^3$ ) is the average seasonal snowpack bulk density. However, this omits the potential dependency of  $\rho_{SB}$  on ground snow depth. This limitation can be overcome if SWE data are available.

An empirical relationship between  $s_{LA-T}$  and  $s_{DA-T}$  was developed by [Tobiasson and Greatorex \(1996\)](#) by using data from the first-order stations operated by the National Weather Service in the United States. This relationship was used in ASCE 7-16 ([ASCE 2017](#)). Other empirical nonlinear relationships for such purposes include those reported by [Sack and Sheikh-Taheri \(1986\)](#), [Sack \(2015\)](#), [Debock et al. \(2017\)](#), [Liel et al. \(2017\)](#), and [Bean et al. \(2021\)](#).

#### 3.6.5.4 Roof Snow Load Estimation and Design Snow Load

A practical and well-known empirical relationship for the ground-to-roof snow load transformation,  $C_{gr}$ , was given by [O'Rourke et al. \(1982\)](#) [see also [Ellingwood and O'Rourke \(1985\)](#)]:

$$C_{gr} = 0.47E_eT_e\varepsilon \quad (3-28)$$

where  $E_e$  is a wind exposure factor ranging from 0.9 to 1.3;  $T_e$  is a thermal characteristic factor ranging from 1.0 to 1.2; and  $\varepsilon$  is the error term, which has a lognormal distribution with a mean value of 1.0 and a coefficient of variation of 0.44. This results in  $C_{gr}$  that ranges from  $0.43\varepsilon$  to  $0.73\varepsilon$  with an average of  $0.58\varepsilon$ . By considering this factor, the annual maximum roof snow load equals  $C_{gr}S_{LA}$ . If a specified value of  $C_{gr}$ ,  $c_{gr-N}$ , is implemented in a structural design code [such as in the NBCC ([2015](#)), where a value of 0.8 is recommended],  $c_{gr-N}$  needs to be included in the reliability-based code calibration exercise. The recommended (snow component of) snow load for a flat roof,  $s_{fR}$ , in ASCE-7-22 ([ASCE 2021b](#)) is given by

$$s_{fR} = 0.7C_eC_t s_{LA-T} \quad (3-29)$$

where a snow load factor of 1.0 is to be used,  $C_e$  is the exposure factor,  $C_t$  is the thermal factor, and  $s_{LA-T}$  is determined on the basis of the uniform reliability approach and is available from the ASCE 7 Hazard Tool Online ([ASCE 2022a](#)) for structures in different risk categories. Compared to previous versions of ASCE 7, the use of the uniform reliability approach to estimate  $s_{LA-T}$  or the reliability-targeted ground snow loads enhances reliability consistency if the uncertainty in the snow load (e.g., coefficient of variation) is geographically varying.

Besides the snow component of the snow load, there is a rain-on-snow surcharge load recommended in ASCE 7-22, which is applied only to the sloped roof (balanced) load case and need not be used in combination with drift, sliding, unbalanced, minimum, or partial loads. The rationale and evaluation of the parameters for the drift snow load were presented by [O'Rourke et al. \(2020\)](#).

Load combination factors are implemented in structural design codes to evaluate the snow load acting simultaneously with other load types, where the calibration of the load combination factors takes into account the fact that the extreme snow load is unlikely to occur simultaneously with extreme live, wind, or earthquake loads (Section 3.6.8).

### 3.6.5.5 Effect of Climate Change on Snow Load

The investigation of the effects of climate change effects on snow load has been reported in, among others, [Jones and Daly \(2016\)](#), [Jeong and Sushama \(2018\)](#), [Croce et al. \(2018\)](#), [Cannon et al. \(2020\)](#), [Hong et al. \(2022\)](#), and [Tye et al \(2021\)](#) (see also Chapter 2). In general, a warmer climate can result in increased precipitation (in liquid or solid). This leads to a time-dependent (nonstationary) and region-dependent increase or decrease of snow load and rain-on-snow surcharge loads. The study done by [Jones and Daly \(2016\)](#) was based on climate projection data for RCP equal to 4.5 and 8.5 available at the time. Their results for Alaska indicated that the effect of climate change on the snow load  $s_{LA-50}$  is not very significant, although SWE increases in the north of Alaska and decreases in the south of Alaska. To take into account the nonstationary change in the extreme snow load for developing the future edition of NBCC, a reliability-based design code calibration was carried out ([Hong et al. 2022](#)) on the basis of projected climate change effects on the statistics of the time-varying extreme snow loads ([Cannon et al. 2020](#)). Their results indicated that such nonstationarities can be coped with by including an additional scaling factor for climate change effect,  $\eta_s$ , which is to be applied to the calculated design snow load without considering climate change effects. [Cannon et al \(2020\)](#) observed that this factor changes from region to region within Canada. Their calibration results indicated that  $\eta_s = 1.0$  in most regions; in a region termed *North*,  $\eta_s = 1.05$  if RCP of 8.5 was considered (implying a global mean temperature increase relative to the 1986 to 2016 reference period by about 2 °C in 2059).

## 3.6.6 Ice Loads and Atmospheric Icing

### 3.6.6.1 Introduction

Freezing rain is made entirely of liquid droplets and freezes on contact with surfaces. Ice accretion is a hazard to the surface transportation system, aviation, structures, and infrastructure systems. The consideration of ice load is important, especially for transmission line systems and communication towers in cold climate regions, because extreme ice loads can collapse tower line systems and lattice structures ([Mulherin 1998](#), [Milton and Bourque 1999](#)). Ice loads are caused by ice accretion, which can be classified as glaze ice (i.e., icing caused by freezing rain) and rime ice (i.e., in-cloud icing). Often, only the glaze ice is considered in structural design codes (e.g., CAN/CSA C22.3, ([CSA 2006](#)), ASCE 7-16, ([ASCE 2017](#))). The consideration of rime ice for structural design is given in ISO 12494 ([ISO 2017](#)). Ice accretion on structural elements increases the gravity load, changes the dynamic characteristics of the structure, alters the aerodynamics of the structure, and affects the structural responses. The combination of the ice accretion load and wind load can govern the design of electrical transmission lines and cable-supported bridges ([McComber et al. 1983](#), [Sinh et al. 2016](#), [Ma et al. 2020](#)). Ice accretion affects the aerodynamics of bridge cables as well.

Analyses of the frequency of the temporal and spatial variation of freezing rain using data from surface observations across Canada and the United States were presented by [Changnon and Karl \(2003\)](#) and [Cortinas et al. \(2004\)](#). A general formulation to evaluate ice accretion was presented by [Makkonen \(2000\)](#). Ice loads in ASCE Manual 74 ([ASCE 2015b](#)) were evaluated using the CRREL simple model (i.e., the Cold Regions Research and Engineering Laboratory model) ([Jones 1998](#), [Jones et al. 2002](#)). Another simple model for evaluating ice accretion is given by [Chaine and Skeates \(1974\)](#) and [Chaine and Castonguay \(1974\)](#); this model is used in Canada for evaluating the ice load for structural design.

Although current structural design codes do not include the effects of climate change to assign the ice load, projected changes to extreme freezing precipitation and ice load are presented in [Jeong et al. \(2019\)](#) and [Cannon et al. \(2020\)](#) (See also [Tropea and Stewart 2021](#), [McCray et al. 2022](#), [Marinier et al. 2023](#)).

### 3.6.6.2 Modeling Ice Accretion

The CRREL simple model presumes that the collision efficiency is 100%, the rainwater impinging on the cylinder sticks to and freezes on the cylinder, and the ice accretion is uniform around the circumference of the cylinder. The uniform radial ice thickness on a circular cylinder,  $\Delta R$ , for an icing event, which is independent of the radius of the cylinder or rod, is given by

$$\Delta R = \frac{1}{\rho_i \pi} \sum_{j=1}^N \left[ (P_j \rho_w)^2 + (3.6 V_j W_j)^2 \right]^{1/2} \text{ (mm)} \quad (3-30)$$

where

$P_j$  (mm/h) = Precipitation rate during the  $j$ -th hour,

$V_j$  (m/s) = Wind velocity during the  $j$ -th hours,

$W_j = 0.067 P_j^{0.846}$  (g/m<sup>3</sup>) = Liquid water content during the  $j$ -th hour, and

$\rho_i = 0.9$  (g/cm<sup>3</sup>),

$\rho_w = 1.0$  (g/cm<sup>3</sup>), and

$N$  = Duration of the storm in hours.

The calculated values  $(\rho_w/\rho_i)T_h$  and  $(1/\rho_i)T_v$  represent the ice accretion thickness on a horizontal and a vertical surface, respectively, where

$$(T_h, T_v) = \left( \sum_{j=1}^N P_j, \sum_{j=1}^N (3.6 V_j W_j) \right) \text{ (mm, mm)} \quad (3-31)$$

The simpler ice accretion model ([Chaine and Skeates 1974](#), [Chaine and Castonguay 1974](#)) used in Canadian practice leads to a more conservative prediction of ice accretion thickness. The calculation of ice accretion requires hourly precipitation data, which may not be available and needs to be estimated from daily precipitation data. The prorating of accumulation precipitation for each hour can be carried out based on the weights that are given in [Jones et al. \(2002\)](#).

### 3.6.6.3 Statistics of Extreme Ice Accretion and Concurrent Wind Velocity

An extreme-value analysis of the ice accretion thickness can be carried out by using the extracted block maximum (e.g., annual maximum). In such a case, the Gumbel distribution, GEV distribution, or lognormal distribution can be used. The peak-over-threshold approach with the generalized Pareto distribution for the event-based extreme ice accretion analysis can also be used to estimate the  $T$ -year return period of ice accretion amount (Jones et al. 2002).

Ice accretion and wind can act simultaneously on a structure such as transmission towers or bridge cables. The ice accreted on a structural element can last longer than a freezing rainstorm. The largest wind speed experienced by the ice-coated structural component will be greater than that observed during the freezing rain event. This wind speed is typically moderate (Jones et al. 2002), and an (equivalent) concurrent wind speed,  $v_{EC-T}$  can be calculated based on the  $T$ -year return period value of the annual maximum wind-on-ice load  $F, f_T$ , and the  $T$ -year return period of the annual maximum ice thickness,  $a_{A-T}$  resulting in

$$v_{EC-T} = \sqrt{\frac{2f_T}{\rho_a C_D D} \frac{1}{(1 + 2a_{A-T}/D)}} \quad (3-32)$$

where  $\rho_a$  is the density of air,  $D = 25$  mm is the diameter of the bare wire, and  $C_D$  is the drag coefficient. The ratio of the  $v_{EC-50}$  to the 50-year annual maximum wind speed varies from site to site. A typical value of 0.8 may be considered.

### 3.6.6.4 Effect of Climate Change on Ice Accretion

In general, a warmer climate can result in increased precipitation. This leads to a time-dependent and region-dependent increase or decrease in ice accretion, depending on the temperature. However, investigations of climate change effects on the annual maximum of ice accretion thickness are not widely available in the literature. Based on climate projection results for Canada reported by Cannon et al. (2020), it was concluded that the mean of the annual maximum of ice accretion thickness increases for Prairies and Northern regions and decreases for the remaining regions in Canada. Also, their results indicate that the increase and decrease of the coefficient of variation are regionally dependent. Based on their results and following a reliability-based structural design code calibration, it was concluded (Hong et al. 2022) that, similar to the treatment of design snow load, an additional scaling factor for climate change effect on the ice accretion load,  $\eta_I$ , should be considered for structural design, where  $\eta_I$  is applied to the calculated design ice load without considering climate change effects. For RCP equal to 6.0 (i.e., a global mean temperature increase relative to 1986 to 2016 reference period by about 2 °C in 2087 (Cannon et al. 2020, Hong et al. 2021), the calibrated  $\eta_I$  equals 1.03 for British Columbia & Quebec regions, 1.08 for Prairies and Northern regions, and 1.0 for Ontario and Atlantic regions.

### 3.6.7 Rain Loads

Rain loads are an important consideration for designing large flat roof structures, so designated if their slopes are less than ¼ in./foot (approximately 20.8 mm/m, or 1.2 degrees). The first line of defense against the accumulation of rainwater on roofs is to provide sufficient roof slope to facilitate drainage. Without proper drainage, water may accumulate on the roof causing a progressively increasing deflection – a phenomenon known as ponding – which can lead to an instability failure of the roof structure if it does not have sufficient stiffness. Ponding instability is especially dangerous in relatively flexible light-frame roof systems typical in modern building construction, where the weight of the ponded water is relatively high relative to the roof dead load weight. If the roof is flat, a structural analysis is required to check that the stiffness of the roof is sufficient to preclude ponding instability. Roofs with a slope in excess of 1/4 in./foot (1.2 degrees) usually are not susceptible to ponding instability from rainwater unless the drains become blocked and ponds can form.

Assurance of proper roof drainage is a combined structural, architectural, and plumbing issue. Primary and secondary drainage systems are typically provided to minimize the likelihood that excessive rainwater will accumulate. An adequate secondary (overflow) drainage system, which is used to limit the depth of water on the roof in the event of clogging of the primary drains, must be designed for flow associated with intense, short-duration storms. In addition, an exceptionally severe storm in excess of the 100-year return period storm may produce a deluge of such intensity and duration that even properly designed and unblocked primary drainage systems may be temporarily overloaded. In that case, the secondary drainage system, with separate drain lines, may be necessary to accept the overflow.

The rain load,  $R$ , in ASCE 7-22 is

$$R = 5.2(d_s + d_h + d_p); R \text{ in psf; } d_s, d_h \text{ and } d_p \text{ in inches} \quad (3-33a)$$

$$R = 0.0098(d_s + d_h + d_p); R \text{ in kPa; } d_s, d_h \text{ and } d_p \text{ in mm} \quad (3-33b)$$

where

$d_s$  = Static head equal to the depth of water on the undeflected roof up to the inlet of the secondary drainage system when the primary drainage system is blocked, in inches (mm),

$d_h$  = Hydraulic head equal to the depth of water on the undeflected roof above the inlet of the secondary drainage system at its design flow (i.e., the hydraulic head), in inches (mm), and  $d_p$  = Ponding head equal to the depth of water owing to deflections of the roof subjected to unfactored rain and dead loads.

The rain load is based on the assumption that the primary drainage system is blocked and that the hydraulic head ( $d_h$ ) is determined from a flow rate corresponding to a rainfall intensity equal to or greater than a 15-min duration storm with a

return period based on risk category (100, 200, and 500 years, respectively, for Risk Categories II, III, and IV buildings). The definition of rain load was changed in ASCE 7-22 (ASCE 2022b) to include an additional contribution owing to ponding, reflected in  $d_p$ , which was intended to eliminate the need for a separate check of ponding instability. Although it has been customary to design the primary drainage systems in Risk Category II buildings for a rainfall intensity equal to or greater than the 60-min duration/100-year return period storm, this requirement was eliminated in ASCE 7-22. However, the use of a 60-min duration/100-year return period rainfall event for the design of the primary drainage system and a 15 min duration/100-year return period rainfall event for the secondary drainage system (assuming that the primary drainage system is completely blocked) is consistent with the *NFPA 5000 Building Construction and Safety Code* (NFPA 2021), whereas the *International Plumbing Code* (ICC 2021b) requires both the primary and the secondary drainage to be designed for the 60-min/100-year event. The National Weather Service provides rainfall depth and intensity data in inches per hour for durations that range from 5 min to 60 days, with mean recurrence intervals that range from 2 to 1,000 year (NOAA 2021).

The prospect of rain during the winter months in the northern tier of states is taken into account through a rain-on-snow surcharge of 8 psf (0.38 kPa) on all roofs with slopes (in degrees) less than  $W/50$ , where  $W$  is the eave-to-ridge distance in ft (in SI:  $W/15.2$  with  $W$  in m), subject to the limitations of Section 7.3.3 of ASCE 7-22.

Climate change will cause these intensities to be changed to reflect the nonstationary nature of annual extreme rainfall events, but the fundamental design process is not expected to change. The emerging collaboration between ASCE and NOAA will allow rainfall to be included in the ASCE 7 Hazard Tool Online (ASCE 2022a).

### 3.6.8 Load Combinations

As noted in Section 3.4, building codes and standards in the United States have adopted the probability-based limit states design philosophy (Ellingwood 2000), which is implemented in a design criteria format known as Load and Resistance Factor Design (LRFD). LRFD is founded on the premise that the measure of structural performance in the face of uncertainties in strength and loads is the probability of not exceeding stipulated limit states (Ellingwood et al. 1982, Ellingwood 2000), and is implemented through the fundamental design requirement expressed by Equation (3-3), which states that the *required strength*, defined by the demand on the structural member, component, or system placed by a combination of actions owing to design loads, not exceed the *design strength* representing the capacity to resist those design loads. The design strength is determined by the various material specification committees, whereas the load combinations for all materials are determined by ASCE 7-22. The resistance and load factors were selected to be consistent with target reliability indexes or annual probabilities of failure (mean annual frequencies of failure), which now are specified in Table 1.3-1 of ASCE 7-22 (Table 3-1).

With the exception of permanent (dead) loads, most loads vary stochastically in time. If the loads are approximately statistically independent, the maximum value of the *combined* loads during a typical service life (50 years in ASCE 7-22) occurs when one of the loads reaches its maximum value (*principal action*), whereas other loads have their instantaneous or arbitrary-point-in-time values (*companion actions*) (Turkstra and Madsen 1980). The following basic load combinations for the design of new structures are provided in Section 2.3 of ASCE 7-22:

$$\begin{aligned}
 1: & 1.4D \\
 2: & 1.2D + 1.6L + (0.5L_r \text{ or } 0.3S \text{ or } 0.5R) \\
 3: & 1.2D + (1.6L_r \text{ or } 1.0S \text{ or } 1.6R) + (L \text{ or } 0.5W) \\
 4a: & 1.2D + 1.0W + 1.0L + (0.5L_r \text{ or } 0.3S \text{ or } 0.5R) \\
 4b: & 1.2D + 1.0W + 2.0F_a + 1.0L + (0.5L_r \text{ or } 0.3S \text{ or } 0.5R) \\
 5a: & 0.9D + 1.0W \\
 5b: & 0.9D + 1.0W + 2.0F_a
 \end{aligned} \tag{3-34}$$

Additional combinations in ASCE 7-22 address tornado loads,  $W_T$ , lateral earth pressures,  $H$ , temperature effects,  $T$ , weight of ice,  $D_i$ , and wind-on-ice,  $W_p$ , but are ignored in Equation (3.34) for simplicity.

Loads  $D$ ,  $L$ , and  $L_r$  are gravity dead, live, and roof live loads, with nominal values provided in Chapters 3 and 4 of ASCE 7-22. Loads  $S$ ,  $R$ ,  $W$ , and  $F_a$  are nominal snow, rain, wind, and flood loads, each stipulated in separate chapters in ASCE 7-22, with nominal loads currently set in terms of hazard return periods. The load factor on  $L$  in combinations 3 and 4 is permitted to equal 0.5 when the basic live load  $L_0$  is less than, or equal to, 100 psf (4.78 kN/m<sup>2</sup>), with the exception of garages or areas occupied as places of public assembly. Note that the load combinations involving all the aforementioned loads, with the exception of  $D$ ,  $L$ , and  $L_r$ , are climate-dependent. The bridge design specifications (AASHTO 2020) include similar provisions that consider the combination of several climatic parameters, such as water pressure, wind loads on structures, wind loads on vehicles, and ice loads, formatted in equations similar to Equation (3-34) that account for the possibility that such loads may also occur simultaneously with live loads or earthquake loads in addition to dead loads.

The relative importance of the loads in the design load combination, measured by ratios  $L/D$ ,  $W/D$ ,  $S/D$ , etc., depend on the construction technology employed, typically varying from low values for reinforced concrete and masonry structures, which are dead load–dominant, to high values for light-frame wood and steel structures. To make the load combinations equally applicable to all common construction technologies, the design loads (*each equal to the product of a load factor and a nominal load*) were determined to achieve essentially the same target reliability, regardless of load ratio (Ellingwood et al. 1982). As noted previously, there is no evidence after four decades in use that the target reliabilities in Table 3-1 are

inadequate. Therefore, the *nominal loads* and *strengths* in Equations (3-3), (3-4), and (3-34) for use in a changing climate must be selected to achieve essentially the same target reliabilities. Because the current climate parameters were determined under the assumptions that the design strength is time-invariant and the annual extreme loads are stationary, it is possible that the manner in which the design loads are specified may have to be modified to achieve these reliability targets. However, it is not difficult to show that if the conditional failure rate increases linearly by 20% over 50 years, the reliability index for a 50-year service period decreases from 3.0 to approximately 2.97, which is within the scatter provided by current code provisions and will be self-adjusting if the code revision cycle remains on the order of 6 years.

### 3.7 CLIMATE CHANGE IMPACTS ON GEOTECHNICAL SYSTEMS

Assessing climate change impacts on geotechnical systems requires quantifying the impact of climate change on both factors governing the engineering performance and integrity of geotechnical infrastructure: *supplies* (e.g., shear strength and compressibility of soil) and *demands* (e.g., loads imposed on the structure owing to climate extremes). Such quantitative studies can assist us to properly evaluate the failure risk and resilience of current earth structures and safely design future earth structures and foundations for a changing climate.

#### 3.7.1 Impacts on Soil and Earthen Structures

New patterns of extreme weather events exacerbated by climate change affect the short- and long-term performance of soil and earthen structures. These changes may cause soil and earthen structures to weaken through strength reduction, drying, soil desiccation cracking, shrinkage, microbial oxidation of soil organic matter, fluctuation in the groundwater table, surface erosion, and highly dynamic pore pressure changes (Vahedifard et al. 2018). A summary of major climate change features and their effects on existing infrastructure and natural slopes can be found in Table 3-5. A more detailed discussion is provided in the following paragraphs.

An increase in the total precipitation will increase the level of saturation within the unsaturated zone and may decrease the depth of the water table. Resulting increases in pore pressure may decrease suction and lower the shear strength of soil, possibly resulting in failure (Clarke et al. 2006, Dehn et al. 2000, Lee and Jones 2004). Conversely, a decrease in total precipitation will lower the saturation level, increasing the soil's effective strength through higher suction. However, extended drought conditions may result in a loss of these improvements owing to excessive soil drying, resulting in a decreased contribution from suction, desiccation cracks, heavy shrinking, and loss of organic matter (Robinson and Vahedifard 2016).

High precipitation intensity can have a significant negative effect on natural slopes and geotechnical structures. Sudden increases in saturation will reduce the effect of suction, thus lowering the effective strength of the soil. In addition, intense rainfall often causes an erosion of surface materials and has also been

*Table 3-5. Potential Impacts of Climate Change on Soil and Earthen Structures.*

<i>Climate change feature</i>	<i>Fundamental impact</i>	<i>Practical impact</i>
Increased temperature	Higher evaporation rate/soil drying; Soil organic carbon (SOC) oxidation; Changes in vegetation amount; Snow, ice, and permafrost melting.	Increased suction, desiccation cracking, shrinkage; Land subsidence; Varied effects depending on the type of vegetation; Reduced strength of arctic soils, release of entrapped carbon, increased risk of mass wasting at higher elevations.
Decreased mean precipitation	Soil drying and water table lowering; Vegetation reduction.	Possible desiccation cracking and shrinkage, increase in suction; Loss of cover and increased risk of erosion.
Increased mean precipitation	Soil wetting and water table rise.	Decreasing suction leading to reduced shear strength.
Drought	Extreme soil drying and water table lowering.	Significant desiccation cracking and shrinkage, increased susceptibility to intense precipitation owing to increased permeability from cracking and shrinkage.
Intense precipitation	Rapid soil wetting; Overland flow.	Sudden changes in suction possible leading to heightened failure risk; Possible erosion and mass wasting.
Flood/sea level rise	Large pore pressure increases; Soil wetting.	Lower suction within flood protection infrastructure owing to wetting, increased risk of multiple failure mechanisms such as piping and overtopping, erosion.

associated with soil piping within slopes (Jones 2010). These processes may cause or enhance the failure of natural and built slopes (Hungry et al. 2005; Iverson et al. 2011). Furthermore, the effects of intense rainfall can be enhanced if preceded by an extended period of drought (Vahedifard et al. 2016). In addition, models have demonstrated that under partially saturated conditions, even non-extreme above-average rainfall can result in slope failures such as shallow landslides (Leshchinsky et al. 2015).

Rainfall-triggered instabilities in human-engineered and natural geotechnical structures are analyzed primarily using extreme precipitation estimates, derived using the so-called stationary assumption (i.e., statistics of extreme events will not vary significantly over a long period). However, extreme precipitation patterns have been shown to vary substantially because of climate change, leading to unprecedented changes in the statistics of extremes owing to non-stationarity. It has been shown that the use of stationary rainfall data can lead to underestimations in the hydromechanical behavior of natural and human-engineered earthen structures (Robinson et al. 2017, Vahedifard et al. 2017). These findings highlight the importance of site-specific assessments to quantify the potential impacts of climate change on the performance of current and future earthen structures. Rainfall-triggered landslides are widespread natural hazards that annually cause several million dollars in damage to property and infrastructure and occasional loss of human life. Climatic trends have been shown to increase landslide activity because of extreme precipitation patterns (e.g., Coe and Godt 2012, Gariano and Guzzetti 2016). Two major issues obstruct our full understanding of how landslide processes are affected by a changing climate: the high uncertainty in forecasting landslide activation owing to heavy precipitation and the inaccuracies in predicting precipitation and storm patterns (e.g., Coe and Godt 2012). Moreover, landslide studies typically project mean precipitation data as it is very difficult to estimate the variations in the frequency and magnitude of extreme rainfall events (e.g., Coe and Godt 2012).

Extended precipitation events, both extreme and moderate, can cause flood conditions. Floods pose risks similar to extreme precipitation events, with increased levels of erosion, soil wetting, and high pore pressures. Significantly high water levels may cause an overtopping of levees and dams, leading to significant external erosion of the earthen structure. Possible changes in precipitation event occurrence may change the frequency and intensity of floods, threatening the integrity of levees as well as levee-protected communities and infrastructure (Vardon 2015, Vahedifard et al. 2020, Mirae-Ashtiani et al. 2022). In addition, the increased pore pressures may cause piping and other forms of failure to occur. Similar risks are posed by sea level rise to coastal infrastructure. However, although sea level rise will occur gradually, it will not recede like floodwaters; thus, the risk to coastal communities will increase steadily.

An amplifying feedback loop can occur between drought, soil desiccation cracking, and CO<sub>2</sub> emissions (Vahedifard et al. 2024). The feedback can also alter the emissions of other greenhouse gases, such as CH<sub>4</sub> and N<sub>2</sub>O, from soils. Higher temperatures will speed up evaporation and soil organic carbon (SOC) oxidation (Davidson and Janssens 2006, Conant et al. 2011). Increased evaporation rates, combined with precipitation changes, will increase the frequency of pore pressure cycling, which has been known to cause strain softening and changes in permeability (Kovacevic et al. 2001, Potts et al. 1997, Nyambayo et al. 2004). In addition, increased evaporation rates owing to high temperatures may exacerbate the development of negative effects caused by drought conditions. Oxidation of SOC may cause land subsidence in highly organic peat soils and possibly also

an increased rate of sea level rise in some regions. SOC oxidation accounts for approximately 75% of elevation loss owing to peat subsidence, whereas the remaining 25% is attributed to secondary consolidation and compaction of organic soils (Mount and Twiss 2005). This oxidation is not accounted for in current emission estimates (Scharlemann et al. 2014). In addition to these effects, temperature increases cause the melting of permafrost in arctic regions, greatly reducing soil strength as well as melting ice and snow at high elevations, increasing the risk of mass wasting (NRC 2016, Gariano and Guzzetti 2016).

### 3.7.2 Impacts on Geotechnical Infrastructure and Foundations

Changes in the climate parameters presented in the previous paragraphs affect the potential failure modes of existing geotechnical infrastructure. The relationships between these effects and potential failure modes are summarized in Table 3-6.

### 3.7.3 Impacts on Soil–Structure Interaction and Landslides

Under drained conditions, elevated temperatures can increase the stability of unsaturated intact slopes and soil–structure interaction by increasing the soil's effective stress (Thota and Vahedifard, 2021). Coe and Godt (2012) predicted a decrease in the landslide activity in Slumgullion of Colorado, primarily because of forecasted increases in surface temperature and decreases in precipitation over the next century. Bennett et al. (2016) performed aerial photograph analysis, satellite

Table 3-6. Relationships between Atmospheric Events and Geotechnical Failure Modes.

<i>Climate change feature</i>	<i>Impact on earthen structures/slopes</i>	<i>Potential failure modes affected</i>
Increased temperature	Drying; Ice and snowmelt at higher elevations.	Uplift; Slope stability failure.
Decreased mean precipitation	Possible desiccation cracking; Shrinkage; Loss of vegetation cover.	Piping, internal erosion, slope stability; Piping; Piping slope stability.
Increased mean precipitation	Soil wetting and water table rise.	Erosion, slope stability, piping;
Drought	Elevated risk of impacts given for decrease in mean precipitation.	See decreased mean precipitation.
Intense precipitation	Rapid soil wetting; Overland flow.	Piping, slope stability; Slope stability, erosion.
Flood/sea level rise	Large pore pressure increases; Soil wetting.	Piping, internal erosion, slope stability, erosion.

interferometry, and satellite pixel tracking to examine the effect of California's historic 2012 to 2015 drought on 98 slow-moving landslides in Northern California. Their study showed that the historic drought put the brakes on these landslides. [Bennett et al. \(2016\)](#) concluded that drought decelerates earthflow, slows down landslide motion, and reduces the frequency of slope failure ([Bennett et al. 2016](#), [Mackey and Roering 2011](#)). In a follow-on study, [Handwerger et al. \(2019\)](#) employed aerial imagery to examine the postdrought landslide activities in Northern California. They found significant increases in activities of slow-moving landslides in 2017, right after the end of the historic drought. [Nereson and Finnegan \(2018\)](#) used historical aerial imagery data (1937 to 2017) to understand Oak Ridge earthflow motion and reported that the velocity of landslides decreased during periods of drought. Elevated temperatures and moisture deficit associated with drought increase suction, which, in turn, increases the shear strength and the factor of safety of intact unsaturated slopes ([Thota and Vahedifard, 2021](#)). However, elevated temperatures and drying–wetting cycles can possibly trigger the formation of desiccation cracks in fine-grained soils ([Zeng et al. 2022](#), [Tang et al. 2024](#)). Desiccation cracks form on the surface but can propagate several meters below the ground surface. Cracks can adversely affect the integrity and stability of unsaturated slopes and earthen structures by decreasing the soil mass strength, increasing the hydraulic conductivity, and inducing preferred pathways for water infiltration, leading to abrupt losses of suction and generation of the excess pore water pressure during rainfalls ([Vahedifard et al. 2014](#); [Abdollahi et al. 2021](#)). Tensile strength, the key soil property reinstating the formation of desiccation cracks, is shown to decrease under elevated temperatures ([Salimi et al. 2021](#)). Previous studies ([Tang et al. 2010](#); [Salimi et al. 2021](#)) have revealed that subjecting unsaturated clayey soils to elevated temperatures leads to the development of surface tensile stress and desiccation cracks at higher rates. [Salimi et al. \(2021\)](#) performed a set of laboratory tests to examine the effect of temperature on the tensile strength during desiccation of two compacted clays with medium to high plasticity. Their results showed that, at the optimum water content, the tensile strength decreased by 36% and 27% in highly plastic and medium plastic clays, respectively, when the temperature was elevated from 20 °C to 60 °C. Furthermore, elevated temperatures can alter the stability of unsaturated slopes through thermal-induced changes in vegetation cover ([Jamalinia et al. 2019, 2020](#)).

## **3.8 PERFORMANCE-BASED APPROACHES TO CLIMATE CHANGE**

### **3.8.1 Introduction**

The topics of PBD and climate change and resilience (to be discussed in Section 3.9, which follows) are closely coupled. SEI aspires to advance PBD for natural hazards as a way of enhancing the professionalism of the structural engineering community ([Dusenberry 2019](#)). Because this is an SEI Special Project, the SEI position is acknowledged, and some positive suggestions are made on how PBD

will advance structural engineering for impacts of climate change. Appendix D of the SEI Report on PBD (SEI 2018) deals with resilience-based performance standards for buildings and lifeline systems.

The ASCE Code of Ethics (ASCE 2020b), updated on October 26, 2020, states Engineers govern their professional careers on the following fundamental principles:

- create safe, resilient, and sustainable infrastructure;
- treat all persons with respect, dignity, and fairness in a manner that fosters equitable participation without regard to personal identity;
- consider the current and anticipated needs of society; and
- utilize their knowledge and skills to enhance the quality of life for humanity.

These principles can be addressed with PBD methods, where codes and standards are lagging, to address the effects of climate change on civil infrastructure and to *create safe, resilient, and sustainable infrastructure* and to *consider the anticipated needs of society* (Lounis and McAllister 2016; Ellingwood et al 2019).

### 3.8.2 Prescriptive versus Performance-Based Design

PBD is a process that enables the development of structures that will have predictable performance when subjected to defined loading. PBD is founded on the premise that the structural systems and the nonstructural systems they support (e.g., socioeconomic functions) must meet specific performance objectives, which establish the expectations for design regarding safety, functionality, and durability. Traditional approaches to design are dictated by prescriptive provisions in building codes, which are becoming ever more complex as new technologies and data are addressed in practice. However, when prescriptive provisions prevent the engineer from fully leveraging advances in technology to meet the needs of the client, alternative methods are allowed with the approval of the building official. This allows new technology, such as advanced test and analysis capabilities, to supplement a prescriptive approach.

PBD methods include the following steps:

1. Establish the performance objectives, including those for climate effects and associated uncertainties.
2. Conduct initial design.
3. Verify performance through analytical simulation, prototype testing, or a combination thereof.
4. Perform peer review and develop detailed documentation to support design decisions.

#### 3.8.2.1 Advantages of Performance-Based Design

Performance-based design methods rely on an in-depth understanding of expected structural performance under given load effects. There are potential benefits in advancing long-term resilience and sustainability in civil

infrastructure by addressing the effects of climate change with PBD methods. PBD approaches can enable the future use of construction practices and materials that will facilitate the development and utilization of new structural systems with higher performance capabilities compared to traditional structural systems.

PBD is based on structural mechanics and probabilistic methods of analysis. As a result, structural design solutions can make efficient use of materials. PBD can incorporate design solutions that are environmentally sustainable (Lounis and McAllister 2016). Similarly, PBD can also support informed adaptation of infrastructure to changing hazards with different levels of uncertainty, such as climate change.

PBD innovations that lead to improved construction practices and use of sustainable materials may reduce the contributions of civil infrastructure to climate change. Improved construction practices along with structural monitoring may improve the life-cycle management of infrastructure and enable risk-informed decision-making.

PBD can advance codes and standards, as well as education. The required detailed documentation and peer review can ease future assessments of newly designed structures. The fundamental principles of structural mechanics and probabilistic methods of analysis essential to PBD can advance structural engineering education and practice.

### 3.8.2.2 *Current State of Performance-Based Design Practice*

The current state of professional practice with regard to the use of PBD in the United States is fractured along the lines of design loading and the type of structure being designed. Many of the prescriptive requirements in these codes and standards are based on experience. The summary of the present state of practice presented subsequently reflects this fractured nature (Dusenberry 2019, ASCE 2023).

#### Building Hazards:

- Seismic design of buildings—Since the early 2000s, the basis for performance-based seismic design (PBSD) of new buildings has used the performance approaches in ASCE 41-23, *Seismic Evaluation and Retrofit of Existing Buildings* (ASCE 2023). PBSD is also used in the design of new buildings to reduce the code-specified, capacity-based requirements for members that are intended to remain essentially elastic.
- Wind-resistant design of buildings—Use of Performance-Based Wind Design (PBWD) is in its infancy for buildings due, in large measure, to the complex analysis that must be done for the interaction between the buildings cladding and its structural system (ASCE 2019).
- Fire-resistant design of buildings—Although current practice in the United States is primarily prescriptive in nature, performance-based structural fire design has been used on many major international projects and is beginning to have an impact on building design in the United States (ASCE 2020a).

This is particularly true as architects conceive more complex designs and engineers have an increased understanding of structural response to fire from nonclimate-associated extreme disasters, including the World Trade Center collapse (Gross and McAllister 2005) and the Windsor tower fire in Madrid (SCOSS 2008).

- Flood design—At present, PBD criteria are not available specifically for flood events. However, the increasing effects of climate change on flood event intensity and frequency are leading to increased demands for design and performance of the built environment beyond code requirements.

Civil Infrastructure:

- Nonbuilding structures—Use of PBD for the design of nonbuilding structures is virtually nonexistent in the United States, with the exception of bridge structures.
- Bridges—Lack of definitive performance criteria within the *AASHTO Bridge Design Specifications* (AASHTO 2020) is a significant hurdle for a general PBD implementation. For bridge structures that are not specifically addressed in the Code, particularly long span bridge structures, PBD procedures are usually applied for wind and seismic design.
- Nonstructural components—For the foreseeable future, desired performance will more commonly be achieved through good detailing and equipment testing dictated by prescriptive requirements, rather than enhanced analyses.

PBD documents and guidance have been developed by ASCE and other organizations such as FEMA (FEMA P-58-4) (FEMA 2018b). Although several hazards and structural types have been addressed, the basis can vary with regard to performance objectives, design criteria, review requirements, and their application to climate change effects.

PBD, as currently implemented, is applied to individual buildings that are part of infrastructure projects (e.g., buildings as part of a water treatment system). It seems more likely that stakeholders (e.g., owners, clients/, and local governments) will require that new projects contribute to the resilience of the community, including the consideration of future climate effects, which tend to be regional in nature (Ellingwood et al 2019). For voluntary incorporation of resilience and climate effects, financial incentives may be provided.

### 3.8.3 Performance-Based Design in a Changing Climate

Engineers currently use PBD to incorporate resilience goals or to address future climate effects on proposed designs. The general approach is to design the structure according to codes and standards and then make refinements or evaluations using PBD to address specific/defined project performance objectives. This separation of effort based on codes and standards helps with the evaluation by peer reviewers and building officials. PBD methods that address climate effects and community resilience may provide the impetus needed to propel this approach into regular design practice.

### 3.8.4 Performance-Based Design—Linking Community and Individual System Design Objectives

In current PBD practice, performance objectives are established for occupant needs and/or building function (e.g., data centers, specialty manufacturers, hospitals). The role that buildings play in the resilience of a community seldom is considered. Many aspects of resilience, including loss of functionality and recovery, require more comprehensive and standardized assessment methods. To advance the current state of practice, the structural design process should start with individualized community-level goals to inform performance objectives for individual projects, including recovery-based performance objectives. Because codes and standards are likely to remain focused on individual buildings in the US regulatory environment, community performance goals and metrics need to be de-aggregated to the individual facility level, where they can be used to develop risk-informed design standards and guidelines, code approaches, or PBE criteria that can be used by structural engineers and other design professionals (Ellingwood et al 2019). This process is illustrated in Figure 3-10.

### 3.8.5 Performance-Based Design: Needs for Engineering Practice

Guidance is needed to develop standard PBD approaches and tools for use in practice that incorporate climate change. Three key aspects of resilient and



Figure 3-10. De-aggregation of community resilience goals for structural design.

Source: Ellingwood et al. (2020).

sustainable designs for the built environment that need to be addressed are the following:

- Safety:
  - Adjustments, if any, to current load and resistance criteria for a changing hazard frequency or intensity.
  - A comprehensive list of possible limit states that may need to be considered for the effects of climate change effects [e.g., drought on foundations (Section 8), increased riverine flow on bridges (e.g., Subsection 3.6.2)].
- Functionality:
  - Limit states that account for the impact of climate change uncertainty on the failure mode.
  - Recovery curves to estimate time to complete likely repairs and time to functional recovery (discussed in Section 9).
- Durability
  - Deterioration that leads to changes in expected resistance owing to new or different levels of exposure, as discussed in Chapter 4.
  - Modifications to maintenance routines to maintain structural integrity.
  - Possible retrofits to improve the performance of existing structures; criteria for when relocation is the best alternative.

### 3.8.6 Challenges and Barriers to Performance-Based Design

PBD offers opportunities for innovation and creativity and for structural engineers to bring more value to clients and project design teams. Challenges that currently impede a broader application of this approach include the following:

- Additional professional education and training are needed for engineers to apply PBD, including understanding performance levels and associated damage, defining performance objectives, and understanding risk assessment and management.
- Resistance to change by clients and owners, as well as designers, needs to be addressed through a combination of communication of the benefits and solution options.
- The risk of litigation for PBD projects can be mitigated with the peer review process and other steps that keep clients and the design team informed about decisions, risks, and challenges.
- The standard development process needs a new approach that includes performance goals and objectives for structural safety and facility functionality (Ellingwood et al 2020).
- Methods to communicate how additional design cost that may be incurred initially are outweighed by life-cycle cost savings and long-term benefits over the service life of the project.

## 3.9 CLIMATE CHANGE IMPACTS AND COMMUNITY RESILIENCE

### 3.9.1 Community Resilience

Community resilience is the ability to prepare for anticipated hazards, adapt to changing conditions, and withstand and recover rapidly from disruptions (PPD 21) (PPD 2013). When discussing resilience, community refers to a place designated by geographical boundaries that functions under the jurisdiction of a governance structure, such as a town, city, or county (NIST 2015). It is within the local governance structure that resilience decisions, actions, and projects are identified, approved, funded, and implemented.

The concept of resilience affects decisions for the built environment, from individual facilities to regional infrastructure systems. The built environment refers to all engineered systems within a community or region, including buildings, facilities, nature-based systems, and infrastructure components and network systems. Many single-family residential buildings are not engineered construction but must still be included in a community resilience assessment.

To achieve resilience at the community level, individual buildings and infrastructure systems must meet resilience criteria that are based on and support the community level. This dependency between scales of resilience links community planning to the design of individual buildings and infrastructure.

Achieving resilient performance in individual facilities and systems requires going beyond the requirements of current codes and standards, which focus on life safety and on limiting the failure of structural components and systems, particularly when addressing recovery of functionality. The issue of resilience requirements for buildings has been addressed with performance-based design (PBD) guidance (Section 8). Examples include ASCE 7-22 Section 1.3.3 Functionality ([ASCE 2022b](#)) and the *Prestandard for Performance Based Wind Design* ([ASCE 2019](#)).

Buildings and infrastructure systems collectively enable a community to provide shelter, utilities, and other services, such as schools and hospitals, and to support social and economic institutions that are essential for community well-being. Vulnerable populations within communities are often disproportionately affected by hazards resulting from climate change, such as flood owing to land-use policies, economic disadvantage, and other demographics such as race/ethnicity, age, and others. Thus, resilience goals may vary between communities because of differences in sociodemographics, age and condition of buildings and infrastructure, and approaches to address equity in resilience goals.

### 3.9.2 Design Considerations for Resilience and Climate Impacts

The consideration of future extreme weather events (e.g., hurricanes, heat waves, precipitation) is of increasing importance for communities. Although not currently addressed by building codes or standards, many local communities of today are demanding that climate effects be considered in designs ([Vogel et al. 2016](#)). Further, climate change may exacerbate the impacts of extreme hazard

events over time, not only by changing the loads on structures, but also by affecting their capacity through aging and deterioration processes. Therefore, it is important to account for resilience and climate issues in community planning, particularly in the design of buildings and other civil infrastructure.

The impact of compound extreme events (e.g., tsunami following earthquake, storm surge and riverine floods following hurricane winds) may also be increased by climate effects (Bruneau et al. 2017). At present, there are insufficient guidance or tools to consider such compound events and their impact on the built environment. In addition to predicting future hazards, the nonstationarity of future climate effects on hazard events will require new approaches for addressing and communicating uncertainty (Cooke 2015).

The concept of resilience hinges on that of functionality, which can be measured at the individual building/facility, infrastructure system, or community levels. For this reason, resilience analyses need to be tailored to the spatial scale being evaluated with clear methods of aggregating and de-aggregating between various spatial scales. Multiple scales of resilience analysis have similar implications for regional climate projections, where correlated climate projections may be needed at individual sites across regions.

Buildings and civil infrastructure systems are designed and maintained using separate regulations, codes, standards, and best practices, each of which has its own design and reliability basis for performance evaluation (McAllister et al. 2022). Each system is designed for different performance objectives (e.g., life safety in buildings for design (rare) events, loss of electric and water service for frequent events). The lack of coordination in their development causes disparities in performance of the built environment for a given hazard event across a community. These disparities become even more accentuated when the performance in terms of recovery is considered. Although reliability helps measure whether specified performance objectives are achieved, different measures are needed for recovery of function.

For some systems, the recovery phase is measured in hours (e.g., power distribution systems), whereas for others, recovery may be measured in months (e.g., repairing a damaged bridge or tunnel). Such disparities can be best identified and addressed with a community-level assessment to inform specific needs at the individual project level. A common tool used to address this need is the so-called resilience table, first introduced in San Francisco (Poland 2009) and then adopted in many other contexts (Washington State Emergency Management Council: Seismic Safety Committee 2012, OSSPAC 2013, NIST 2015). In these tables, one of which is illustrated in Figure 3-11, the community sets the desired time to reach a set of performance metrics for various components of the built environment (e.g., 75% of the roads functional in 3 months). These targets are compared to the predicted recovery time, as assessed by technical experts. The sectors for which the discrepancy between desired recovery performance and predicted recovery performance is the largest are those where interventions are most needed. This simple tool is typically used for a set of scenario events that encompass likely hazard realizations. Currently, these scenarios are identified for each community

Summary Resilience Table	Design Hazard Performance								
	Phase 1: Short-Term			Phase 2: Intermediate			Phase 3: Long-Term		
	Days			Weeks			Months		
	0	1	1-3	1-4	4-8	8-12	4	4-24	24+
<b>Critical Facilities</b>									
Buildings	90%								X
Transportation	Desired Performance	90%	X				Gap		Anticipated Performance
Energy		90%	X						
Water			90%		X				
Wastewater				90%					X
Communication	90%				X				

Figure 3-11. Resilience table illustrating gaps between the desired time to recovery of function (green box) and the current anticipated time to recovery of function (blue box).

Source: NIST (2015).

on the basis of the anticipated hazards and available guidance. The effect of climate change can be incorporated by selecting a portfolio of extreme-event scenarios that will be representative of future climate. To advance resilience analyses and outcomes, a standard approach to identifying hazard scenarios is needed.

Buildings, bridges, and other infrastructure systems tend to be designed for service lives ranging from 50 to 100 years. Many buildings and infrastructure systems are in use beyond these service lives, with their continued performance dependent on retrofits, upgrades, and maintenance. Thus, as discussed in the other sections of this book, the service life of buildings, bridges, and other civil infrastructure systems spans a time period over which climate may change substantially, exposing such systems to climatic conditions and loads that differ from those specified for their design. The same consideration applies to resilience assessment. The entire process of a community resilience assessment, from the selection of anticipated hazards to the assessment of representative analysis scenarios to the specific quantitative evaluations of performance, needs to account for the nonstationarity of the climatic effect. Protocols similar to those discussed in Section 3.5 can inform resilience assessment in such a way as to consider climate change.

When assessing the effect of climate change and the way it may impact design, maintenance, and retrofit, ownership plays an important role. For buildings and infrastructure that have the same owner throughout the service life of the system, there are stronger incentives to include resilience and climate considerations in the planning, design, and maintenance over the service life of the system. Systems that are planned, designed, occupied, and maintained by different entities are more likely to conform to minimum requirements unless there is a perceived consumer demand for resilience, climate considerations, or costs associated with improvements that can be passed to the users/customers.

Dependencies and interdependencies among infrastructure systems in a community require coordination among multiple owners that can be challenging

to achieve. Improving the resilience of one system against future climate effects may be less effective than planned if the owners or managers of interdependent infrastructure systems do not do the same.

### 3.9.3 Functional Performance of the Built Environment

Community-level performance goals are often stated as long-term aspirations for functionality of physical, social, and economic systems. The addition of climate change to the long-term functionality of community systems is now occurring across the nation and many parts of the world. Designers need quantitative performance objectives and design criteria for evaluation of individual facilities and systems that can support community goals and the considerable uncertainty associated with climate change and future events.

Acceptable performance of the built environment is a necessary but insufficient condition to establish community resilience. Community resilience includes social and economic goals, as well as physical service goals. To link the response of infrastructure systems and facilities to community resilience goals, their collective performance must be quantified using metrics related to functionality and recovery. Development of community metrics to support typical community goals is a critical aspect of the cooperative partnership between NIST and the Center for Risk-Based Community Resilience Planning for addressing community resilience on a national scale. Examples of community resilience goals and resilience metrics are given in [Table 3-7](#).

Resilience metrics for physical infrastructure services are of most direct interest to structural engineers. However, the resilient performance of the built environment enables the attainment of the social and economic resilience goals outlined in [Table 3-7](#) and, therefore, such community goals should be considered when evaluating solutions for structural design, maintenance, or improvements.

*Table 3-7. Examples of Community Performance Goals and Example Resilience Metrics.*

<i>Community performance goals</i>	<i>Example resilience metrics</i>
Population stability	Dislocation and migration; housing availability.
Economic stability	Change in employment, taxes and revenue (resources), community budget (needs).
Social services stability	Access to healthcare, education, retail, banking.
Physical services stability	Functionality of buildings, transportation, water, wastewater, electric power, gas, communications.
Governance stability	Access to police and fire protection; essential public governmental services.

Source: [Ellingwood et al. \(2020\)](#).

Functional recovery refers to the post-event recovery of basic intended functions associated with the pre-event use or occupancy of a building or infrastructure system. The resilience perspective for the design of individual buildings or infrastructure systems requires a consideration of potential damage and recovery during the design or assessment process. This issue is addressed to some degree for critical facilities such as hospitals and emergency care centers and shelters, primarily through increasing load and deformation requirements to design and build more robust structures. From a community resilience perspective, other buildings may also meet the definition of a critical facility based on their function, such as nursing homes, K-12 schools, and some businesses. However, current codes and standards focus on life safety issues for individual buildings and infrastructure systems; they do not explicitly consider the likely modes of failure and associated repairs required to restore the facility functionality within a specified time frame. Changes in the regulatory process will be required to incorporate standards that prescribe performance goals in terms of postdisaster functionality and resilience in addition to life safety. Such a change will need to include a shift from component design to a systems approach.

Best practice guidance and design criteria with performance objectives that support community resilience goals are needed to advance the inclusion of functional recovery in design practice. As noted in NIST (2015) and NIST/FEMA (2021), functional performance goals and design criteria are needed to better address the role of infrastructure in the community, including expected levels of damage, subsequent impact on building and other infrastructure functionality, repairs required to achieve recovery of function, and potential impacts on community social and economic recovery.

As the engineering profession strives to bring resilience and functional recovery concepts into practice, the issue of climate change must be addressed in parallel. ASCE (2015) highlighted a key dilemma for practicing engineers: “Even though the scientific community agrees that climate is changing, there is significant uncertainty about the spatial and temporal distributions of the changes over the lifetime of infrastructure designs and plans. The requirement that engineering infrastructure meets future needs, and the uncertainty of future climate, leads to a dilemma for practicing engineers.”

Changes in climatic conditions can affect civil infrastructure structures, and their resilient performance, in a variety of ways. ASCE MOP 140 (ASCE 2018) identified the types of climate-related hazard impacts that need to be addressed by ASCE 7 (ASCE 2021b), in particular, flood impacts (e.g., increased elevations, flow velocities, wave heights), precipitation impacts (e.g., rain and snow loads on roofs, increased ice loads on structures), and wind impacts (e.g., increased intensity and frequency of windstorms and hurricanes). ASCE MOP 144 (ASCE 2021) uses probabilistic methods for risk analysis and management of infrastructure projects to address uncertainties within a planning horizon timeframe. This approach includes identifying and analyzing hazards, system failures, associated

probabilities and consequences including direct and indirect losses, failure and recovery quantification for resilience, effects on communities, economics of resilience, and technologies for enhancing resilience for new as well as existing infrastructure.

Resilience brings in the time dimension through the recovery process at the individual facility or network level, but models for recovery are still in early stages of development. There is also the need to consider interdependencies during recovery such as when a building or system is functional, but another system on which it depends (e.g., utility) is not yet able to provide a service. When buildings in a community are not functional owing to delays in repair funding or other causes, the local tax base decreases. Further, delays in return to functionality for buildings directly affect the population, keeping them displaced and increasing the likelihood of outmigration, which negatively affect population stability metrics (Table 3-7). Outmigration is further dependent on social cohesion and a household's source of shelter, employment, and education for children.

### 3.9.4 Challenges to Community Resilience in a Changing Climate

Best practices of design professionals and decisions by city planners and regulatory authorities are likely to evolve in the coming decade to support how climate change is addressed in community resilience. PBD provides a path forward for addressing this conflict and resolving the inherent challenges that will arise in addressing both facility and community needs. Developing and incorporating PBD approaches that address climate change hazards and impacts into best practices, standards, and codes is an urgent need for the engineering profession and society.

The challenges for structural engineers include the following (Ellingwood et al. 2020):

- Common community resilience goals that address future impacts of climate change should be identified by a broadly based stakeholder group.
- Performance objectives for buildings by functional categories or groupings (e.g., residential buildings, commercial facilities, government) or socioeconomic institutions (e.g., education, health care) should be expressed as requirements that are compatible with engineering practice and practical to implement from an engineering perspective.
- Reliability targets for individual buildings in current structural design practice (e.g., ASCE 7-22 Section 1.3) identify *minimum performance requirements* at the *component* level for most design loads, except earthquake loads. Target reliabilities and performance criteria at the *system* level for all loads are needed to support community resilience goals.
- Codes, standards, and regulations for infrastructure systems (e.g., buildings, bridges, lifelines) should be coordinated to support community resilience goals and climate change impacts and to address functionality and recovery of civil infrastructure as well as life safety.

### 3.10 OBSERVATIONS, RECOMMENDATIONS, AND FUTURE NEEDS

Climate change is expected to have a substantial impact on structural design criteria for buildings, bridges, and other civil infrastructure. Damage owing to natural hazards has been increasing in recent decades as a result of urbanization brought on by population growth and socioeconomic development. This trend is likely to be accelerated by a changing climate, especially in urban areas subject to more frequent or intense hazards. Chapter 3 has presented an overview of climatic loads appearing in structural design guidelines, standards, and codes used for buildings, bridges, and coastal infrastructure. A brief summary of the principles of structural reliability theory and reliability targets used for setting structural design criteria is followed by a comprehensive discussion of the treatment of nonstationarity for climate-dependent variables and design parameters, with a focus on snow and ice, rain, windstorms, and riverine and coastal flooding hazards, drawing on an extensive review of the literature. Uncertainties in these climate variables, especially when projected over the latter decades of the 21st century, are extremely large, especially for wind, ice, and snow loads and, along with nonstationarities, will require special consideration in code revisions. Opportunities afforded by performance-based design in dealing with climate change are introduced. The chapter concludes with a discussion of climate impacts on community resilience, a topic of urgency in light of increasing losses to infrastructure systems as a result of extreme climate hazards with large geographic footprints. An international workshop on Effect of Climate Change on Life-Cycle Performance, Safety, Reliability, and Risk of Structures and Infrastructure Systems, held on September 30, 2022, has confirmed some of the observations in Chapter 3 and added other considerations. The proceedings of that workshop are summarized in Appendix B of this book and are reflected in this summary.

The study summarized in Chapter 3 has led to the following observations, conclusions, and recommendations for mitigating the risk of climate change to buildings, bridges, and other civil infrastructure:

#### 3.10.1 Statistical Modeling and Analysis of Nonstationary Climatic Variables

- Until the present time, climate variables in ASCE 7 have been determined assuming that the annual extreme climate variable of interest forms a stationary sequence, which can be fitted to an extreme-value probability distribution from which the design value is selected at a small annual probability of exceedance (typically on the order of 0.001 to 0.02). The corresponding return periods for design typically range from 50 to 1,000 years and the hazard maps or tables that provide design values are developed on this basis. These return period maps (or tables) are the basis of what is termed a *uniform hazard* approach, because the probability that the climate variable is exceeded is essentially uniform everywhere. In recent decades, ASCE 7 has moved toward a *uniform reliability* approach, where the same

probability of failure is expected everywhere rather than the same hazard intensity, as summarized in Section 3.4. Structural engineers in the United States have become accustomed to and have accepted these approaches.

- New statistical methods will be needed to take nonstationarities in climate variables into account (Pandey and Lounis 2023). The assumption of stationarity underlying the concept of a return period, which is used in current climate statistical modeling, is invalid under climate change because the distributions of the annual extreme climatic variables are not identical. Alternatives to the return period for specifying the design parameter that reflect this nonstationarity will have to be developed and communicated to the professional engineering community and its client base. Section 3.5 discusses some of these alternatives.
- Uncertainties—both aleatory (inherent variability) and epistemic (model-based)—will assume a new level of importance in a changing climate, because the climate variables for design purposes will be based on downscaled climate projections, supplemented by traditional climate data. In contrast to current practice, epistemic uncertainties are likely to dominate after 2060 in extreme-event prediction because of limitations in global climate models or in methods for downscaling them to the local resolution required for building or bridge design.
- Uncertainties in climate variables essential for structural design, for example, wind, snow, and flooding, will be greater than uncertainties in basic temperature and precipitation parameters on account of larger epistemic uncertainties. Further investigation will be required as to the uncertainty associated with the resolution required for structural design in downscaled projections.
- The climate science community should strive to provide, as a minimum, estimates of changes in mean value, variability (measured by standard deviation or coefficient of variation), and probability distribution of annual extremes of individual climatic variables, as this information will be the starting point for incorporating climate change in developing maps of flood, wind, snow, and other climate variables for design purposes in building codes.
- Sequences of annual extreme climatic variables are neither identically distributed nor statistically independent under climate change because of common climate forcings. In the longer term, the correlation structure of the annual extremes should be considered in determining design values of climate variables. If the autocorrelation function for this sequence is nonnegative, the estimates of the maximum values of the climate variables under the independence assumption will be nonconservative, with a corresponding impact on design costs. Expertise for performing such an autocorrelation analysis of climate variables is more likely to be found in the climate science community than in the structural engineering profession.

- Codes and standards dealing with different natural hazards traditionally assess them independently (with a few exceptions) and subsequently combine them in the design process with load combination equations (Section 3.6.8). Climate change is likely to introduce correlations in the way climatic variables evolve over time (e.g., hurricane wind pressures, storm surge, wave action). As discussed, if these individual actions are positively correlated, the design load (and limit state probability; see Section 3.4) will be underestimated. An integrated approach to combining these different structural actions in a multihazard approach that takes these correlations into account should be initiated. Expertise for performing this analysis should be identified in SEI.

### 3.10.2 Climate Variables for Reliability-Based Structural Design

- The uniform reliability approach to structural design for ultimate limit states is based on reliability targets for buildings ( $\beta = 3.0$  for Risk Category II buildings with a 50-year service life) and for bridges ( $\beta = 3.5$  for a 75-year service life). These reliability targets are based on calibration to existing structural design practice over much of the twentieth century, and there is no evidence from more than four decades of design experience to suggest that they are inadequate. Absent information to the contrary, it is recommended that the reliability targets stipulated in current codes and standards remain unchanged at this time. Otherwise, design conservatism and cost may increase without useful purpose.
- If the load process is stationary and structural deterioration is not considered, the conditional failure rate is constant and there is a simple relation between the “N-yr” service life for reliability and annual conditional failure rate. For example, if the target reliability index for a Risk Category II Building is  $\beta = 3.0$  for a service life of 50 years, the conditional failure rate is approximately  $3.0 \times 10^{-5}$ /year (Table 3-1). The selection of a 50-year service life for buildings (or 75-year period for bridges) in probability-based limit states design under stationary conditions was made for convenience more than 40 years ago. The current return periods in building codes and standards for specifying nominal loads are unrelated to building service lives.
- In contrast to historical practice, the planning horizon for structural design in a changing climate must be selected carefully because climate loads are nonstationary. Thus, the conditional failure rates needed to achieve exactly the same target reliabilities (Table 3-1) over a 50-year (or 100-year) service life may increase and the design loads will increase correspondingly. The implications of increasing loads over a service life require further examination prior to codification. The code should define a minimum service life, but an online tool can provide the designer the ability to obtain loads for longer time periods.
- Nonstationarities in climate variables must be integrated in time-dependent structural reliability analysis to estimate future behavior and to demonstrate compliance with performance objectives expressed in reliability terms (e.g., ASCE 7-22, Section 1.3.1.3, Table 1.3-1).

- Climate change will cause many climatic variables (and loads) in US structural design practice to increase (e.g., by the end of the 21st century, increases in 3 s gust wind speed may require Risk Category II structures to be designed with the parameters currently used for Risk Category IV). Such increases are likely to be regionally dependent. This being the case, many respondents to the preworkshop survey (Appendix A) favored increasing climate variables analyzed under stationary conditions by an arbitrary factor (on the order of 1.05). This seemingly simple strategy would reverse a two-decade trend in ASCE 7 to move from a *uniform hazard* basis toward a *uniform reliability* basis for structural design. It is likely that the reliabilities of buildings and bridges in coastal areas would decrease in comparison with those in the interior of the United States if this approach were to be taken.
- Major changes to climatic loads may also affect systematically aspects of structural design that may be rejected by designers on economic grounds. Therefore, hazard analyses should avoid overconservatism.

### 3.10.3 Implementation in Codes and Standards

- Code development in the United States is a bottom-up process developed through a voluntary consensus process. There is no national building code in the United States, and the federal government has no building code authority, having relegated that to the individual states. Provisions to address climate change in building codes and standards must be implemented within the structure of the current building regulatory process in the United States (2019).
- ASCE (and other professional and intergovernment organizations such as AASHTO) facilitates the development of new model code provisions on a 5- to 6-year cycle, which must be adopted through the voluntary consensus process. This revision cycle provides ample opportunity for new climate science to be incorporated in a timely fashion.
- Codes and standards in the US regulatory system focus on providing life safety. Although life safety will always be of paramount importance in the US building regulatory system, it may not be sufficient in a changing climate, where serviceability and functionality of buildings and other civil infrastructure under time-dependent climate effects may also become essential considerations.
- Current codes and standards for buildings and other civil infrastructure systems usually do not take structural deterioration into account. However, structural deterioration may be accelerated by climate change, which will affect safety (see discussion in Chapter 4). For buildings, this will be relevant especially for the building envelope because the structural system is often protected from the environment. In contrast, the structural system of a bridge is fully exposed to the environment and accelerated climate-related deterioration becomes a significant concern. Modeling structural resistance capacities of many common structures is the responsibility of

material-specific organizations such as ACI, AISC, and others. SEI/ASCE should initiate collaborations with these organizations to ensure that design criteria ensure adequate performance of all types of structural systems.

### 3.10.4 Performance-Based Engineering

- Performance-based engineering (e.g., ASCE 7-22, Section 1.3) offers a framework for introducing new design approaches under the “alternative means and methods” provisions of codes that provides a path forward for addressing and resolving the inherent challenges and constraints that will arise in considering both individual facility and community needs under a changing climate.
- Design adaptability has been recognized as a tool for addressing climate change. Low-regret building and bridge design strategies might be necessary to deal with the deep uncertainties in climate variables, especially in the final decades of the 21st century (ASCE 2015a, 2018). Such concepts can be better addressed in the context of performance-based design than under traditional prescriptive methods found in building codes and standards and may be useful in building a business case for solutions in which accounting for climate change would otherwise lead to prohibitive costs.

### 3.10.5 Climate Change and Urban Resilience

- The impact of natural hazard events on communities has been increasing because of the effects of climate impacts on communities, both large and small, in hazard-prone areas. For this reason, the National Academy (NRC 2012) and Presidential Policy Directive PPD 21 (PPD 2013) have designated community resilience a *national imperative*.
- Design for resilience requires a new way of thinking—a focus on the performance of the built environment as a system, as opposed to individual facilities, and an emphasis on posthazard event functionality in addition to life safety (NIST 2015).
- Community resilience will be impacted by increasing losses to infrastructure systems owing to climate change if not addressed in structural design. Therefore, codes and standards for infrastructure systems (e.g., buildings, bridges, lifelines) should be coordinated to support community resilience goals and climate change impacts and to address functionality and recovery of civil infrastructure as well as life safety.
- Current codes and standards on their own are unlikely to be sufficient for resilience-based design because, by their nature, they are not community-specific. Therefore, code development should recognize that common community resilience goals, performance objectives, and metrics identified by a broad stakeholder group are likely to be community-dependent and based on community experiences with natural hazard events and local socioeconomic institutions and structures (Ellingwood et al. 2020).

### 3.10.6 Implementation in Professional Engineering Practice

- Simple processes to implement the best climate science in structural engineering without disrupting professional practices of structural engineering must be developed.
- An established model with delegated responsibilities is needed to develop and maintain climate projections for structural design. The ASCE 7 Hazard Tool Online ([ASCE 2022a](#)) for environmental and geophysical loads introduced for the first time in ASCE 7-22, provides access to digital data in the hazard tool databases. The US Geological Survey has taken responsibility for the seismic hazard modeling in ASCE 7 under the National Earthquake Hazard Reduction Act of 1977 for more than three decades. The new collaboration between ASCE and NOAA offers exciting opportunities for developing similar partnerships between climate scientists and engineers for climate-related load parameters. This collaboration will be most useful for structural load assessment if NOAA provides information on climate extremes, which currently are simulated by engineers rather than NOAA scientists. Moreover, having the ASCE 7 Hazard Tool Online supported entirely by federal agencies with the necessary expertise will put the hazard analyses and databases in the public domain with a level of transparency needed in ASCE 7 for future risk-informed structural design.
- The scope of ASCE's collaboration with NOAA and other federal agencies to reinforce the ASCE 7 Hazard Tool Online should be expanded to aspects that are not covered currently, such as storm surge and flood maps, with a focus on developing flood databases aimed at supporting structural design rather than insurance underwriting.
- The structural engineering profession, building and bridge industries, public agencies, and the public must be persuaded to accept changes in project design and development in the national interest, even if the initial project construction costs increase in some instances. A business case must be made to facilitate the adoption of future climate-based loads, emphasizing life-cycle analysis (Chapter 4), financial incentives, access to insurance, municipal bonds for public sector construction, among others.
- Professional liability for practicing structural engineers might be reduced if climate change is taken into consideration.
- The preworkshop survey (Appendix A) indicated that changes of more than about 10% in load or in resulting construction costs will encounter resistance from the structural engineers, developers, and the construction industry without comprehensive cost-benefit studies. There is precedent for using such studies to support increases in seismic design requirements in the Eastern United States.
- The Structural Engineering Institute should develop and implement a portfolio of continuing education courses incorporating the role of climate change in structural design practice, as appropriate, to support any climate

change initiative in the profession. Such courses should be tailored to professional structural engineers to provide them with sufficient information to make intelligent choices in structural design and project development. The current continuing education offerings that support new editions of ASCE 7 are models for content and level of instruction.

### 3.11 ACKNOWLEDGMENTS

Contributions by sections: 3.1. B. R. Ellingwood, P. Bocchini; 3.2. B. R. Ellingwood, P. Bocchini; 3.3. B. R. Ellingwood, P. Bocchini, Z. Lounis; 3.4. M. Ghosn, B. R. Ellingwood, M. Liu, D. Yang, L. Capacci, S. Diniz. 3.5; P. Bocchini, L. Capacci, M. Ghosn, N. Lin; 3.6.1. G. Tsiatas, B. R. Ellingwood, F. Biondini; 3.6.2. M. Ghosn, J. W. van de Lindt, B. R. Ellingwood, D. M. Frangopol; 3.6.3. M. Akiyama, G. Tsiatas, Y. Li; 3.6.4. J. W. van de Lindt, Y. Li, M. Barbato; 3.6.5. H. Hong, Z. Lounis, B. R. Ellingwood; 3.6.6. H. Hong, Z. Lounis; 3.6.7. B. R. Ellingwood, T. P. McAllister; 3.6.8. B. R. Ellingwood, M. Barbato; 3.7. Farshid Vahedifard; 3.8. T. P. McAllister, G. Tsampras, B. R. Ellingwood; 3.9. J. W. van de Lindt, T.P. McAllister, P. Bocchini; 3.10. B. R. Ellingwood, P. Bocchini.

### References

- AASHTO (American Association of State Highway and Transportation Officials). 1973. *Standard specifications for highway bridges*, 11th ed. Washington, DC: AASHTO.
- AASHTO. 2020. *LRFD bridge design specifications*, 9th ed. Washington, DC: AASHTO.
- Abdollahi, M., F. Vahedifard, M. Abed, and B. A. Leshchinsky. 2021. "Effect of tension crack formation on active earth pressures encountered in unsaturated retaining wall backfills." *J. Geotech. Geoenviron. Eng.* 147 (2): 06020028, DOI: 10.1061/(ASCE)GT.1943-5606.0002434.
- ACI (American Concrete Institute). 2019. *Building code requirements for structural concrete*. Farmington Hills, MI: ACI.
- Adhikari, S., E. R. Ivins, and E. Larour. 2016. "ISSM-SESAW v1.0: Mesh-based computation of gravitationally consistent sea-level and geodetic signatures caused by cryosphere and climate driven mass change." *Geosci. Model. Dev.* 9 (3): 1087–1109. <https://doi.org/10.5194/gmd-9-1087-2016>.
- Ahmed, K. 2011. "Temperature effects in multi-story buildings." *J. Eng. Sci.* 39 (2): 249–267.
- AISC (American Institute of Steel Construction). 2022. *Specification for structural steel buildings*. ANSI/AISC 360-22. Chicago: AISC.
- Alhamid, A. K., M. Akiyama, H. Ishibashi, K. Aoki, et al. 2022. "Framework for probabilistic tsunami hazard assessment considering the effects of sea-level rise due to climate change." *Struct. Saf.* 94: 102152.
- ANSI (American National Standards Institute). 1982. "Building code requirements for minimum design loads in buildings and other structures." ANSI A58.1-1982. New York: ANSI.
- ASCE. 2010. *Minimum design loads for buildings and other structures*. ASCE 7-10. Reston, VA: ASCE.

- ASCE. 2015a. *Adapting infrastructure and civil engineering practice to a changing climate*. Reston, VA: ASCE.
- ASCE. 2015b. *Guidelines for electrical transmission line structural loading*, MOP 74. Reston, VA: ASCE.
- ASCE. 2017. *Minimum design loads and associated criteria for buildings and other structures*. ASCE 7-16. Reston, VA: ASCE.
- ASCE. 2018. *Climate-resilient infrastructure: Adaptive design and risk management*, MOP 140. Reston, VA: ASCE.
- ASCE. 2019. *Prestandard for performance-based wind design*. Reston, VA: ASCE.
- ASCE. 2020a. *Performance-based structural fire design: exemplar designs of four regionally diverse using ASCE 7-16, Appendix E*. Reston, VA: ASCE. <https://ascelibrary.org/doi/epdf/10.1061/9780784482698>
- ASCE. 2020b. *Code of ethics*. Reston, VA: ASCE.
- ASCE. 2021. *Hazard-resilient infrastructures: Analysis and design*, MOP 144. Reston, VA: ASCE.
- ASCE. 2022a. *ASCE 7 hazard tool online*. Reston, VA: ASCE.
- ASCE. 2022b. *Minimum design loads and associated criteria for buildings and other structures*. ASCE 7-22. Reston, VA: ASCE.
- ASCE. 2023. *Seismic evaluation and retrofit of existing buildings*. ASCE 41-23. Reston, VA: ASCE.
- Bartlett, F. M., H. P. Hong, and W. Zhou. 2003. "Load factor calibration for the proposed 2005 edition of the National Building Code of Canada: Statistics of loads and load effects." *Can. J. Civ. Eng.* 30 (2): 429–439.
- Bastidas-Arteaga, E., and M. G. Stewart. 2019. *Climate adaptation engineering: Risks and economics for infrastructure decision-making*. London: Butterworth-Heinemann.
- Bean, B., M. Maguire, Y. Sun, J. Wagstaff, et al. 2021. *The 2020 national snow load study*. Milwaukee, WI: Mathematics and Statistics Faculty Publications.
- Bennett, G. L., J. J. Roering, B. H. Mackey, A. L. Handwerker, et al. 2016. "Historic drought puts the brakes on earthflows in northern California." *Geophys. Res. Lett.* 43 (11): 5725–5731.
- Bindschadler, R. A., S. Nowicki, A. Abe-ouchi, A. Aschwanden, et al. 2013. "Ice-sheet model sensitivities to environmental forcing and their use in projecting future sea level (the SeaRISE project)." *J. Glaciol.* 59 (214): 195–224. <https://doi.org/10.3189/2013JoG12J125>.
- Brooks, H. E. 2013. "Severe thunderstorms and climate change." *Atmos. Res.* 123: 129–138.
- Brooks, H. E., G. W. Carbin, and P. T. Marsh. 2014. "Increased variability of tornado occurrence in the United States." *Science* 346 (6207): 349–352.
- Bruneau, M., M. Barbato, J. E. Padgett, A. E. Zaghi, et al. 2017. "State-of-the-art on multihazard design." *J. Struct. Eng.* 143 (10): 03117002.
- Buchanan, M. K., R. E. Kopp, M. Oppenheimer, and C. Tebaldi. 2016. "Allowances for evolving coastal flood risk under uncertain local sea-level rise." *Clim. Change* 137 (3): 347–362.
- Buchanan, M. K., M. Oppenheimer, and R. E. Kopp. 2017. "Amplification of flood frequencies with local sea level rise and emerging flood regimes." *Environ. Res. Lett.* 12 (6): 064009.
- Cannon, A. J., D. Jeong, X. Zhang, and F. W. Zwiers. 2020. *Climate-resilient buildings and core public infrastructure 2020: An assessment of the impact of climate change on climatic design data in Canada*. Gatineau, QC, Canada: Environment and Climate Change.
- Ceyhan, E., P. Basuchowdhuri, T. Judeh, S. Ou, et al. 2007. "Towards a faster and improved ADCIRC (Advanced Multi-Dimensional CIRCulation) model." *J. Coast. Res.* 50: 949–954.
- Chaine, P. M., and G. Castonguay. 1974. *New approach to radial ice thickness concept applied to bundle-like conductors, Industrial Meteorology—Study IV*. Toronto: Environment Canada.

- Chaine, P. M., and P. Skeates. 1974. *Ice accretion handbook: Freezing precipitation*. Toronto: Environment Canada.
- Changnon, S. A., and T. R. Karl. 2003. "Temporal and spatial variations of freezing rain in the contiguous United States: 1948–2000." *J. Appl. Meteorol.* 42 (9): 1302–1315.
- Chow, V. T., D. R. Maidment, and L. W. Mays. 1988. *Applied hydrology*. New York: McGraw-Hill Series in Water Resources.
- Church, J. A., P. U. Clark, A. Cazenave, J. M. Gregory, et al. 2013. "Sea level change." In Chap. 13 of *Climate change 2013: The physical science basis. Contribution of working group I to fifth assessment report of the intergovernmental panel on climate change*, 1137–1216. Cambridge, UK: Cambridge University Press.
- Clarke, G. R. T., D. A. B. Hughes, S. L. Barbour, and V. Sivakumar. 2006. "The implications of predicted climate changes on the stability of highway geotechnical infrastructure: A case study of field monitoring of pore water response." In *EIC Climate Change Technology*, 1–10. New York: IEEE.
- Coe, J. A., and J. W. Godt. 2012. "Review of approaches for assessing the impact of climate change on landslide hazards." *Landslides and engineered slopes, protecting society through improved understanding*, Vol. 1. In *Proc., 11th Int. and 2nd North American Symp. on Landslides and Engineered Slopes*, edited by E. Eberhardt, C. Froese, A. K. Turner, and S. Leroueil, pp. 371–377. London: Taylor & Francis.
- Coles, S. 2001. *An introduction to statistical modeling of extreme values*. London: Springer.
- Conant, R. T., M. G. Ryan, G. I. Agren, H. E. Birge, et al. 2011. "Temperature and soil organic matter decomposition rates—Synthesis of current knowledge and a way forward." *Global Change Biol.* 17 (11): 3392–3404.
- Cooke, R. M. 2015. "Messaging climate change uncertainty." *Nat. Clim. Change* 5 (1): 8–10.
- Cortinas, J. V., Jr., B. C. Bernstein, C. C. Robbins, and J. W. Strapp. 2004. "An analysis of freezing rain, freezing drizzle, and ice pellets across the United States and Canada: 1976–90." *Weather Forecast* 19 (2): 377–390.
- Croce, P., P. Formichi, F. Landi, and F. Marsili. 2018. "Climate change: Impact on snow loads on structures." *Cold Reg. Sci. Technol.* 150: 35–50.
- CSA (Canadian Standard Association). 2006. *Design criteria of overhead transmission lines*. CAN/CSA C22.3. Rexdale, ON: CSA.
- CSA. 2019. *Canadian highway bridge design code*. CSA S6:19. Toronto, ON: CSA.
- Cui, W., and L. Caracoglia. 2016. "Exploring hurricane wind speed along US Atlantic coast in warming climate and effects on predictions of structural damage and intervention costs." *Eng. Struct.* 122: 209–225.
- Davidson, E. A., and I. A. Janssens. 2006. "Temperature sensitivity of soil carbon decomposition and feedbacks to climate change." *Nature* 440 (7081): 165–173.
- Debock, D. J., A. B. Liel, J. R. Harris, B. R. Ellingwood, et al. 2017. "Reliability-based maps for design snow loads. I: Site-specific probability models for ground snow loads." *J. Struct. Eng.* 143 (7): 04017046.
- Dehn, M., G. Bürger, J. Buma, and P. Gasparetto. 2000. "Impact of climate change on slope stability using expanded downscaling." *Eng. Geol.* 55 (3): 193–204.
- de Lima, A. S., A. Khalid, T. W. Miesse, F. Cassalho, et al. 2020. "Hydrodynamic and waves response during storm surges on the Southern Brazilian coast: A hindcast study." *Water (Switzerland)* 12 (12): 3538.
- Deryugina, T., L. Kawano, and S. Levitt. 2018. "The economic impact of hurricane Katrina on its victims: Evidence from individual tax returns." *Am. Econ. J. Appl. Econ.* 10 (2): 202–233.

- Dusenberry, D. O. 2019. "Performance-based design is the future." Accessed October 2, 2024. <https://www.structuremag.org/article/performance-based-design-is-the-future/>.
- Ellingwood, B., T. V. Galambos, J. G. MacGregor, and C. A. Cornell. 1980. *Development of probability-based load criteria for American National Standard A58*. NBS SP 577. Gaithersburg, MD: National Bureau of Standards.
- Ellingwood, B., J. G. MacGregor, T. V. Galambos, and C. A. Cornell. 1982. "Probability based load criteria: Load factors and load combinations." *J. Struct. Div.* 108 (5): 978–997.
- Ellingwood, B., and M. O'Rourke. 1985. "Probabilistic models of snow loads on structures." *Struct. Saf.* 2 (4): 291–299.
- Ellingwood, B., and R. K. Redfield. 1983. "Ground snow loads for structural design." *J. Struct. Eng.* 109 (4): 950–964.
- Ellingwood, B. R. 2000. "LRFD: Implementing structural reliability in professional practice." *Eng. Struct.* 22 (2): 106–115.
- Ellingwood, B. R., N. Wang, J. R. Harris, and T. P. McAllister. 2019. "The role of performance-based engineering in achieving community resilience." Chap. 6 in *Handbook of sustainable and resilient infrastructure*, edited by P. Gardoni, 94–112. London: Routledge.
- Ellingwood, B. R., J. W. van de Lindt, and T. McAllister. 2020. "Community resilience: A new challenge to the practice of structural engineering." *Struct. Mag.* 27 (11): 28–30.
- Elms, D. G. 1992. "Risk assessment." In *Engineering safety*, edited by D. Blockley, 28–46. Berkshire, UK: McGraw-Hill UK.
- Elsner, J. B. 2006. "Evidence in support of the climate change—Atlantic hurricane hypothesis." *Geophys. Res. Lett.* 33 (16): 1–3.
- El-Tayeb, E. H., S. E. El-Metwally, H. S. Askar, and A. M. Yousef. 2017. "Thermal analysis of RC beams and frames." *HBRC J.* 13 (1): 8–24.
- Emanuel, K. 2005. "Increasing destructiveness of tropical cyclones over the past 30 years." *Nature* 436 (7051): 686–688.
- Emanuel, K., R. Sundararajan, and J. Williams. 2008. "Hurricanes and global warming: Results from downscaling IPCC AR4 simulations." *Bull. Am. Meteorol. Soc.* 89 (3): 347–367.
- Emanuel, K., K. Oouchi, M. Satoh, H. Tomita, et al. 2010. "Comparison of explicitly simulated and downscaled tropical cyclone activity in a high-resolution global climate model." *J. Adv. Model. Earth Syst.* 2 (Art. 9): 1–9.
- Emanuel, K. A. 2013. "Downscaling CMIP5 climate models shows increased tropical cyclone activity over the 21st century." In *Proc., Natl Acad. Sci. U.S.A.* 110 (30): 12219–12224.
- Esmaili, M., and M. Barbato. 2021. "Predictive model for hurricane wind hazard under changing climate conditions." *Nat. Hazards Rev.* 22 (3): 04021011.
- FEMA (Federal Emergency Management Agency). 2001. *Engineering principles and practices for flood-prone residential structures*. Tech. Rep. 259. Washington, DC: FEMA.
- FEMA. 2016. *Flood facts*. Washington, DC: FEMA.
- FEMA. 2018a. *Seismic performance assessment of buildings, Volume 1—Methodology*. 2nd ed. FEMA P-58-1. Washington, DC: FEMA.
- FEMA. 2018b. *Seismic performance assessment of buildings, Volume 4—Methodology for assessing environmental impacts*. FEMA P-58-4. Washington, DC: FEMA.
- FHWA (Federal Highway Administration). 2012. *Evaluating scour at bridges*, 5th ed. Hydraulic Engineering Circular No. 18, FHWA-HIF-12-003. Washington, DC: FHWA.
- Fintel, M., and F. Khan. 1965. "Effects of column exposure in tall structures—Temperature variations and their effects." *ACI J. Proc.* 62 (12): 1533–1556.

- Fox-Kemper, B., H. T. Hewitt, C. Xiao, G. Aðalgeirsdóttir, et al. 2021. "Ocean, cryosphere and sea level change." In Chap. 9 of *Climate change 2021: The physical science basis. Contribution of working group I to the sixth assessment report of the intergovernmental panel on climate change*. Cambridge, UK: Cambridge University Press.
- Galambos, T. V., B. Ellingwood, J. G. MacGregor, and C. A. Cornell. 1982. "Probability based load criteria: Assessment of current design practice." *J. Struct. Div.* 108 (5): 959–977.
- Gariano, S. L., and F. Guzzetti. 2016. "Landslides in a changing climate." *Earth-Sci. Rev.* 162: 227–252.
- Gayathri, R., P. K. Bhaskaran, and F. Jose. 2017. "Coastal inundation research: An overview of the process." *Curr. Sci.* 112 (2): 267–278.
- Geis, J., K. Strobel, and A. Liel. 2012. "Snow induced building failures." *J. Perform. Constr. Facil.* 26 (4): 377–388.
- Genç, O., M. Ardiçlioğlu, and N. Ağırlioğlu. 2015. "Calculation of mean velocity and discharge using water surface velocity in small streams." *Flow Meas. Instrum.* 41: 115–120.
- Georgiou, P. N., A. G. Davenport, and B. J. Vickery. 1983. "Design wind speeds in regions dominated by tropical cyclones." *J. Wind Eng. Ind. Aerodyn.* 13 (1–3): 139–152.
- Ghosn, M., and B. R. Ellingwood. 2024. "Risk-informed design and safety assessment of structures in a changing climate: A review of U.S. practice and a path forward." *Struct. Infrastruct. Eng.* 20 (7–8): 1–15.
- Ghosn, M., F. Moses, and J. Wang. 2003. *Design of highway bridges for extreme events*. NCHRP Rep. 489. Washington, DC: Transportation Research Board.
- Gross, J., and T. McAllister. 2005. *Federal building and fire safety investigation of the World Trade Center Disaster: Structural fire response and probable collapse sequence of the World Trade Center towers*. NIST NCSTAR 1-6. Gaithersburg, MD: NIST, National Construction Safety Team Act Reports (NIST NCSTAR). [https://tsapps.nist.gov/publication/get\\_pdf.cfm?pub\\_id=101279](https://tsapps.nist.gov/publication/get_pdf.cfm?pub_id=101279)
- Hagedorn, R. 2016. "Impact of extreme summer temperatures on bridge structures." Ph.D. thesis, Dept. of Civil and Structural Engineering, University of Arkansas.
- Hagedorn, R., J. S. Martí-Vargas, C. N. Dang, W. M. Hale, et al. 2019. "Temperature gradients in bridge concrete I-girders under heat wave." *J. Bridge Eng.* 24 (8): 1–14.
- Hague, B. S., and A. J. Taylor. 2021. "Tide-only inundation: A metric to quantify the contribution of tides to coastal inundation under sea-level rise." *Nat. Hazard.* 107 (1): 675–695.
- Hall, J. A., S. Gill, J. Obeysekera, W. Sweet, et al. 2016. *Regional sea level scenarios for coastal risk management: Managing the uncertainty of future sea level change and extreme water levels for department of defense coastal sites worldwide*. Washington, DC: Department of Defense, Strategic Environmental Research and Development Program.
- Handwerger, A. L., E. J. Fielding, M. H. Huang, G. L. Bennett, et al. 2019. "Widespread initiation, reactivation, and acceleration of landslides in the northern California coast ranges due to extreme rainfall." *J. Geophys. Res.: Earth Surf.* 124 (7): 1782–1797.
- He, J., H. Xin, Y. Wang, and J. A. F. O. Correia. 2021. "Effect of temperature loading on the performance of a PC bridge in Oklahoma: Reliability analysis." *Structures* 34: 1429–1442.
- Hintermaier, A., and N. Lin. 2024. Investigation of climate change effects on design wind speeds along the US east and Gulf coasts. *J. Struct. Eng.* ASCE 150 (9): 04024123-1–04024123-14. <https://doi.org/10.1061/JSENDH.STENG-11899>
- Hock, R., A. Bliss, B. E. N. Marzeion, R. H. Giesen, et al. 2019. "GlacierMIP—A model intercomparison of global-scale glacier mass-balance models and projections." *J. Glaciol.* 65 (251): 453–467.

- Holicky, M., and M. Sykora. 2009. "Failures of roofs under snow load: Causes and reliability analysis." In *Forensic engineering*, 444–453. Reston, VA: ASCE.
- Hong, H. P., D. Kennedy, Z. Lounis, D. Gagnon, et al. 2022. "Calibration of new design wind and ice loads for Canadian highway bridge design code based on ultimate return period and considering climate change effects." In *Proc., 11th Int. Conf. on Short and Medium Span Bridges*. Surry, BC: Canadian Society for Civil Engineering.
- Hong, H. P., Q. Tang, S. C. Yang, X. Z. Cui, et al. 2021. "Calibration of the design wind load and snow load considering the historical climate statistics and climate change effects." *Struct. Saf.* 93: 102135.
- Hong, H. P., and W. Ye. 2014. "Analysis of extreme ground snow loads for Canada using snow depth records." *Nat. Hazard.* 73: 355–371.
- Hungr, O., S. McDougall, and M. Bovis. 2005. "Entrainment of material by debris flows." In *Debris-flow hazards and related phenomena*, edited by M. Jakob and O. Hungr, 135–158. Berlin: Springer.
- Hunter, J. 2012. "A simple technique for estimating an allowance for uncertain sea-level rise." *Clim. Change* 113 (2): 239–252.
- ICC (International Code Council). 2021a. *International building code (IBC)*. Washington, DC: ICC.
- ICC. 2021b. *International plumbing code (IPC)*. Washington, DC: ICC.
- Imbsen, R. A., D. E. Vandershaf, R. A. Schamber, and R. V. Nutt. 1985. *Thermal effects in concrete bridge superstructures*. NCHRP 276. Washington, DC: National Cooperative Highway Research Program.
- IPCC. 2014. *Climate change 2014: Synthesis report*. Contribution of Working Groups I, II and III to the Fifth Assessment Report of the Intergovernmental Panel on Climate Change. Geneva: IPCC.
- IPCC. 2022. *Climate change 2022—Impacts, adaptation and vulnerability*. IPCC Sixth Assessment Report (AR6). Geneva: IPCC.
- ISO (International Standardization Organization). 2017. *Atmospheric icing of structures*. ISO 12494. Geneva: ISO.
- Iverson, R. M., M. E. Reid, M. Logan, R. G. LaHusen, et al. 2011. "Positive feedback and momentum growth during debris-flow entrainment of wet bed sediment." *Nat. Geosci.* 4 (2): 116–121.
- Jackson, L. P., and S. Jevrejeva. 2016. "A probabilistic approach to 21st century regional sea-level projections using RCP and high-end scenarios." *Global Planet. Change* 146: 179–189.
- Jamalinia, E., P. J. Vardon, and S. C. Steele-Dunne. 2019. "The effect of soil–vegetation–atmosphere interaction on slope stability: A numerical study." *Environ. Geotech.* 8 (7): 430–441.
- Jamalinia, E., P. J. Vardon, and S. C. Steele-Dunne. 2020. "The impact of evaporation induced cracks and precipitation on temporal slope stability." *Comput. Geotech.* 122: 103506.
- Jeong, D. I., A. J. Cannon, and X. Zhang. 2019. "Projected changes to extreme freezing precipitation and design ice loads over North America based on a large ensemble of Canadian regional climate model simulations." *Nat. Hazards Earth Syst. Sci.* 19 (4): 857–872.
- Jeong, D. I., and L. Sushama. 2018. "Projected changes to extreme wind and snow environmental loads for buildings and infrastructure across Canada." *Sustainable Cities Soc.* 36: 225–236.

- Jevrejeva, S., A. Grinsted, and J. C. Moore. 2009. "Anthropogenic forcing dominates sea level rise since 1850." *Geophys. Res. Lett.* 36 (20): L20707.
- Jones, J. A. A. 2010. "Soil piping and catchment response." *Hydrol. Process* 24 (12): 1548–1566.
- Jones, K., and S. Daly. 2016. *Effect of Arctic amplification on design snow loads in Alaska*. Hanover, NH: Engineering Research and Development Center.
- Jones, K. F. 1998. "A simple model for freezing rain ice loads." *Atmos. Res.* 46 (1–2): 87–97.
- Jones, K. F., R. Thorkildson, and J. N. Lott. 2002. "The development of the map of extreme ice loads for ASCE Manual 74." In *Proc., Electrical transmission in a new age*, 9–31. Reston, VA: ASCE.
- Jun, M., R. Knutti, and D. W. Nychka. 2008. "Spatial analysis to quantify numerical model bias and dependence." *J. Am. Stat. Assoc.* 103 (483): 934–947.
- Keper, J., and Y. Wang. 2001. "The dynamics of boundary layer jets within the tropical cyclone core. Part II: Nonlinear enhancement." *J. Atmos. Sci.* 58 (17): 2485–2501.
- Khan, F., and M. Fintel. 1966. "Effect of column exposure in tall structures—Analysis for length changes of exposed columns." *ACI J. Proc.* 63 (8): 843–862.
- Khan, F., and M. Fintel. 1968. "Effects of column exposure in tall structures—Design considerations and field observations of buildings." *ACI J. Proc.* 65 (2): 99–110.
- Khan, F. R., and A. F. Nassetta. 1970. "Temperature effects on tall steel framed buildings. Part 3—Design considerations." *Eng. J.* 7 (4): 121–131.
- Kopp, R. E., R. M. Horton, C. M. Little, J. X. Mitrovica, et al. 2014. "Probabilistic 21st and 22nd century sea-level projections at a global network of tide-gauge sites." *Earth's Future* 2 (8): 383–406.
- Koshimura, S., and N. Shuto. 2015. "Response to the 2011 Great East Japan Earthquake and Tsunami disaster." *Philos. Trans. R. Soc. A Math. Phys. Eng. Sci.* 373 (2053).
- Kotani, T., K. Tozato, S. Takase, S. Moriguchi, et al. 2020. "Probabilistic tsunami hazard assessment with simulation-based response surfaces." *Coast. Eng.* 160: 103719.
- Kovacevic, K., D. M. Potts, and P. R. Vaughan. 2001. "Progressive failure in clay embankments due to seasonal climate changes." In *Proc., 5th Int. Conf. on Soil Mechanics and Geotechnical Engineering*, Vol. 3, 2127–2130. London: International Society for Soil Mechanics and Geotechnical Engineering
- Kunreuther, H., R. Meyer, and C. van den Bulte. 2004. *Risk analysis for extreme events: Economic incentives for reducing future losses*. NIST Rep. GCR 04-871. Gaithersburg, MD: National Institute of Standards and Technology.
- Lagasse, P. F., M. Ghosn, P. A. Johnson, L. W. Zevenbergen, et al. 2013. *Risk-based approach for bridge scour prediction*. Washington, DC: Transportation Research Board.
- Landerer, F. W., and S. C. Swenson. 2012. "Accuracy of scaled GRACE terrestrial water storage estimates." *Water Resour. Res.* 48 (4): 4531.
- Lee, C. Y., M. K. Tippett, A. H. Sobel, and S. J. Camargo. 2018. "An environmentally forced tropical cyclone hazard model." *J. Adv. Model. Earth Syst.* 10 (1): 223–241.
- Lee, E. M., and D. K. C. Jones. 2004. *Landslide risk assessment*. London: Thomas Telford.
- Lee, J. Y., and B. R. Ellingwood. 2017. "A decision model for intergenerational life-cycle risk assessment of civil infrastructure exposed to hurricanes under climate change." *Reliab. Eng. Syst. Saf.* 159: 100–107.
- Lee, K. H., and D. V. Rosowsky. 2005. "Site-specific snow load models and hazard curves for probabilistic design." *Nat. Hazards Rev.* 6 (3): 109–120.
- Leshchinsky, B., F. Vahedifard, H. B. Koo, and S. H. Kim. 2015. "Yumokjeong Landslide: An investigation of progressive failure of a hillslope using the finite element method." *Landslides* 12 (5): 997–1005.

- Levermann, A., R. Winkelmann, S. Nowicki, J. L. Fastook, et al. 2014. "Projecting antarctic ice discharge using response functions from SeaRISE ice-sheet models." *Earth Syst. Dyn.* 5 (2): 271–293.
- Li, L., A. D. Switzer, Y. Wang, C. H. Chan, et al. 2018. "A modest 0.5-m rise in sea level will double the tsunami hazard in Macau." *Sci. Adv.* 4 (8): eaat1180.
- Liel, A. B., D. J. DeBock, J. R. Harris, B. R. Ellingwood, et al. 2017. "Reliability-based maps for design snow loads: II. Reliability assessment and mapping procedures." *J. Struct. Eng.* 143 (7): 04017047.
- Lin, N., R. E. Kopp, B. P. Horton, and J. P. Donnelly. 2016. "Hurricane Sandy's flood frequency increasing from year 1800 to 2100." In *Proc., National Academy of Science U.S.A.* 113 (43): 12071–12075.
- Lindgren, J., D. K. Jonsson, and A. Carlsson-Kanyama. 2009. "Climate adaptation of railways: Lessons from Sweden." *Eur. J. Transp. Infrastruct. Res.* 9 (2):164-181.
- Lounis, Z., and T. P. McAllister. 2016. "Risk-based decision making for sustainable and resilient infrastructure systems." *J. Struct. Eng.* 142 (9): F4016005.
- Ma, Y., Q. Dai, and W. Pang. 2020. "Reliability assessment of electrical grids subjected to wind hazards and ice accretion with concurrent wind." *J. Struct. Eng.* 146 (7): 04020134.
- Maguire, M., B. Bean, J. Harris, A. Liel, et al. 2021. *Ground snow loads for ASCE 7-22—What has changed and why?* Logan, UT: Utah State University.
- Mackey, B. H., and J. J. Roering. 2011. "Sediment yield, spatial characteristics, and the long-term evolution of active earthflows determined from airborne LiDAR and historical aerial photographs, Eel River, California." *GSA Bull.* 123 (7-8): 1560–1576. <https://doi.org/10.1130/B30306.1>
- Makkonen, L. 2000. "Models for the growth of rime, glaze, icicles and wet snow on structures." *Philos. Trans Royal Soc. London. Series A: Mathematical, Physical and Engineering Sciences* 358 (1776): 2913–2939. <https://www.jstor.org/stable/2666835>
- Marinier, S., J. M. Thériault, and K. Ikeda. 2023. "Changes in freezing rain occurrence over eastern Canada using convection-permitting climate simulations." *Clim. Dyn.* 60 (5): 1369–1384. <https://doi.org/10.1007/s00382-022-06370-6>.
- Marsooli, R., N. Lin, K. Emanuel, and K. Feng. 2019. "Climate change exacerbates hurricane flood hazards along US Atlantic and Gulf Coasts in spatially varying patterns." *Nat. Commun.* 10: 3785.
- Mayo, T., and N. Lin. 2019. "The effect of the surface wind field representation in the operational storm surge model of the National Hurricane Center." *Atmosphere* 10: 193.
- McAllister, T. P., N. Wang, and B. R. Ellingwood. 2018. "Risk-informed mean recurrence intervals for updated wind maps in ASCE 7-16." *J. Struct. Eng.* 144 (5): 06018001.
- McAllister, T., R. Walker, and A. Baker. 2022. "Assessment of resilience in codes, standards, regulations, and best practices for buildings and infrastructure systems." *NIST Technical Note 2209*, Gaithersburg, MD: National Institute of Standards and Technology. <https://doi.org/10.6028/NIST.TN.2209>
- McComber, P., G. Morin, R. Martin, and L. V. Van. 1983. "Estimation of combined ice and wind load on overhead transmission lines." *Cold Reg. Sci. Technol.* 6 (3): 195–206.
- McCray, C. D., D. Paquin, J. M. Thériault, and É. Bresson. 2022. "A multi-algorithm analysis of projected changes to freezing rain over North America in an ensemble of regional climate model simulations." *J. Geophys. Res.: Atmospheres* 127 (14): e2022JD036935. <https://doi.org/10.1029/2022JD036935>
- McLaughlin, E. R. 1970. "Temperature effects on tall steel framed buildings part 1: Response of steel columns to temperature exposure." *Eng. J.* 7 (4): 105–109.

- Milton, J., and A. Bourque. 1999. *A climatological account of the January 1998 ice storm in Quebec: Scientific report*. Toronto: Environment Canada, Quebec Region, Atmospheric Sciences & Environmental Issues Division.
- Mirae-Ashtiani, S., F. Vahedifard, M. Karimi-Ghartemani, J. Zhao, et al. 2022. "Performance degradation of levee-protected electric power network due to flooding in a changing climate." *IEEE Trans. Power Syst.* 37 (6): 4651–4660.
- Mo, H. M., L. Y. Dai, F. Fan, T. Che, et al. 2016. "Extreme snow hazard and ground snow load for China." *Nat. Hazard.* 84 (3): 2095–2120.
- Molk, P. 2016. "Private versus public insurance for natural hazards: Individual behavior's role in loss mitigation." In *Societal risk management of natural hazards*, edited by P. Gardoni, C. Murphy, and A. Rowell. Berlin: Springer.
- Molodecka, V., N. Devineni, and M. Ghosn. 2020. "Effect of climate change on reliability of bridges under threat from flood-related scour." In *American Geophysical Union, Fall Meeting 2020*. Abstract GC092-08. <https://ui.adsabs.harvard.edu/abs/2020AGUFMGC092..08M/abstract>.
- Mount, J., and R. Twiss. 2005. "Subsidence, sea level rise, seismicity in the Sacramento-San Joaquin Delta." *San Francisco Estuary Watershed Sci.* 3 (1).
- Mudd, L., Y. Wang, C. Letchford, and D. Rosowsky. 2014. "Assessing climate change impact on the US East Coast hurricane hazard: Temperature, frequency, and track." *Nat. Hazards Rev.* 15 (3): 04014001.
- Mulherin, N. D. 1998. "Atmospheric icing and communication tower failure in the United States." *Cold Reg. Sci. Technol.* 27 (2): 91–104.
- Nasr, A., E. Kjellström, I. Björnsson, D. Honfi, et al. 2020. "Bridges in a changing climate: A study of the potential impacts of climate change on bridges and their possible adaptations." *Struct. Infrastruct. Eng.* 16 (4): 738–749.
- NBCC (National Building Code of Canada). 2015. *Canadian Commission on Building and Fire Codes*. Ottawa, ON, Canada: National Research Council of Canada.
- NBCC. 2020. *Canadian Commission on Building and Fire Codes*. Ottawa, ON, Canada: National Research Council of Canada.
- NEHRP (National Earthquake Hazards Reduction Program). 2020. *Recommended seismic provisions for new buildings and other structures. Vol. II: Part 3 resource papers*. FEMA P-2082-2. Washington, DC: NEHRP, Building Seismic Safety Council, National Institute of Building Sciences.
- Nereson, A. L., and N. J. Finnegan. 2019. "Drivers of earthflow motion revealed by an 80 yr record of displacement from Oak Ridge earthflow, Diablo Range, California, USA." *GSA Bull.* 131 (3-4): 389–402. <https://doi.org/10.1130/B32020.1>
- Newark, M. J., L. E. Welsh, R. J. Morris, and W. V. Dnes. 1989. "Revised ground snow loads for the 1990 national building code of Canada." *Can. J. Civ. Eng.* 16 (3): 267–278. <https://cdnsiencepub.com/doi/pdf/10.1139/l89-052>
- NFPA (National Fire Protection Association). 2021. *Building construction and safety code*. NFPA 5000. Quincy, MA: NFPA.
- NIST (National Institute of Standards and Technology). 2016. *Community resilience planning guide for buildings and infrastructure systems*. NIST SP 1190 (Volumes 1 and 2). Gaithersburg, MD: NIST.
- NIST/FEMA (Federal Emergency Management Agency). 2021. *Recommended options for improving the built environment for post-earthquake reoccupancy and functional recovery time*. NIST SP 1254/FEMA P-2090. Gaithersburg, MD: NIST.

- NOAA (National Oceanographic and Atmospheric Administration). 2021. *Precipitation frequency data server*. Silver Spring, MD: Hydrometeorological Design Studies Center.
- Nowak, A. S. 1999. *Calibration of LRFD bridge design code*. NCHRP Rep. 368. Washington, DC: Transportation Research Board, National Academies Press.
- NRC (National Research Council). 2012. *Disaster resilience: A national imperative*. Washington, DC: National Academies Press.
- NRC. 2016. *Transportation resilience: Adaptation to climate change*. Washington, DC: NRC, National Academies Press.
- Nyambayo, V. P., D. M. Potts, and T. I. Addenbrooke. 2004. "The influence of permeability on the stability of embankments experiencing seasonal cyclic pore water pressure changes." In *Vol. 2 of Advances in Geotechnical Engineering: Skempton Conf.*, 898–910. London: Thomas Telford.
- Orlić, M., and Z. Pasarić. 2013. "Semi-empirical versus process-based sea-level projections for the twenty-first century." *Nat. Clim. Change* 3: 735–738.
- O'Rourke, M., H. N. Sinh, J. Cocca, and T. Williams. 2020. "Winter wind parameter for snow drifts." *J. Struct. Eng.* 146 (7): 04020124.
- O'Rourke, M. J., R. Redfield, and P. Von Bradsky. 1982. "Uniform snow loads on structures." *J. Struct. Div.* 108 (ST12): 2781–2798.
- OSSPAC (Oregon Seismic Safety Policy Advisory Commission). 2013. *Oregon resilience plan*. Salem, OR: OSSPAC.
- Palu, S., and H. Mahmoud. 2019. "Impact of climate change on the integrity of the superstructure of deteriorated U.S. bridges." *PLoS ONE* 14 (10): e0223307.
- Pandey, M. D. and Z. Lounis. 2023. "Stochastic modeling of non-stationary environmental loads for reliability analysis under the changing climate." *Struct. Saf.* 103:102348.
- Pant, S., and E. J. Cha. 2018. "Effect of climate change on hurricane damage and loss for residential buildings in Miami-Dade County." *J. Struct. Eng.* 144 (6): 04018057.
- Poland, C. D. 2009. *The resilient city: Defining what San Francisco needs from its seismic mitigation policies*. San Francisco Planning and Urban Research Association Report. San Francisco, CA: Earthquake Engineering Research Institute.
- Potts, D. M., K. Kovacevic, and P. R. Vaughan. 1997. "Delayed collapse of cut slopes in stiff clay." *Géotechnique* 47 (5): 953–982.
- PPD (Presidential Policy Directive). 2013. *Critical infrastructure security and resilience*. PPD 21. Washington, DC: The White House.
- Rahmstorf, S. 2007. "A semi-empirical approach to projecting future sea-level rise." *Science* 80 (315): 368–370.
- Rappaport, E. N. 2000. "Loss of Life in the United States associated with recent Atlantic tropical cyclones." *Bull. Am. Meteorol. Soc.* 81 (9): 2065–2073.
- Rappaport, E. N. 2014. "Fatalities in the United States from Atlantic tropical cyclones: New data and interpretation." *Bull. Am. Meteorol. Soc.* 95 (3): 341–346.
- Ribereau, P., A. Guillou, and P. Naveau. 2008. "Estimating return levels from maxima of non-stationary random sequences using the Generalized PWM method." *Nonlinear Processes Geophys.* 15 (6): 1033–1039.
- Richter, K., R. E. M. Riva, and H. Drange. 2013. "Impact of self-attraction and loading effects induced by shelf mass loading on projected regional sea level rise." *Geophys. Res. Lett.* 40 (6): 1144–1148.
- Robinson, J. D., and F. Vahedifard. 2016. "Weakening mechanisms imposed on California's levees under multiyear extreme drought." *Clim. Change* 137 (1–2): 1–14.

- Robinson, J. D., F. Vahedifard, and A. AghaKouchak. 2017. "Rainfall-triggered slope instabilities under a changing climate: Comparative study using historical and projected precipitation extremes." *Can. Geotech. J.* 54 (1): 117–127.
- Roeder, C. W. 2002. *Thermal design procedure for steel and concrete bridges*. Final Report for NCHRP 20-07/106. Washington, DC: National Cooperative Highway Research Program, The National Academies.
- Rootzén, H., and R. W. Katz. 2013. "Design life level: Quantifying risk in a changing climate." *Water Resour. Res.* 49 (9): 5964–5972.
- Sack, R., and A. Sheikh-Taheri. 1986. *Ground and roof snow loads for Idaho*. Moscow, ID: Department of Civil Engineering, University of Idaho.
- Sack, R. L. 2015. "Ground snow loads for the western United States: State of the art." *J. Struct. Eng.* 142 (1): 4015082.
- Salas, J. D., and J. Obeysekera. 2014. "Revisiting the concepts of return period and risk for nonstationary hydrologic extreme events." *J. Hydrol. Eng.* 19 (3): 554–568.
- Salimi, K., A. B. Cerato, F. Vahedifard, and G. A. Miller. 2021. "Tensile strength of compacted clays during desiccation under elevated temperatures." *Geotech. Test. J.* 44 (4): 1119–1134.
- Scharlemann, J., E. Tanner, R. Hiederer, and V. Kapos. 2014. "Global soil carbon: Understanding and managing the largest terrestrial carbon pool." *Carbon Manage.* 5 (1): 81–91.
- SCOSS (Standing Committee on Structural Safety). 2008. "The fire at the Torre Windsor office building, Madrid 2005. Failure Data Sheet, London: Standing Committee on Structural Safety. <https://www.cross-safety.org/sites/default/files/2005-06/torre-windsor-building-fire-madrid.pdf>.
- SEI (Structural Engineering Institute). 2018. *Advocating for performance-based design*. Task Committee Report to the Structural Engineering Institute Board of Governors. Reston, VA: ASCE.
- Sharma, S., and S. B. Mohan. 2011. "Status of bridge failures in the United States (1800–2009)." In *Annual Meeting of the Transportation Research Board*. Washington, DC: Transportation Research Board.
- Shinozuka, M., M. Q. Feng, J. Lee, and T. Naganuma. 2000. "Statistical analysis of fragility curves." *J. Eng. Mech.* 126 (12): 1224–1231.
- Sinh, N. H., F. T. Lombardo, C. W. Letchford, and D. V. Rosowsky. 2016. "Characterization of joint wind and ice hazard in Midwestern United States." *Nat. Hazards Rev.* 17 (3): 04016004.
- Steenbergen, R. D. J. M., C. P. W. Geurts, and C. A. van Bentum. 2009. "Climate change and its impact on structural safety." *HERON* 54 (1): 3–35 (TNO Delft, The Netherlands)
- Stocker, T. F., et al. 2013. "Climate change 2013: The physical science basis." In *Proc., Contribution of Working Group I to the 5th Assessment Report of the Intergovernmental Panel on Climate Change*. Cambridge, UK: Cambridge University Press.
- Sturm, M., B. Taras, G. E. Liston, C. Derksen, et al. 2010. "Estimating snow water equivalent using snow depth data and climate classes." *J. Hydrometeorol.* 11 (6): 1380–1394.
- Swiss Re. 2020. "Swiss Re Institute estimates USD 83 billion global insured catastrophe losses in 2020, the fifth-costliest on record." <https://www.swissre.com/media/press-release/nr-20201215-sigma-full-year-2020-preliminary-natcat-loss-estimates.html>.
- Tang, C.-S., Y.-J. Cui, A.-M. Tang, and B. Shi. 2010. "Experiment evidence on the temperature dependence of desiccation cracking behavior of clayey soils." *Eng. Geol.* 114 (3 – 4): 261–266.
- Tang, C.-S., B. Liu, F. Vahedifard, N. J. Jiang, et al. 2024. "Enhancing soil resilience to climatic wetting-drying cycles through a bio-mediated approach." *J. Geophys. Res.* 129 (5): e2023JF007573.

- Taylor, K. E., R. J. Stouffer, and G. A. Meehl. 2012. "An overview of CMIP5 and the experiment design." *Bull. Am. Meteorol. Soc.* 93 (4): 485–498.
- Thota, S. K., and F. Vahedifard. 2021. "Stability analysis of unsaturated slopes under elevated temperatures." *Eng. Geol.* 293: 106317.
- Tobiasson, W., and A. Greatorex. 1996. "Database and methodology for conducting site specific snow load case studies for the United States." In *Snow engineering: Recent advances*, edited by I. Izumi, T. Nakamura, and R. L. Sack, 249–256. Rotterdam, Netherlands: Balkema.
- Tropea, B., and R. Stewart. 2021. Assessing past and future hazardous freezing rain and wet snow events in Manitoba, Canada using a pseudo-global warming approach. *Atmos. Res.* 259: 105656. <https://doi.org/10.1016/j.atmosres.2021.105656>
- Turkstra, C. J., and H. O. Madsen. 1980. "Load combinations in codified structural design." *J. Struct. Div.* 106 (12): 2527–2543.
- Tye, M. R., J. P. Giovannetone, A. Aghakouchak, R. E. Beighley, et al. 2021. *Impacts of future weather and climate extremes on United States infrastructure: Assessing and prioritizing adaptation actions*. Report of the Task Committee on Future Weather and Climate Extremes. Reston, VA: ASCE.
- USGS (US Geological Survey). 2024. USGS flood indicator mapper. <https://fim.wim.usgs.gov/fim/>
- Vahedifard, F., B. A. Leshchinsky, S. Sehat, and D. Leshchinsky. 2014. "Impact of cohesion on seismic design of geosynthetic-reinforced earth structures." *J. Geotech. Geoenviron. Eng.* 140 (6): 04014016.
- Vahedifard, F., J. D. Robinson, and A. AghaKouchak. 2016. "Can protracted drought undermine the structural integrity of California's earthen levees?" *J. Geotech. Geoenviron. Eng.* 142 (6): 02516001.
- Vahedifard, F., F. S. Tehrani, V. Galavi, E. Ragno, et al. 2017. "Resilience of MSE walls with marginal backfill under a changing climate: Quantitative assessment for extreme precipitation events." *J. Geotech. Geoenviron. Eng.* 143 (9): 04017056.
- Vahedifard, F., Williams, J. M., and AghaKouchak, A. (2018). "Geotechnical Engineering in the Face of Climate Change: Role of Multi-Physics Processes in Partially Saturated Soils." In *Proc., 2018 International Foundations Congress and Equipment Exposition, IFCEE 2018: Advances in Geomaterial Modeling and Site Characterization, Geotechnical Special Publication No. 295*. 353–364. Reston, VA: ASCE. DOI: 10.1061/9780784481585.035.
- Vahedifard, F., F. H. Jasim, F. T. Tracy, M. Abdollahi, et al. 2020. "Levee fragility behavior under projected future flooding in a warming climate." *J. Geotech. Geoenviron. Eng.* 146 (12): 04020139.
- Vahedifard, F., C. C. Goodman, V. Paul, and A. AghaKouchak. 2024. "Amplifying feedback loop between drought, soil desiccation cracking, and greenhouse gas emissions." *Environ. Res. Lett.* 19 (3): 031005.
- Vardon, P. J. 2015. "Climatic influence on geotechnical infrastructure: A review." *Environ. Geotech.* 2 (3): 166–174.
- Vickery, P. J., P. F. Skerlj, and L. A. Twisdale. 2000. "Simulation of hurricane risk in the US using empirical track model." *J. Struct. Eng.* 126 (10): 1222–1237.
- Vickery, P. J., D. Wadhwa, J. Galsworthy, J. A. Peterka, et al. 2010. "Ultimate wind load design gust wind speeds in the United States for use in ASCE-7." *J. Struct. Eng.* 136 (5): 613–625.
- Vogel, J., K. M. Carney, J. B. Smith, C. Herrick, et al. 2016. *Climate adaptation: The state of practice in US communities*. Troy, MI: The Kresge Foundation and Abt Associates.
- Washington State Emergency Management Council: Seismic Safety Committee. 2012. *Resilient Washington State—A framework for minimizing loss and improving statewide*

- recovery after an earthquake. Camp Murray, WA: Washington State Emergency Management Council.
- West, H. H., and A. K. Kar. 1970. "Temperature effects on tall steel framed buildings part 2—Structural analysis." *Eng. J.* 7 (4): 110–120.
- Xu, H., N. Lin, M. Huang, and W. Lou. 2020. "Design tropical cyclone wind speed when considering climate change." *J. Struct. Eng.* 146 (5): 04020063.
- Xue, X., N. Wang, B. R. Ellingwood, and K. Zhang. 2018. "The impact of climate change on resilience of communities vulnerable to riverine flooding." In Chapter 8 of *Climate Change and Its Impacts: Risks and Inequalities*, edited by C. Murphy, P. Gardoni, and R. McKim, 129–144. Berlin: Springer.
- Yang, D. Y., and D. M. Frangopol. 2019. "Physics-based assessment of climate change impact on long-term regional bridge scour risk using hydrologic modeling: Application to Lehigh River watershed." *J. Bridge Eng.* 24 (11): 04019099.
- Yang, K., V. A. Paramygin, and Y. P. Sheng. 2020. "A rapid forecasting and mapping system of storm surge and coastal flooding." *Weather Forecast* 35 (4): 1663–1681.
- Yin, K., S. Xu, W. Huang, and Y. Xie. 2017. "Effects of sea level rise and typhoon intensity on storm surge and waves in Pearl River Estuary." *Ocean Eng.* 136: 80–93.
- Zeng, H., C. S. Tang, C. Zhu, F. Vahedifard, et al. 2022. "Desiccation cracking of soil subjected to different environmental relative humidity conditions." *Eng. Geol.* 297: 106536.
- Zhang, J., A. A. Taflanidis, N. C. Nadal-Caraballo, J. A. Melby, et al. 2018. "Advances in surrogate modeling for storm surge prediction: Storm selection and addressing characteristics related to climate change." *Nat. Hazards* 94: 1225–1253.

### *Additional Reading on Design in an Era of Climate Change (Not cited in the text)*

- Alfraidi, Y., and A. H. Boussabaine. 2015. "Design resilient building strategies in face of climate change." *Int. J. Archit. Environ. Eng.* 9 (1): 6.
- Barros, A. P., and J. L. Evans. 1997. "Designing for climate variability." *J. Prof. Issues Eng. Educ. Pract.* 123 (2): 62–65.
- Bastidas-Arteaga, E., and M. G. Stewart. 2018. "Cost-effective adaptation to address climate change impacts." In *Cost-effective design to address climate change impacts*, 613–636. Sawston, UK: Woodhead Publishing.
- Bjarnadottir, S., Y. Li, and M. G. Stewart. 2011b. "A probabilistic-based framework for impact and adaptation assessment of climate change on hurricane damage risks and costs." *Struct. Saf.* 33 (3): 173–185.
- Bjarnadottir, S., Y. Li, and M. G. Stewart. 2014. "Regional loss estimation due to hurricane wind and hurricane-induced surge considering climate variability." *J. Struct. Infrastruct. Eng.* 10 (11): 1369–1384.
- Chester, M., S. Markolf, A. Fraser, D. Burillo, et al. 2018. "Infrastructure and climate change." In *Routledge handbook of sustainable and resilient infrastructure*, 605–625. London: Taylor and Francis.
- Contento, A., H. Xu, and P. Gardoni. 2018. "A physics-based transportable probabilistic model for climate change dependent storm surge." In *Routledge Handbook of Sustainable and Resilient Infrastructure*, edited by P. Gardoni, 662–682. London: Routledge.
- Czajkowski, J., K. Simmons, and D. Sutter. 2011. "An analysis of coastal and inland fatalities in landfalling US hurricanes." *Nat. Hazard.* 59 (3): 1513–1531.

- Devendiran, D. K., S. Banerjee, and A. Mondal. 2021. "Impact of climate change on multihazard performance of river-crossing bridges: Risk, resilience, and adaptation." *J. Perform. Constr. Facil.* 35 (1): 04020127.
- Dong, Y., and D. M. Frangopol. 2016. "Probabilistic time-dependent multihazard life-cycle assessment and resilience of bridges considering climate change." *J. Perform. Constr. Facil.* 30 (5): 04016034.
- Ellingwood, B. R., J. W. van de Lindt, and T. P. McAllister. 2019. "A fully integrated model of interdependent physical infrastructure and social systems." *Bridge* 49 (2): 43–51.
- Gudipudi, P., B. S. Underwood, and A. Zalgout. 2017. "Impact of climate change on pavement structural performance in the United States." *Transp. Res. Part D: Transp. Environ.* 57: 172–184.
- Kim, D. K., H. M. Son, and J. W. Hu. 2015. "An analytical study on the performance of wind resistant system considering climate change." *Appl. Mech. Mater.* 752–753: 656–661.
- Lacasse, M. A. 2019. "An overview of durability and climate change of building components." *Can. J. Civ. Eng.* 46 (11): v–viii.
- Lee, J. Y., and B. R. Ellingwood. 2017. "A decision model for intergenerational life-cycle risk assessment of civil infrastructure exposed to hurricanes under climate change." *Reliab. Eng. Syst. Saf.* 159: 100–107.
- Lowe, R. 2007. "Addressing the challenges of climate change for the built environment." *Build. Res. Inf.* 35 (4): 343–350.
- Mondoro, A., D. M. Frangopol, and L. Liu. 2018. "Bridge adaptation and management under climate change uncertainties: A review." *Nat. Hazards Rev.* 19 (1): 04017023.
- Mosalam, K. M., U. Alibrandi, H. Lee, and J. Armengou. 2018. "Performance-based engineering and multi-criteria decision analysis for sustainable and resilient building design." *Struct. Saf.* 74: 1–13.
- Nasr, A., I. Bjornsson, D. Honfi, and O. L. Ivanov, et al. 2019. "A review of the potential impacts of climate change on the safety and performance of bridges." *Sustainable and Resilient Infrastruct.* 6 (4): 1–21.
- Nordenson, G., and C. Seavitt. 2015. "Structures of coastal resilience: Designs for climate change." *Social Res.* 82 (3): 655–671.
- Pongiglione, M., and C. Calderini. 2016. "Sustainable structural design: Comprehensive literature review." *J. Struct. Eng.* 142 (12): 04016139.
- Stemers, K. 2003. "Towards a research agenda for adapting to climate change." *Build. Res. Inf.* 31 (3–4): 291–301.
- Stewart, M. G., X. Wang, and M. N. Nguyen. 2011. "Climate change impact and risks of concrete infrastructure deterioration." *Eng. Struct.* 33 (4): 1326–1337.
- Stewart, M. G., X. Wang, and M. N. Nguyen. 2012. "Climate change adaptation for corrosion control of concrete infrastructure." *Struct. Saf.* 35: 29–39.
- Suh, K.-D., S.-W. Kim, N. Mori, and H. Mase. 2012. "Effect of climate change on performance-based design of caisson breakwaters." *J. Waterway Port Coastal Ocean Eng.* 138 (3): 215–225.
- US Climate Resilience Toolkit. Accessed June 25, 2021. <https://toolkit.climate.gov/>.
- Wang, X., M. G. Stewart, and M. Nguyen. 2012. "Impact of climate change on corrosion and damage to concrete infrastructure in Australia." *Clim. Change* 110 (3–4): 941–957.
- Yassaghi, H., and S. Hoque. 2019. "An overview of climate change and building energy: Performance, responses and uncertainties." *Buildings* 9 (7): 166.